NOTE TO USERS

Page(s) not included in the original manuscript and are unavailable from the author or university. The manuscript was scanned as received.

124

This reproduction is the best copy available.

UMI®

Structure, Photochemistry and Charge-Transfer-To-Solvent Relaxation Dynamics of Anionic Clusters

Kadyr K. Timergazine
(Qadir K. Timerghazin)

A Thesis

in

The Department

of

Chemistry and Biochemistry

Presented in Partial Fulfillment of the Requirements
for the Degree of Doctor of Philosophy at
Concordia University
Montréal, Québec, Canada

January 2006

Your file Votre référence
ISBN: 978-0-494-16267-5
Our file Notre référence
ISBN: 978-0-494-16267-5

Abstract

Structure, Photochemistry and Charge-Transfer-To-Solvent Relaxation Dynamics of Anionic Clusters

Kadyr K. Timergazine, Ph.D. Chemistry
Concordia University, 2006

In this work, various methods of computational chemistry have been applied to study the structure, photochemistry and dynamics of small anionic clusters in order to obtain some insight into the fundamental nature of molecule-molecule and electron-molecule interactions. The main theme of this Thesis evolves around charge-transfer-to-solvent (CTTS) excited states of small halide-polar molecule clusters and concomitant phenomena, with specific attention to iodide-acetonitrile clusters $I^-(CH_3CN)_n$.

The structure of ground-state halide-acetonitrile complexes is determined by a competition between ion-dipole interactions and hydrogen bonding. The latter is dominant for complexes formed by all halide ions, except for the binary iodide-acetonitrile complex $I^-(CH_3CN)$, which is stabilized by only ion-dipole interactions. On the other hand, in the excited or ionized iodide complexes and clusters, the non-uniform electron density distribution around the neutral iodine atom due to the unpaired electron and spin-orbit coupling effects plays a very important role in interactions of the iodine atom with molecules or ions. The CTTS excitation of iodide-solvent clusters leads to the transfer of an electron from iodide to a diffuse dipole-bound orbital. The calculated excitation energies for the iodide-acetonitrile complex, as well as the vertical detachment energies of the excited electron have been found to be in a good agreement with available experimental data. For the first time, the relaxation dynamics of CTTS excited states in clusters has been studied by means of first-principles excited-state molecular dynamics simulations for paradigm iodide-acetonitrile $I^-(CH_3CN)$ and iodide-water $I^-(H_2O)_3$ clusters. Whereas the departure of a neutral iodine atom can lead to

stabilization of the excited electron, in agreement with state-of-the-art femtosecond spectroscopy experimental data, the solvent dynamics should not be neglected when interpreting experimental results. The photoexcitation and subsequent relaxation of $I^-(CH_3CN)_n$ clusters can lead to formation of acetonitrile cluster anions, which are characterized by the binding of the excess electron in a dipole-bound orbital outside of acetonitrile molecules, as shown for the prototype acetonitrile dimer anion. At the same time, in solution or relatively large clusters, two acetonitrile molecules can dimerize, forming a weak covalent carbon-carbon bond and allowing for delocalization and binding of the excess electron in their valence orbitals.

Acknowledgments

I wish to thank Dr. Gilles H. Peslherbe for the time I have spent in his research group, for his help, guidance and friendly support.

I also would like to thank my committee members, Dr. Heidi M. Muchall and Dr. Peter H. Bird. As well, I wish to thank our research group members, past and present. In particular, I would like to acknowledge fruitful collaboration with Tao-Nhân Nguyen and Denise Koch over the years, and stimulating discussions with Grygoriy Dolgonos, Robert Mawhinney and Paul Loncke.

I wish to acknowledge the financial support from Concordia University. Calculations were performed at the computational facilities of Centre for Research in Molecular Modeling (CERMM), Réseau québécois de calcul de haute performance (RQCHP) and the Western Canada Research Grid (WestGrid).

Finally, I would like to thank my wife Elena for her constant support, understanding and love.

Elenağa, mineñ iñ yaratqan keşemä

Table of Contents

List of figures

List of tables

Glossary

AE	All-electron
AIL	Atomic interaction line
AIM	Atoms in molecules
B3LYP	Becke's three-parameter hybrid exchange/Lee-Yang-Parr correlation functional
BCP	Bond critical point
BSSE	Basis set superposition error
CAS	Complete active space
CASPT2	Second-order multireference perturabtion theory
CASSCF	Complete active space self-consistent field
CBS	Complete basis set
CCSD(T)	Coupled clusters with single, double and perturbative triple excitations
CCSD-EOM	Coupled cluster (with single and double excitations) equation-of-motion
CIS	Configuration interaction with single excitations
CP	Counterpoise or critical point
CPCM	Conductor-like polarizable continuum model
CPP	Core polarization potential
CT	Charge transfer
CTTS	Charge transfer to solvent
DB	Dipole-bound
DBCC	Dipole-bound charge concentration
DFT	Density functional theory
ECP	Effective core potential
EPR	Electron paramagnetic resonance
ESP	Electrostatic potential
GGA	Generalized gradient approximation
HB	Hydrogen bonding
HF	Hartree-Fock
IAS	Interatomic surface
IP	Ionization potential
IR	Infrared
LIF	laser-induced fluorescence
MP2	Second-order Møller-Plesset theory

MRCI	Multi-reference configuration interaction
MRCI+Q	Multi-reference configuration interaction with the multireference Davidson correction
NBO	Natural Bond orbital
NNA	Non-nuclear attractor
NPA	Natural Population Analysis
PBEO	1-parameter hybrid exchange/correaltion functional by Perdew, Burke and Ernzerhof
PES	Potential energy surface
PP	Pseudopotential
RCP	Ring critical point
ROHF	Restricted open-shell Hartree-Fock
SET	Solvated electron technology
SO	Spin-orbit
SVP	Split valence polarized
TD-DFT	Time-dependent density-functional theory
UCCSD(T)	Spin-unrestricted open-shell coupled cluster method with single and double excitations and perturbative triples correction
UDFT	Unrestricted density-functional theory
UHF	Unrestricted Hartree-Fock
UMP2	Unrestricted second-order Møller-Plesset theory
VB	Valence-bound
VDE	Vertical detachment energy
VSCC	Valence shell charge concentration
VSXC	Exchange-correlation functional by van Voorhis and Scuseria
ZPE	Zero-point vibrational energy

Contributions of authors

Chapter II: "Theoretical investigation of charge transfer to solvent in photoexcited iodide acetonitrile clusters"

K. K. Timergazine: research work and manuscript preparation

G. H. Peslherbe: project supervisor

Chapter III: "Halide anions in a 'methyl pocket': Competition between hydrogen bonding and ion-dipole interactions in acetonitrile-halide complexes"

K. K. Timergazine: research work and manuscript preparation

T. N. Nguyen: early research work, NPA and ESP population analyses

G. H. Peslherbe: project supervisor

Chapter IV: "Electrostatic interactions and spin-orbit coupling in iodine atom complexes: accurate ab initio potential for the $Na^+\cdots I^\cdot$ complex"

K. K. Timergazine: research work and manuscript preparation

D. M. Koch: model potential development and manuscript preparation

G. H. Peslherbe: project supervisor

Chapter V: "Photoexcitation and charge-transfer-to-solvent relaxation dynamics of the $I^-(CH_3CN)$ complex"

K. K. Timergazine: research work and manuscript preparation

G. H. Peslherbe: project supervisor

Chapter VI: "Further insight into the relaxation dynamics of photoexcited $I^-(H_2O)_n$ clusters"

K. K. Timergazine: research work and manuscript preparation

G. H. Peslherbe: project supervisor

Chapter VII: "A theoretical study of the dipole-bound and valence-bound acetonitrile anions"

K. K. Timergazine: research work and manuscript preparation

G. H. Peslherbe: project supervisor

Chapter I

General Introduction

I.1. Preamble

Recent advances in experimental techniques and computational methods now permit high-accuracy investigations of an intermediate form of matter – clusters. Gas-phase clusters are defined as agglomerates of two or more ions, atoms or molecules, bound to each other by interatomic/intermolecular forces. The properties of clustered monomers can be considered to lie in between those of the gas and condensed phases. Therefore, cluster studies provide a unique opportunity to study many fundamental chemical and physical processes such as solvation, chemical, photochemical, and biochemical reactions, and may provide very useful insight into the properties of molecules in the condensed phase.

Recently, state-of-the-art experimental studies have uncovered extremely interesting photochemical properties of small clusters formed by the iodide anion and a few polar solvent molecules. The charge-transfer-to-solvent (CTTS) excited states formed upon photoexcitation of these clusters are known to lead to the formation of dipole-bound solvent cluster anions closely related to the solvated electron, which is implicated in many important chemical and biochemical processes, including radiation damage to living cells. Hence, investigation of the properties and time-evolution of ground and excited state anionic clusters, including iodide-solvent clusters as well as pure solvent cluster anions may shed light on to many important chemical, biochemical and physical problems. In this Thesis, methods of computational and theoretical chemistry are applied to address some of the structural, photochemical and dynamical properties of small anionic clusters.

I.2. The solvated electron in the bulk

The history of the solvated electron goes back to the mid-nineteenth century, when the unusual coloration of alkali metal solutions in liquid ammonia was first observed.[1] In the beginning of the twentieth century, the solvated electron was identified as a reason for the color and high electrical conductivity of these solutions.[2] Later, with the advent of studies of chemical processes caused by high-energy radiation, it was recognized that the solvated electron is a ubiquitous transient species in irradiated aqueous systems.[3] The solvated electron was also found to play a key role in the radiation damage of living cells.[4]

An electron trapped in a solvent is characterized by some general features, like a wide and structureless absorption band in the visible and infrared (IR) spectra, and a narrow singlet line in the electron paramagnetic resonance (EPR) spectra.[3] Depending on the solvent, the solvated electron can be very stable (*e.g.* in ammonia and some ethers) or just transient species (*e.g.* in water and alcohols). The solvated electron is the most reducing agent known to chemists – it is used to synthesize some metal ions in exotic oxidation states, carbanions, and other organic species.[3,5] Recently, it was even proposed to use solvated-electron solutions for the destruction of hazardous chemical wastes and chemical weapons (the so-called solvated electron technology – SET).[6]

The first attempts of a theoretical treatment of the solvated electron made use of very simple continuum models where the solvated electron was placed in a spherical cavity surrounded by a polarizable continuous dielectric, such as the model developed by Jortner.[7] In these models, the electron was envisioned to be trapped by the polarization of the solvent, which is promoted by the excess electron itself (self-trapping). Later, these models were enhanced by representing the first solvation shell by a set of dipoles, resulting in semi-continuum models.[8,9] Despite some limited success in reproducing

experimental results (using a number of fitted parameters), continuum and semi-continuum theories failed to explain many experimentally observed features of the solvated electron, such as the shape of the absorption line in the electronic spectrum.

Attempts to treat the solvent molecules explicitly were made in the 1970s using quantum-chemical calculations with semi-empirical methods and very simplistic cluster models.[10] Since realistic quantum-chemical calculations are not feasible for bulk systems with solvated electrons, mixed quantum-classical molecular dynamics simulations of the solvated electron in the liquid phase became very popular during the last two decades. In work by the groups of Rossky,[11,12] Borgis,[13,14] Berne,[15-17] Barnett,[18,19] and others, the solvent (usually water) molecules were represented by some classical model and the excess electron either by a description in terms of a wavefunction (with the water-electron interactions represented by some model potential), or by a Feynman path integral representation.[16] Using these sophisticated approaches, many experimental results (absorption line shape and its temperature and pressure dependence) were rationalized and qualitatively reproduced. However, a complete understanding of the nature of the free electron interaction with polar solvent molecules, which is essential to provide a reliable theoretical description of the solvated electron, may require thorough investigation of an electron bound to one or a few solvent molecules in gas-phase clusters.

I.3. The dipole-bound and solvated electron in clusters

The idea that an electron can be trapped in the field of a fixed dipole consisting of two point charges was first explored by Fermi and Teller in 1947.[20] They showed that, if the dipole moment is larger than a critical value of 1.62 D, the trapped electron can have an infinite number of bound states. Further theoretical investigations showed that, for actual polar molecules in the gas phase, the critical value of the dipole moment necessary

to bind an excess electron in the dipole-bound state (DBS) should be around 2.5 D.[21-23] Only in 1974 was the first experimental observation of a dipole-bound anion reported by Compton and co-workers, who obtained a weakly bound acetonitrile anion CH_3CN^- by charge-exchange collisions of acetonitrile with excited Rydberg atoms.[24] On the other hand, attempts to prepare CH_3CN^- by direct electron attachment to acetonitrile molecules failed, confirming the dipole-bound character of the acetonitrile anion with a very diffuse, Rydberg-type excess electron distribution.

A very important breakthrough was made by Haberland and co-workers in 1984, when negatively charged water clusters $(H_2O)^-_n$ were synthesized by direct attachment of slow electrons to neutral $(H_2O)_n$ clusters.[25] Since then, water cluster anions have been the subject of intense research from the experimental as well as theoretical sides, since these species are very important for the understanding of the bulk hydrated electron and electron-water interactions in general.[26] The occurrence of "magic numbers" at n= 2, 6, 7 and 11 for $(H_2O)_n$ clusters[27] initiated a long-standing debate about the origin and structure of the corresponding clusters.[26] There is currently, an ever increasing interest in the structure, electron binding and dynamics of water cluster anions,[28-37] and in December 2004, *Science* magazine named the developments in the field of water chemistry and physics, which include studies of "water clusters to determine how electrons and protons dissolve in water" among the "Breakthroughs of the Year".[38]

The first quantum-chemical calculations of dipole-bound anions were performed by Jordan and co-workers in the late 1970s on such species as $LiCl^-$, the CH_3CN^- molecular anions and the $(HF)_2^-$ cluster anion, with Hartree-Fock theory.[39,40] This work showed that *ab initio* calculations can readily reproduce the binding of an electron to a molecular dipole. It should be noted that the extremely diffuse nature of dipole-bound anions dictates the use of specially constructed, very diffuse basis sets in addition to the regular valence basis sets used to describe the valence-shell electrons.[41] In recent

publications by Gutowski *et al.*,[42-47] different contributions to the binding energy of the excess electron to neutral polar host molecules were examined in great detail, and the dispersion interaction between the excess electron and the host molecule was found to account for up to 50% of the total interaction energy. Thus, the dipole binding of an electron to a molecule appears to be much more complex and subtle than considered earlier on the basis of simple electrostatic models. Furthermore, since the dispersion interaction plays such an important role for dipole-bound anions, quantum-chemical calculations of these systems must include proper electron correlation effects.[26]

Recent quantum-chemical investigations uncovered another interesting feature of negatively charged cluster anions, as some of them were predicted to bind an electron in two ways: on the surface of the cluster, as for classical dipole-bound anions, and inside the cluster, giving rise to so-called "solvated electron" cluster anions.[44,45,48] In the latter, the excess electron is trapped in between two or more molecular dipoles, making these clusters direct cluster precursors of the bulk solvated electron. The combined experimental and theoretical work of Bowen, Gutowski and co-workers[48] on $(HF)_3^-$ clusters unequivocally proved the co-existence of the dipole-bound and asymmetric "solvated electron" isomers under experimental conditions. It thus appears that an electron captured by a cluster of polar molecules is a key model to understand the bulk solvated electron and concomitant phenomena like charge transfer to solvent.

I.4. Charge-transfer-to-solvent (CTTS) phenomena in the bulk

The strong, wide and structureless absorption bands in the ultraviolet (UV) spectra of many anions, especially halides, dissolved in water and other polar solvents

has fascinated chemists for a long time.[49] Indeed, the photochemical behavior of the same ions in the gas phase is completely different – normally, there are no bound excited states observed in these conditions and absorption of light only leads to photodetachment of the excess electron. For example, in the gas phase, all the excited states of the iodide anion I^- lie above its ionization potential (IP). In water and acetonitrile solutions, on the other hand, wide absorption bands with λ_{max}= 230 nm and 250 nm, respectively are observed. Early studies demonstrated a strong dependence of λ_{max} on the nature of the solvent. This solvent dependence, together with the observation of two absorption bands with a λ_{max} difference corresponding to the value of the $^2P_{3/2}$–$^2P_{1/2}$ spin-orbit splitting of the *free* iodine atom, led to the conclusion that, upon photoexcitation, an electron is being ejected from the iodide anion and becoming trapped by the solvent.[49] Therefore, this absorption phenomenon was said to involve a charge-transfer-to-solvent (CTTS) transition. Jortner and co-workers experimentally proved that the photoexcitation of dissolved halide salts in water indeed leads to hydrated electron production.[50]

Since the CTTS excited states and the solvated electron seem to share common features, the first theoretical investigations of CTTS problems exploited solvated electron models existing at the moment. For example, the model by Platzman and Frank[49,51] used the polarizable continuum model of Jortner,[7] augmented by a thermodynamic scheme akin to the Born cycle to calculate CTTS excitation energies. These early models evidently inherited the drawbacks of the continuum solvated-electron theories.[52]

Quantum-classical molecular dynamics simulations of the photoexcitation and excited-state dynamics of halides in water were relatively successful in reproducing some experimental observations,[53-55], including recent femtosecond spectroscopy results.[56-58] In 1994, Combariza, Kestner and Jortner reported one of the first detailed *ab initio* investigations of the structure and thermodynamics of small halide-water clusters

$X^-(H_2O)_n$, n=1–6.[59] Furthermore, possible bound excited states of the clusters were investigated, but the predicted excitation energies were found to be so high that these excited states were essentially thought to be unlikely. Thus, it was concluded that "bound electronic excitation in clusters, which constitutes the precursor of the CTTS transition in bulk water, sets in at n > 6".[59] At that time, a lack of thorough understanding of the nature of the expected CTTS precursor states in clusters, and consequently, an inappropriate choice of methods (configuration interaction with single excitations (CIS) with a small basis set and no extra diffuse functions) prevented a theoretical prediction of CTTS states in clusters. The first evidence for cluster analogs of bulk CTTS states was to be provided by experimental studies.

I.5. CTTS precursor states of iodide-solvent clusters

I.5.a.Iodide-acetonitrile and iodide-acetone clusters

The first experimental characterization of CTTS precursor states in small clusters of an anion and polar solvent molecules were reported by Johnson and co-workers in 1995 for the iodide-acetone complex,[60] and for the iodide-acetonitrile complex.[61] This was achieved by a combination of photoelectron and "action" spectroscopies. The photoelectron spectra of these species demonstrated the shift of the vertical detachment energies (VDE, or in other words, the ionization potential – IP) from that of bare gas-phase iodide, a well-known feature of anion-solvent clusters.[59,62,63] But in addition to the detection of photoejected electrons by means of photoelectron spectroscopy, the yield of possible neutral and anionic fragments due to photodetachment or photoexcitation were monitored (separately) as a function of photon energy – *i.e.* both photoneutral and anionic photofragment "action" spectroscopies were used to obtain absorption

spectra.[60,64] Both photoneutral and anionic action spectra of the same complex possess rather well-resolved maxima, which coincide with each other, and strikingly, always lie slightly *below* (≤0.01 eV) the VDE of the complex. Hence, in contrast to bare iodide, iodide complexes with polar molecules absorb light with energy *less* than that necessary to completely eject the excess electron, suggesting the existence of excited states below the ionization limit for these complexes.

Another very important observation by Johnson and co-workers lies in the fact that the mass spectra of the anionic photofragments formed after excitation of the iodide-acetonitrile and iodide-acetone complexes show the corresponding dipole-bound anions, CH_3CN^- and $(CH_3)_2CO^-$, as the only charged products. All these observations led to the conclusion that photoexcitation of the iodide-polar molecule complex with photon energy just below the VDE leads to the formation of dipole-bound excited states, which relax with the formation of the corresponding dipole-bound anion and ejection of the neutral iodine atom,[60,61,64]

$$I^-(S) \rightarrow [I^-(S)]^* \rightarrow I^\cdot + S^-$$

Hence, the excited states observed for photoexcited $I^-(CH_3CN)$ and $I^-((CH_3)_2CO)$ complexes can be attributed to cluster precursors of bulk CTTS states, a general feature that can be expected of anions clustered with one or more polar solvent molecules. This experimental discovery of CTTS precursor states prompts further computational studies, following the initial failure to predict the existence of these states.

Interestingly, in the case of ternary $I^-(CH_3CN)_2$ cluster,[61] both photoelectron and absorption spectra suggested the existence of two isomers for $I^-(CH_3CN)_2$. The structures that were postulated for these two isomers have acetonitrile molecules either on both sides of the iodide anion (symmetric solvation) or aligned on the same side of the ion (asymmetric solvation):[61,65]

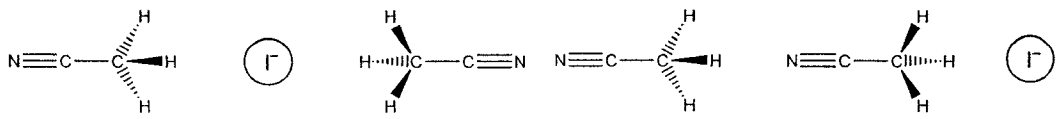

symmetric solvation asymmetric solvation

Upon excited-state relaxation, the symmetrically solvated cluster is unlikely to yield a negatively charged acetonitrile dimer, so the other linear structure was assumed to be responsible for the formation of the $(CH_3CN)_2^-$ anion observed in experiments, which is also expected to be linear.[61] The excess electron could be stripped off the anionic dimer, supposedly forming a linear, high-energy, neutral acetonitrile dimer that had not been observed before.[61,66] In previous experimental work,[67] the only $(CH_3CN)_2$ isomer that could be isolated had the acetonitrile molecules antiparallel to each other. Thus it appears that asymmetric solvation in $I^-(CH_3CN)_2$ could be exploited to generate new neutral cluster species.[66]

I.5.b.Iodide-water clusters

Although the experimental observation of CTTS precursor states in iodide-acetone and iodide-acetonitrile clusters was a major breakthrough, it is the subsequent work by the same group on iodide-water clusters that really caught the attention of the scientific community. The bound CTTS precursor excited states were reported for clusters with two, three and four water molecules.[68] Moreover, a very neat progression of the excitation energy and absorption coefficient towards the bulk limit was observed as a function of cluster size.

Neumark and co-workers[34,69,70] later applied state-of-the-art femtosecond photoelectron spectroscopy techniques to study the relaxation dynamics of photoexcited $I^-(H_2O)_n$ and $I^-(D_2O)_n$ clusters (n= 3–28) (*cf.* Figure 1). This work revealed interesting, even puzzling, dynamical characteristics of the excited electron, whose binding energy

was found to increase gradually for some time after photoexcitation, suggesting that the cluster undergoes some kind of reorganization which leads to the stabilization of the excited electron.

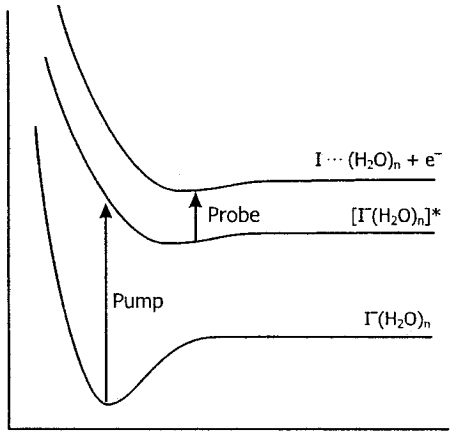

Figure 1. Schematic representation of the femtosecond photoelectron spectroscopy experiments by Neumark and co-workers.[69] The pump laser pulse excites the iodide-water cluster $I^-(H_2O)_n$, and the probe pulse monitors the evolution of the excited state $[I^-(H_2O)_n]^*$ via ejection of the loosely bound excited electron and measuring the electron kinetic energy

In order to rationalize these observations, Neumark and co-workers put forward the hypothesis[69,71] that the rise in the electron binding energy is due to the reorganization of the network of water molecules to gain a configuration that can support the excess electron much more efficiently than in the initial cluster configuration. This model is based solely on the consideration of solvent dynamics, neglecting the possible role of the neutral iodine atom formed upon photoexcitation, and is hereafter referred to as the solvent-driven relaxation model. This model also accounts for the pronounced isotope effects observed, *i.e.* a slower relaxation in the case of $I^-(D_2O)_n$ clusters compared to that for $I^-(H_2O)_n$.

Chen and Sheu proposed an alternative interpretation of the femtosecond experimental observations, based on quantum-chemical calculations, in which the

stabilization of the excited electron is rationalized by the ejection of the neutral iodine atom from the water cluster.[72,73] Quantum-chemical calculations show that the presence of the neutral iodine atom can considerably destabilize the excited electron in excited $I^-(H_2O)_n$ clusters, and thus, as the iodine atom departs from the water cluster, the electron binding energy must increase significantly. According to this iodine-driven relaxation model, iodine would depart from the water cluster in the excited state relatively slowly, giving rise to the experimentally observed rise of the excited electron vertical binding energy. The main problem with the latter model is that it is based on static quantum-chemical calculations, which have the water cluster moiety frozen in the geometry of the cluster before photoexcitation, and it thus neglects solvent motion and cannot account for the observed isotope effect. At this stage, the majority of the models proposed so far to interpret femtosecond experimental results do not treat the relaxation of iodide-water clusters as a whole, neglecting either the role of the iodine atom or that of solvent reorganization.

Thus, it appears that modeling of the relaxation dynamics of photoexcited iodide-water clusters is a considerable challenge for modern computational chemistry. However, there is another type of halide-solvent clusters whose CTTS relaxation may lead to even more complex and fascinating dynamics, with two very different excited/excess electron binding regimes, as discussed in the next section.

I.6. Solvent clusters which can support a valence-bound electron: multi-channel CTTS relaxation dynamics

So far, we have only discussed solvent molecules or clusters which can support an excess electron exclusively by trapping in the field of the solvent dipole moment (*e.g.*

acetonitrile or water). However, a number of molecules can bind an excess electron, not only in the field of their dipole, but also in valence orbitals. Nitromethane (CH_3NO_2) was one of the first molecules found to bind an excess electron in these two ways: its dipole moment is large enough (μ = 3.46 D) to support a dipole-bound electron, and it can also accommodate the excess electron in the π^* orbital of the NO_2 group, giving rise to a valence-bound anion. Adamowicz[74] was the first one to point out the possibility of the existence of a dipole-bound anionic state (DBS) for nitromethane, and Compton *et al.* [75] experimentally showed that it could be prepared by charge exchange between Rydberg atoms and CH_3NO_2. On the other hand, conventional electron capture techniques only produce the valence-bound anionic state (VBS), which is more stable. The valence and dipole electron affinities of nitromethane were found to be 0.26±0.08 eV and 12±3 meV, respectively. An extensive computational study by Gutsev and Bartlett[76] showed that the geometry of the DBS species does not differ significantly from that of the neutral parent, whereas the VBS equilibrium geometry is characterized by a pyramidal nitrogen atom. Therefore, when studying the conversion between the dipole- and valence bound states, the most important geometrical coordinate is the tilt angle of the NO_2 group θ:

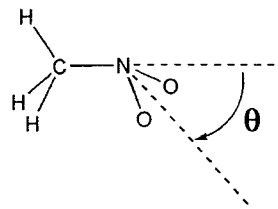

Desfrançois *et al.* showed that the solvation of the dipole-bound form of $CH_3NO_2^-$ by a few argon atoms greatly facilitates the transition into the more stable valence-bound state.[77]

These interesting features of the nitromethane anion lead to a very complicated behavior for photoexcited halide-nitromethane clusters. Johnson and co-workers[78] studied the photoexcitation of $X^-(CH_3NO_2)$ complexes [X=Cl, Br, and I] and found that

the relaxation of the excited clusters results in production of not only $CH_3NO_2^-$ anions, as was expected by analogy with $I^-(CH_3CN)$ cluster studies, but also in products of nucleophilic substitution

$$X^{\bullet} + CH_3NO_2^- \leftarrow [X^-(CH_3NO_2)]^* \rightarrow NO_2^- + CH_3X$$

Quite surprisingly, it was also found that regeneration of the initial species, *i.e.* X^- and CH_3NO_2, also takes place, in contrast to iodide-acetonitrile cluster relaxation, which only produces the CH_3CN^- anion.[61] In the case of the chloride-nitromethane complex the situation is even more complicated: in addition to the products of nucleophilic substitution, the ClO^- and NCO^- ions were also observed in the mass spectrum.

To explain the formation of the halide X^- and $NO_2^{\bullet -}$ ions upon photoexcitation of $X^-(CH_3NO_2)$, Johnson and co-workers proposed that the system hops from the DBS to the classic Evans-Polanyi excited state surface of the S_N2 reaction (*cf.* Figure 2), which connects to the ground state at the conical intersection in the region of the ground-state transition structure. When reaching the top of the ground-state barrier, the system can relax in both directions, leading to either X^- or $NO_2^{\bullet -}$ ions and the corresponding neutral products. The complex interplay between the ground-state, dipole-bound and valence-bound CTTS excited states the $X^-(CH_3NO_2)$ cluster, may thus lead to extremely interesting and complicated relaxation dynamics for these systems. The possibility of photochemical initiation of the endothermic S_N2 reaction $X^-(CH_3NO_2) \rightarrow NO_2^- + CH_3X$ also appears to be of great interest from the point of view of the general theory of S_N2 reactions.[79]

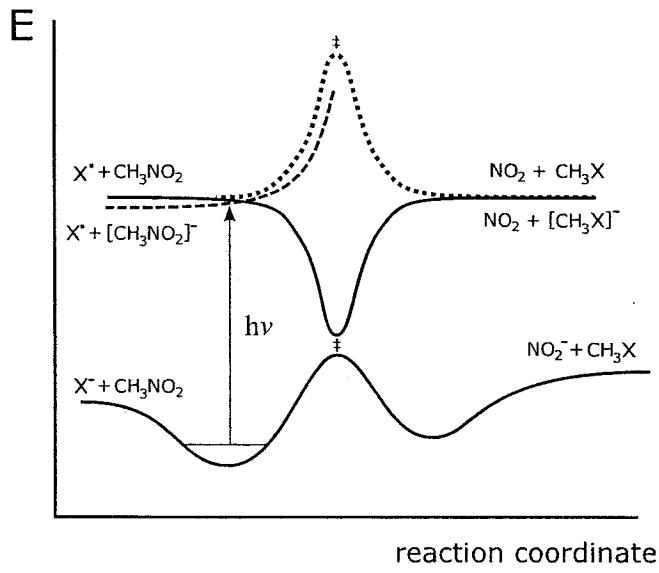

Figure 2. Schematic representation of the gas-phase S_N2 reaction $X^- + CH_3NO_2 \rightarrow NO_2^- + CH_3X$ (bottom curve) and the corresponding neutral reaction (top dotted curve). The dipole-bound state is shown as a dashed line, and the transitions states indicated as ‡ (Ref. 78)

Thus, when a solvent molecule not only is able to bind an electron in a dipole-bound fashion, but also can accommodate the electron in one of its empty valence orbitals, the interplay of dipole-bound and valence-bound states makes the CTTS relaxation dynamics enormously complicated. Relaxation process can proceed via more than one possible channel, since the system can jump from one excited state to another during the relaxation process. The dynamics of CTTS relaxation in these cases, where actual chemical transformation of the molecules is possible, is probably one of the most fascinating aspects of the photochemistry of iodide-polar molecule clusters. However, modeling of these processes is hindered by serious technical problems, due to the complex nature of the dipole- and valence-bound states.[80] We hope that the present work, which mostly deals with simpler, purely dipole-bound CTTS excited states, will provide a solid basis for computational investigations of multi-channel CTTS relaxation dynamics.

I.7. Objectives and outline

The short review given so far shows that various properties of anionic solvent clusters (*e.g.* halide-solvent clusters or solvent cluster anions) are closely related to important problems of contemporary Chemistry, Physics and Biology. Hence, experimental and theoretical studies of these systems are of tremendous importance for understanding the most fundamental characteristics of molecular aggregates, their structure and reactivity.

The objectives of this Thesis are to develop and apply methods of modern computational/theoretical chemistry to investigate the structure, photochemistry and dynamics of small anionic clusters. This work focuses on the CTTS photoexcitation and the excited-state relaxation of halide-solvent clusters and related issues, including the structure and potential energy surface (PES) of the ground and excited-state clusters, the products of relaxation of the CTTS excited states, and other problems which are essential to the understanding of the photochemistry of anionic clusters. Our goal is to rationalize experimental results reported in the literature up to date and to attempt to resolve a number of existing controversies. We expect that our computational work will lead to further experimental studies, providing increased insight into the nature of the processes of interest, and additional data to validate computational methods for quantitative predictions.

To accomplish this goal, a wide variety of computational methods is employed, including single- and multi-reference quantum-chemistry approaches with inclusion of electron correlation and spin-orbit effects at various levels, as well as ground- and excited-state first-principles molecular dynamics simulations. Special attention is devoted not only to the numerical results of the computations, but also to the general

physical picture of the factors determining the static and dynamical properties of the systems of interest.

The outline of this manuscript-based Thesis is as follows. Background information concerning the solvated electron and the charge-transfer-to-solvent excited states in the bulk and in clusters has been reviewed in Chapter I. In Chapter II a preliminary quantum-chemical study of the charge-transfer-to-solvent photoexcitation of the binary iodide-acetonitrile complex is descibed in order to reveal the most basic features of the photoexcitation process in iodide-acetonitrile clusters. Although the investigation reported in Chapter II provided important insight into the most basic properties of the CTTS states of iodide-acetonitrile clusters, it clearly suggests that, in order to obtain a truly quantitative description of the CTTS photoexcitation, one needs to apply more advanced techniques that correctly treat the excited electron as well as spin-orbit coupling effects.

An accurate treatment of ground-state geometries and binding energies is essential in order to be able to correctly model the photoexcitation of halide-solvent clusters. However, the current knowledge of the ground-state structure of halide-acetonitrile complexes and the exact nature of the intermolecular interactions in these clusters is limited. Hence, the main objective of Chapter III is to perform a detailed study of the ground-state $X^-(CH_3CN)$ complexes. Extensive testing of the various model chemistries and an in-depth investigation of the complex potential energy surfaces and the nature of bonding revealed a very subtle interplay between the ion-dipole interactions and hydrogen bonding in halide-acetonitrile clusters, and similar systems where a halide ion interacts with a methyl group of a solvent molecule. However, extensive knowledge of ground state halide-solvent clusters is not the only prerequisite to the deep understanding of the CTTS excited states of these clusters.

Photoionization and photoexcitation of halide-solvent clusters lead to formation of open-shell complexes involving a neutral iodine atom, which presents a number of challenges because of the (quasi)degeneracy of the ground electronic state and strong spin-orbit interactions. Therefore, the objective of Chapter IV is to perform a detailed study of complexes formed with iodine, focusing on the relatively simple $Na^+\cdots I^\bullet$ paradigm complex. The nature of the interaction of iodine with charged species is investigated, as well as the role of spin-orbit effects, which was studied with both *ab inito* and semi-empirical approaches to spin-orbit interactions.

In Chapter V, a detailed investigation of the photoexcitation and CTTS excited-state relaxation dynamics of the binary iodide-acetonitrile complex is carried out, with the help of important insight obtained from studies presented in the preceding chapters. The nature of photoexcitation and the various ingredients of the CTTS excitation energy are discussed, along with the role of spin-orbit coupling effects, to provide a truly quantitative description of the photoexcited iodide-acetonitrile complex. The potential energy curves for the excited and ionized electronic states are also utilized to obtain further insight into the nature of these states. The information on the potential energy curves is used to develop an efficient approach for first-principles excited-state molecular dynamics simulations of the CTTS relaxation dynamics. Using this approach, realistic *ab inito* molecular dynamics simulations of the CTTS excited-state relaxation for a small iodide-solvent cluster have been performed for the first time, and the time-evolution of the excited electron vertical binding energy discussed in connection with available experimental data for the relaxation dynamics of more complex iodide-water clusters.

The relaxation mechanism of the CTTS excited state of binary iodide-acetonitrile clusters is probably one of the simplest cases of CTTS relaxation dynamics. As was discussed above (*cf.* p. 10), significantly more complex excited-state dynamics of iodide-

water clusters became a matter of debate in the scientific literature. Thus, Chapter VI presents the results of a preliminary investigation of charge-transfer-to-solvent excited-state dynamics of model $I^-(H_2O)_3$ clusters. This preliminary study provides important insight into the puzzling dynamics of the CTTS excited states of iodide-solvent clusters.

The relaxation of photoexcited iodide-acetonitrile complexes is known to produce acetonitrile cluster anions. However, their structure, stability and electronic structure are not very well known. Thus, the objective of Chapter VII is to perform an investigation of the various ways acetonitrile molecules can interact with an excess electron. Recent experimental studies suggested that relatively small acetonitrile clusters can not only support an excess electron in a dipole-bound fashion, but they can also accept the electron it into their valence orbitals, just like in the case of the nitromethane molecule (*cf.* Section I.6). Hence, both dipole-bound and valence bound acetonitrile dimer anions are investigated, with particular attention to their peculiar electronic structure and the topology of the electron density distribution.

The general conclusions of this Thesis are presented in Chapter VIII.

Chapter II

Theoretical investigation of charge transfer to solvent in photoexcited iodide-acetonitrile clusters

Published as:

Qadir K. Timerghazin and Gilles H. Peslherbe, Chemical Physics Letters 354, 31-37 (2002)

II.1. Introduction

The role of solvation in the photochemical behavior of chemical species has been a long-standing issue, and charge transfer to solvent (CTTS) is undoubtedly one of the most pronounced cases of the solvent role in photochemistry.[49] Whereas many anions such as halides do not possess electronically bound excited states in the gas phase and undergo simple electron detachment when exposed to light of sufficient wavelength, they exhibit a strong and broad absorption band in a number of polar solvents. These absorption bands were assigned to transitions to bound excited states, hereafter called CTTS states, presumably supported by a concerted action of solvent molecules.[49] A number of theories, treating the solvent as a dielectric continuum which traps and stabilizes an excited electron, have been developed to model the CTTS phenomenon.[51,81] In the last few years, CTTS states were investigated by femtosecond spectroscopy[82,83] and modeled with quantum molecular dynamics.[54,84]

Recent advances in experimental investigative techniques of chemical reactions in molecular clusters – an intermediate state between the gas and condensed phases,[85] made it possible to investigate CTTS in clusters. Dipole-bound excited states resulting from photoexcitation of clusters containing an iodide ion and a few molecules of acetone,[60] acetonitrile,[61] water,[68,69] nitromethane and methyl iodide[64] have been recently observed experimentally and are thought to be precursors of the solution CTTS states. Bound excited states were also observed for iodide in clusters of highly polarizable xenon atoms $I^-(Xe)_n$ ($n \geq 4$).[86,87] In the case of water clusters, two or more solvent molecules seem to be needed to stabilize the excited state, while acetone and acetonitrile complexes with iodide of 1:1 composition already demonstrate well-developed excited-state precursors of the bulk CTTS states. This suggests that the excited states of the anionic clusters are more stable with increasing solvent polarity. It was also shown that the

larger the number of solvent molecules in the cluster, the larger the blue shift of the absorption maxima towards the bulk values.[61,68,86] Finally, it was observed that further evolution of photoexcited complexes of acetone, acetonitrile and water leads to dissociation into an iodine atom and a negatively charged solvent cluster $(S)_n^-$, where S = CH_3CN, $(CH_3)_2CO$ or H_2O[60,61,69]

$$I^-(S)_n \rightarrow [I^-(S)_n]^* \rightarrow I\bullet + (S)_n^-$$

On the theoretical side, CTTS precursor states have only been investigated for iodide-water clusters.[72,88-90] It was shown that quantum-chemical calculations such as configuration interaction with single excitations (CIS) and time-dependent density-functional theory (TD-DFT) qualitatively reproduce experimentally observed trends for the dependence of the CTTS excitation energy on cluster size.[88,90] Chen and Sheu studied the photoexcitation of $I^-(H_2O)_n$ and the resulting electron distribution in CTTS precursor states with the simple initial-guess method,[89] and reported results in good agreement with experiment. Recently, the same approach was used for investigating the relaxation of iodide-water clusters following photoexcitation.[72]

More detailed studies are needed to provide a thorough description of photoexcitation processes in ionic clusters. Of particular interest is the nature of the electronic transition to the CTTS state, i.e. the charge flow between ground and excited states. Furthermore, studies of photoexcitation processes in iodide clusters with molecules of varying polarity and polarizability should bring some more insight into CTTS phenomena. In this Letter, we present a preliminary investigation of the excited states of the $I^-(CH_3CN)$ complex, and contrast our results to those for $I^-(H_2O)_3$ clusters, while we defer a more systematic and detailed investigation of $I^-(CH_3CN)_n$ clusters to a later publication. Vertical excitation energies are calculated with several quantum-chemical methods and successfully compared to experimental data. The charge flow

between the ground and excited states is then analyzed in order to shed some light into the nature of the electronic transitions in these clusters.

II.2. Computational procedure

Cluster equilibrium geometries were optimized with second-order Møller-Plesset (MP2) theory[91] and vertical excitation energies were calculated by configuration interaction with single excitations (CIS),[92] time-dependent density-functional theory (TD-DFT)[93] with the B3LYP hybrid functional,[94] and the coupled cluster (with single and double excitations) equation-of-motion approach (CCSD-EOM).[95] For first row atoms, we used a standard 6-311++G(df,p) basis set.[91] For iodine, we employed an all-electron (AE) 6-311G basis[96] or a Stuttgart-Dresden-Bonn quasi-relativistic ECP46MWB effective core potential (ECP),[97] with valence basis sets augmented by diffuse *s* and *p* as well as polarization *d* and *f* functions.[98] Geometry optimizations were performed with the ECP basis set, while vertical excitation energies were calculated with both the all-electron and ECP basis sets. Atomic charges were calculated by Löwdin population analysis and the atoms-in-molecules (AIM) approach.[99] Calculations were performed with the Gaussian 98,[100] GAMESS[101] and MOLPRO[102] quantum chemistry packages.

II.3. Results and discussion

The structure of iodide–acetonitrile complexes was previously investigated with the MP2/6-311+G* model chemistry.[103] These calculations predict the $I^-(CH_3CN)$ complex (shown in Figure 3) to have C_{3v} cylindrical symmetry, with the ion residing on the methyl side along the acetonitrile principal symmetry axis, at a distance of 3.70 Å from the methyl carbon. The binding energy of this complex was found to be 10.5

kcal/mol with CCSD(T)/6-311+G(2df,pd)//MP2/6-311+G* (including approximate zero-point-energy and basis-set-superposition-error corrections), in good agreement with the experimental value of 11.10 ± 0.40 kcal/mol.[63] The complex was re-optimized with the larger basis set described in the previous section for consistency, but no change of consequence was observed in the geometry of the complex. The complex is stabilized mostly due to electrostatic interactions of the negatively charged iodide with the highly dipolar acetonitrile molecule, but some charge transfer is observed, as can be seen from the results of the ground state population analyses in Table 1.

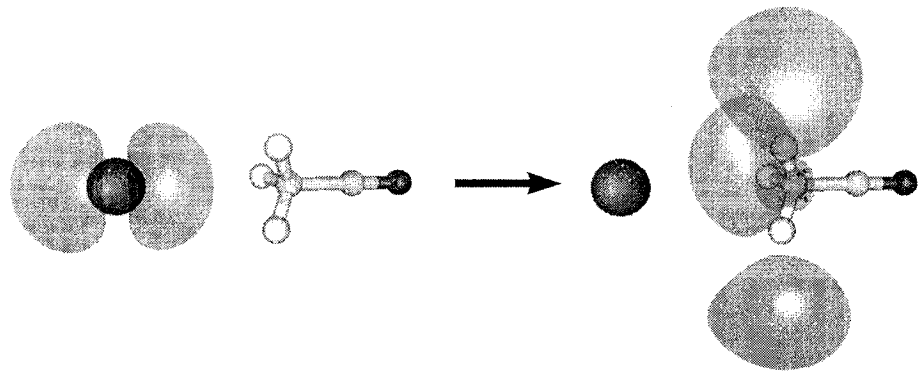

Figure 3. Electron density difference between the $I^-(CH_3CN)$ ground and excited states for the $1^1A_1 \rightarrow 2^1A_1$ transition calculated with CIS/6-311++(df,p). The negative density difference isosurface is plotted on the left side, while the positive difference isosurface is plotted on the right side

The results of excited state calculations for the $I^-(CH_3CN)$ complex are collected in Table 1. All the methods employed (CIS, TD-DFT, CCSD-EOM) consistently suggest that the experimentally observed absorption of the $I^-(CH_3CN)$ complex corresponds to transitions to the first three singlet excited states, one doubly degenerate 1^1E state and one 2^1A_1 state. Inspection of Table 1 shows that TD-DFT reproduces the experimental vertical excitation energies reported by Johnson et al[61] within 0.2 eV, whereas CIS and CCSD-EOM overestimate the excitation energies by about 1.4 and 0.8 eV, respectively. Including higher-order excitations in the coupled cluster equation-of-motion approach

may improve the calculated excitation energies, but one should note that a proper treatment of spin-orbit coupling might be needed for truly quantitative results. The energy difference between the ^1E and $^1A_1$ states is only 0.06 eV with TD-DFT, and other methods give even smaller differences. Calculations with all-electron basis sets tend to give higher excitation energies than with effective core potential bases. Finally, oscillator strengths calculated with a given method are very similar for both the $1^1A_1 \rightarrow 1^1E$ and $1^1A_1 \rightarrow 2^1A_1$ transitions, but CIS predicts values about 5 times larger than TD-DFT.

Table 1. Ground and excited state properties of the iodide-acetonitrile complex[a]

State		CIS		TD-DFT		CCSD-EOM		Expt.[d]
		AE[b]	ECP[c]	AE[b]	ECP[c]	AE[b]	ECP[c]	
1^1A_1	$q(I)_{Löwdin}$	-0.88	-0.89					
	$q(I)_{AIM}$	-0.97		-0.95				
1^1E	E	4.92	4.77	3.39	3.33	4.33	4.18	3.53
	f	0.091	0.100	0.021	0.023			
	$q(I)_{Löwdin}$	-0.04	-0.04					
	$q(I)_{AIM}$	-0.31						
2^1A_1	E	4.94	4.80	3.44	3.39	4.34	4.19	
	f	0.101	0.099	0.040	0.041			
	$q(I)_{Löwdin}$	-0.07	-0.08					
	$q(I)_{AIM}$	-0.33						

[a] q(I) is the iodine atomic charge, E is the vertical excitation energy (in eV), and *f* is the oscillator strength.
[b] All-electron 6-311++G(df,p) basis set for all atoms
[c] Stuttgart-Dresden-Bonn ECP basis set for iodine, 6-311++G(df,p) basis set for all other atoms
[d] Taken from Ref. 61

To gain insight into the nature of the electronic transitions upon photoexcitation of the $I^-(CH_3CN)$ complex, we calculated the CIS electron density difference between the ground and excited states. The density difference diagrams show areas of the molecule from where some negative charge is removed upon excitation (negative difference) and

where it is promoted (positive difference). It is seen from Figure 3 that the $1^1A_1 \rightarrow 2^1A_1$ transition involves electron promotion from the iodide valence p_z orbital to diffuse orbitals mostly located on the methyl group of acetonitrile. The $1^1A_1 \rightarrow 1^1E$ transitions (not shown here) are similarly associated with electron density moving out of the iodide valence p_x and p_y orbitals orthogonal to the complex symmetry axis. We note from Table 1 that the excitation energy for these transitions is lower than for the $1^1A_1 \rightarrow 2^1A_1$ transition. This may be attributed to the fact that, in the ground state cluster, electrons in the p_z orbital are stabilized by interactions with the solvent dipole – which is aligned with the p_z orbital – to a greater extent than those in the p_x and p_y orbitals. This picture of electrons being promoted from the iodide valence p orbitals to diffuse orbitals of the acetonitrile methyl group is representative of charge transfer to solvent, and is further supported by the charge analysis of the excited complex. The Löwdin charge on iodine drops to zero in the excited complex, indicating full transfer of the iodide negative charge to the solvent. The AIM charge analysis also supports that picture of electron transfer to the solvent, but to a lesser extent, as the difference in the iodine charge between the ground and excited state is only about 0.7 e.

For comparison with previous work on iodide-water clusters,[72,88-90] we calculated the excited states of the C_3-symmetry $I^-(H_2O)_3$ cluster shown in Figure 4. The total solvent dipole in this $I^-(H_2O)_3$ cluster is aligned along the complex symmetry axis and has a magnitude of 3.8 D very similar to that of acetonitrile (3.9 D). As for the $I^-(CH_3CN)$ complex, the results of our calculations, collected in Table 2, suggest that the first three lowest singlet excited states of the cluster –1^1E and 2^1A_1 – are possible candidates for the experimentally observed CTTS precursor states. Our calculations of vertical excitation energies for $I^-(H_2O)_3$ are in good agreement with previous TD-DFT, CIS and initial-guess calculations.[88,89] Again, TD-DFT appears to perform well, reproducing the experimental excitation energy within 0.3 eV, while CIS and CCSD-EOM overestimate the excitation

energy by 1.3 and 0.6 eV, respectively. All the methods employed consistently show a larger spacing between the 1^1E and 2^1A_1 states for $I^-(H_2O)_3$ than for $I^-(CH_3CN)$. Both TD-DFT and CIS predict larger oscillator strengths for photoexcitation of the iodide–water cluster.

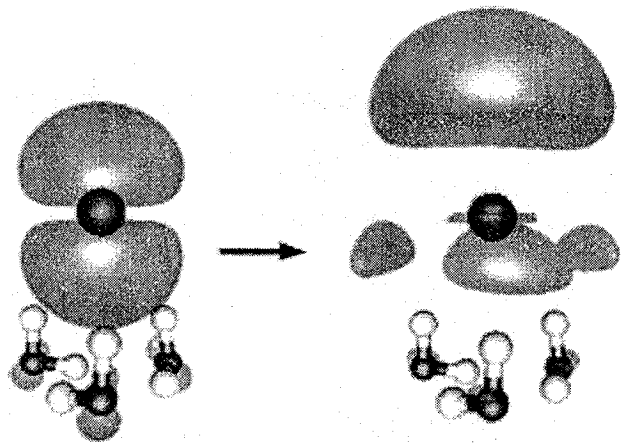

Figure 4. Electron density difference between the $I^-(H_2O)_3$ ground and excited states for the $1^1A_1 \rightarrow 2^1A_1$ transition calculated with CIS/6-311++(df,p). The negative density difference isosurface is plotted on the left side, while the positive difference isosurface is plotted on the right side.

Analysis of the electron density difference between the ground and excited states of the $I^-(H_2O)_3$ cluster, shown in Figure 4, indicate that the transition to the 1^1E state involves electron excitation out of the degenerate iodide valence p_x and p_y orbitals, while the transition to the 2^1A_1 state involves electron excitation out of the iodide valence p_z orbital (pointing towards the solvent cluster), very much like for the $I^-(CH_3CN)$ complex. However, the photoexcited electron seems to reside in the area above the iodine atom and not towards the solvent cluster, unlike for the $I^-(CH_3CN)$ complex. We note that initial-guess calculations by Chen and Sheu predict essentially the same distribution of the excited electron density for $I^-(H_2O)_3$ (*cf.* Figure 3 in [89]). Population analyses in Table 1 and Table 2 also indicate a higher negative charge on the iodine atom for the excited $I^-(H_2O)_3$ cluster than for the $I^-(CH_3CN)$ complex, and thus apparently much less electron

transfer to solvent in the case of water. Thus, for iodide–water cluster, a picture emerges, which seems to contrast with that for acetonitrile, and in contradiction with charge transfer to solvent upon photoexcitation.

Table 2. Ground and excited state properties of the complex of iodide with three water molecules.[a]

State		CIS		TD-DFT		CCSD-EOM	UMP2[d]	TD-DFT[e]	CIS[e]	Expt[f]
		AE[b]	ECP[c]	AE[b]	ECP[c]	ECP[c]				
1^1A_1	$q(I)_{Löwdin}$	-0.74	-0.73							
	$q(I)_{AIM}$	-0.90		-0.85						
1^1E	E	5.57	5.49	4.49	4.41	4.83	4.18	4.29	5.49	4.25
	f	0.125	0.160	0.072	0.078					
	$q(I)_{Löwdin}$	-0.25	-0.16							
	$q(I)_{AIM}$	-0.67								
2^1A_1	E	5.67	5.58	4.61	4.55	4.87				
	f	0.179	0.204	0.155	0.159					
	$q(I)_{Löwdin}$	-0.29	-0.21							

[a] q(I) is the iodine atomic charge, E is the vertical excitation energy (in eV), and *f* is the oscillator strength.
[b] All-electron 6-311++G(df,p) basis set for all atoms
[c] Stuttgart-Dresden-Bonn ECP basis set for iodine, 6-311++G(df,p) basis set for all other atoms
[d] Initial-guess UMP2 results from [89]
[e] CIS and TD-DFT results from [88]
[f] Taken from Ref. 68

This apparent contradiction can be explained if we compare the electronic structure of the corresponding solvent anions to that of the excited iodide clusters, taking into account the fact that the iodine core tends to repel the excited electron due to exchange repulsion, as recently discussed by Chen and Sheu.[89] In the dipole-bound acetonitrile anion, the excess electron is mostly located "outside" the molecule, on the methyl group, as shown in Figure 5. In many dipole-bound anions, the negative charge tends to settle on the electrophilic sites of the host molecule, which usually involve so-

called "dangling" hydrogen atoms.[104] A similar situation is observed for the $(H_2O)_3^-$ anion, where the excess electron is located above the plane of three hydrogen atoms, as shown in Figure 5. We now consider the changes that would take place upon insertion of a neutral iodine atom into these anions to form the excited iodide-solvent clusters. Repulsion with the iodine core shifts the excited electron into areas where it is still stabilized by the solvent dipole, but does not interact much with the occupied orbitals of the iodine atom. In the case of the acetonitrile complex, it is clear from Figure 3 that the excited electron is located further towards the methyl group than it is in the bare acetonitrile anion because of repulsions from the iodine core. The stabilization of the excited electron by the acetonitrile dipole may be slightly less than that of the electron in the acetonitrile anion, but interactions with the electrophilic "dangling" hydrogen atoms and the local C-H bond dipoles may compensate for this loss of stabilization. As for the water cluster, the distance between the hydrogen atoms pointing at iodine and the iodine atom is smaller than that in the $I^-(CH_3CN)$ complex (2.82 vs. 3.54 Å), and the excited electron tends to shift to the area above the iodine atom, where it is stabilized by the solvent dipole, as seen from Figure 4. Even if there is some electron density located near the hydrogen atoms, the excited electron density is located above the iodine atom for the most part. However, even in this case where the excited electron does not seem to "transfer" to the solvent, the excited state is essentially stabilized by the solvent. As was recently shown by Chen and Sheu,[72] upon relaxation, the excited cluster ejects the neutral iodine atom, the excited electron passes around the iodine core and shifts to the water cluster, forming the $(H_2O)_n^-$ anion. Depending on cluster size, the nascent negatively charged solvent cluster may either vibrationally autodetach or rearrange in order to stabilize the excess electron.[69] In contrast, the relaxation of the excited $I^-(CH_3CN)$ complex is presumably a much simpler process, involving very little change in the excited electron density and simply ejection of the iodine atom from the cluster. This

may explain the high yields of CH_3CN^- anions observed experimentally upon photoexcitation of the iodide-acetonitrile complex.[61]

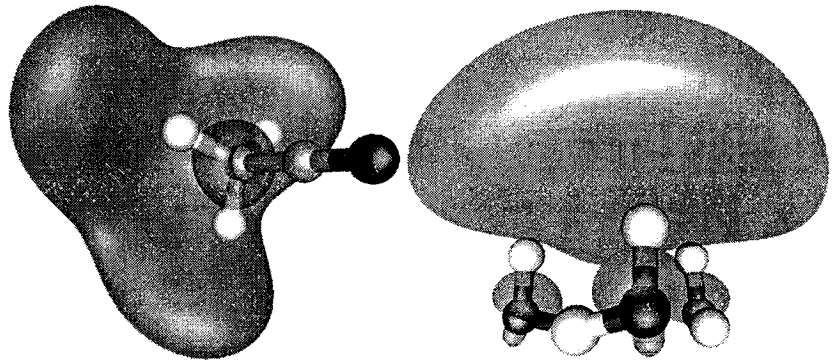

Figure 5. Electron density in the highest occupied molecular orbitals of the CH_3CN^- and $(H_2O)_3^-$ anions calculated with the MP2/6-311++G(df,p) model chemistry. The molecular geometries of acetonitrile and the water cluster are taken unrelaxed, from the iodide-solvent cluster structure.

II.4. Concluding remarks

Charge-transfer-to-solvent (CTTS) precursor states of the iodide-acetonitrile complex have been investigated by means of quantum-chemical calculations and compared with those of iodide-water clusters. The calculated vertical excitation energies are found to be in good agreement with experimental results, and TD-DFT seems to perform particularly well for these systems. A detailed analysis of the electron density difference between the ground and excited states indicate that, upon photoexcitation, an electron is promoted from one of the iodide valence *p* orbitals to the acetonitrile molecule. In the case of iodide-water cluster photoexcitation, transfer of the electron to the solvent network is not as obvious and the excited electron appears mostly located on top of the iodine atom, even though it is stabilized by a concerted action of the solvent. Analysis of the electron density in the corresponding solvent anions shows that the

apparent difference in the electronic structure of the excited $I^-(CH_3CN)$ and $I^-(H_2O)_3$ clusters can be rationalized in terms of the repulsion between the excited electron and the neutral iodine core, as well as the availability of solvent electrophilic sites which help stabilize the excess negative charge.

Chapter III

Halide anions in a "methyl pocket": competition between hydrogen bonding and ion-dipole interactions in acetonitrile-halide complexes

Submitted as:

Qadir K. Timerghazin, Tao-Nhân V. Nguyen, and Gilles H. Peslherbe, *Journal of the American Chemical Society*, 2006

III.1. Introduction

Among various types of intermolecular interactions, hydrogen bonding (HB) is undoubtedly of paramount importance in both chemistry and biology. It has been the subject of intense research for almost a century[105] and still remains one of the hottest topics of research.[106-109,110] In recent years, studies of HBs formed by so-called non-conventional hydrogen bond donors and acceptors[111] have attracted a lot of attention. In fact, until very recently, HBs formed with C–H bond as a donor of hydrogen were considered as rather uncommon and a fairly unimportant type of hydrogen bonding, and their very existence was even considered as highly improbable by many researchers.[112] However, nowadays, the C–H···X hydrogen bonds are widely accepted as an abundant and important inter- and intramolecular interaction in structural chemistry and biology,[108,110,113-117] and the last few years have seen an increased interest in these hydrogen bonds in the context of studies of improper, blue-shifting hydrogen bonds.[118-120] Although these unusual hydrogen bonds, which exhibit shortening of the donor Y–H bond and concomitant blue shifting of the corresponding vibrational frequency, were observed for a number of HB donors (e.g. N–H, Si–H, and P–H),[120,121] the majority of the blue-shifting hydrogen bonds known to date involve C–H donors.[118,120] Unfortunately, despite the significant research effort in this field,[118,121-125] there is still no generally accepted theory which can thoroughly explain the origin of the blue-shifting hydrogen bonding phenomenon.

Even though halide ions (X^-) are known to be the strongest HB acceptors,[108,] their interaction with polar mono-substituted methanes are often considered the result of a simple ion-dipole attraction, which leads to linear structures (usually of C_{3v} symmetry) of the resulting $YCH_3\cdots X^-$ complexes, where the halide moiety resides in the middle of a "methyl pocket".[61,64-66,126-129] Hobza and co-workers[118,130] investigated

computationally several complexes of monohalosubstituted methanes with halide anions and proposed that their linear C_{3v} structures are due to "trifurcated blue-shifting" hydrogen bonds formed by the halide with all three hydrogen atoms of the CH_3 group. On the other hand, structures with lower symmetry, where the halide ion is coordinated to just one of the hydrogen atoms of the methyl group, thus forming a regular, red-shifting hydrogen bond, were found computationally[65,131-133] for some combinations of YCH_3 and X^-, or proposed on the basis of experimental data.[134]

In this article, we address the competition between the various attractive forces between halide anions and molecules of polar mono-substituted methanes by investigating of the halide-acetonitrile binary complexes. Acetonitrile (CH_3CN) is one of the most widely used non-aqueous polar solvents in chemistry. Due to its large dipole moment, the acetonitrile molecule can be involved in strong electrostatic intermolecular interactions with various ions, while the fairly high acidity of the methyl group suggests the possibility of hydrogen-bond formation with CH_3CN.[134] We report a systematic and detailed quantum-chemical investigation of the structure, stability, potential energy surface (PES), and nature of the intermolecular interactions in $X^-(CH_3CN)$ complexes (X=I, Br, Cl, and F), and show the subtle balance between the ion-dipole interaction of the anion with the YCH_3 molecule and hydrogen bonding with one of the methyl hydrogen atoms. Indeed, as we show with some examples, the existence of hydrogen-bonded isomers of $X^-(YCH_3)_n$ complexes and clusters is very often overlooked.

The outline of this article is as follows. Computational details are presented in section 2, and results about the structure, stability and PES of the $X^-(CH_3CN)$ complexes are given in section 3. The detailed analysis of the geometry, PES, and charge distribution is then presented in section 4, in order to reveal the nature of bonding in the $X^-(CH_3CN)$ complexes. The insight gained from section 4 is used in section 5 to critically discuss recent experimental and theoretical results about the interaction of halide ions

with various mono-substituted methanes. The summary and concluding remarks follow in section 6.

III.2. Computational procedure

The structures and properties of the $X^-(CH_3CN)$ clusters were calculated using the Gaussian 98[100] and MOLPRO 2002.6[102] quantum chemistry packages. To locate global minimum energy structures, the complex geometries were optimized with all coordinates relaxed, while conserving symmetry constraints. Subsequent frequency calculations were performed to characterize the nature of the stationary points and obtain harmonic vibrational frequencies and zero-point energies. To gain a better understanding of the $X^-(CH_3CN)$ complex potential energy surface we performed a number of relaxed potential energy scans along the C-C_M-X (α tilt angle of the halide from the acetonitrile symmetry axis (*cf.* Figure 6).

Throughout this work, two triple-zeta (TZ) quality and one quadruple-zeta (QZ) quality Gaussian basis sets were used. The smallest basis set, referred as TZ1, was based on the 6-311++G(df,p) basis set by Pople and co-workers.[91] In the case of iodine, this basis set was combined with the iodine ECP46MWB quasi-relativistic effective core potential (ECP) and the corresponding valence basis set by Bergner *et al.*,[97] augmented with additional polarization and diffuse functions (exponents α_s=0.0405, α_d=0.276, α_f=0.434).[98] More extended basis sets, referred to as TZ2 and QZ1, were based on Dunning's correlation-consistent triple- and quadruple-zeta basis sets augmented with diffuse functions (aug-cc-pVTZ and aug-cc-pVQZ).[135] For bromine and iodine, the ECP28MWB and ECP46MWB pseudopotentials[97] were used, in combination with the augmented correlation-consistent triple- and quadruple-zeta valence basis sets developed by Martin and Sundermann.[136] In the case of iodine, an effective core

polarization potential (CPP)[97] was also used to test the effects of core-valence correlation effects which are neglected in calculations using ECPs. Wavefunctions for Atoms-In-Molecules (AIM) analysis[99] were generated using the all-electron version of the TZ2 basis set (TZ2AE), where the aug-cc-pVTZ basis set[135] was used for bromine, and the (19s,15p,12d,4f)/[11s,9p,6d,2f] basis set by Sadlej[137] was used for iodine.

Geometry optimizations and frequency calculations were performed with second-order Møller-Plesset (MP2) perturbation theory,[91] and with Density Functional Theory (DFT), using the hybrid 3-parameter B3LYP functional by Becke *et al.*[94] A number of other hybrid and pure DFT functionals were also tested (see Supporting Information). Furthermore, single-point energy calculations were performed with the coupled clusters with single, double and perturbative triple excitations [CCSD(T)] level of theory for MP2-optimized geometries. Several geometry optimizations (with numerical gradients) were also performed at the CCSD(T)/TZ1 and CCSD(T)/TZ2 levels.

Intermolecular binding energies (D_0) were calculated with the supermolecule approach, including unscaled zero-point energy corrections. The Basis Set Superposition Error (BSSE) was estimated with the standard Counterpoise (CP) approximation.[138,139] For the chloride-acetonitrilecomplex, CP-corrected optimizations and frequency calculations were also performed, as implemented in Gaussian 98, Revision A.11.[100]

Atoms-In-Molecules (AIM) analysis was performed with the AIMPAC program package by R. W. F. Bader and co-workers[140] for MP2/TZ2AE//MP2/TZ2 wavefunctions. Atomic point charges were also calculated with MP2/TZ2, using Natural Population Analysis (NPA)[141] of the NBO 3.1 program[142] and electrostatic potential fitting (ESP charges),[143,144] as implemented in Gaussian 98.[100]

III.3. Structure and stability of $X^-(CH_3CN)$ complexes

III.3.a.Iodide-acetonitrile complex

All previously published quantum-chemical calculations [65,103,126] point toward a complex with a linear structure of C_{3v} symmetry. Indeed, MP2/TZ1 and MP2/TZ2 geometry optimizations predict a linear structure (shown in Figure 6a) as the global minimum on the potential energy surface. On the other hand, DFT calculations paint a different picture: the global minimum found in B3LYP calculations with the TZ1, TZ2 and QZ1 basis sets is a bent structure of C_s symmetry, as shown in Figure 6b, and the C_{3v} linear structure corresponds to a second order saddle point (with imaginary frequencies in the range $8i$-$15i$ cm^{-1}).

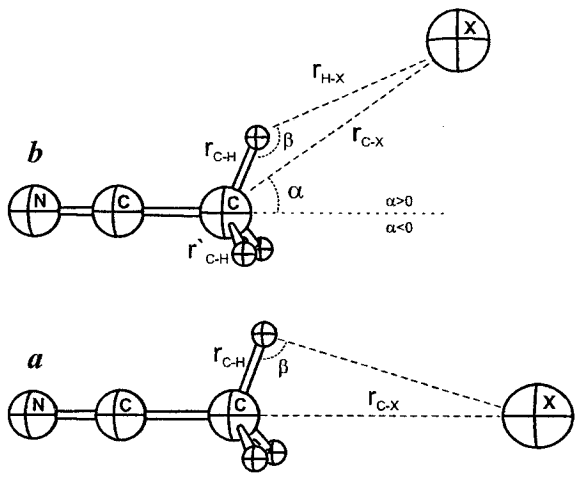

Figure 6. Generic linear (a) and bent (b) structures of halide-acetonitrile complexes, and geometrical parameters used in Table 5

To gain a better understanding of the iodide-acetonitrile PES, relaxed potential energy scans along the tilt angle α between iodide and the acetonitrile molecule symmetry axis are shown in Figure 7a. During the scan, the iodide moiety was kept in a given C–C–H plane, and α=0° corresponds to the linear structure (*cf.* Figure 6). The potential

energy profiles (Figure 7a) appear to be relatively flat in the -10° to 50° range, with an energy change not exceeding 0.2 kcal/mol. The MP2 and B3LYP potential energy profiles are similar, but the B3LYP interaction energies are lower by ca. 1.8 kcal/mol, compared to MP2 values computed with the same basis set. However, the B3LYP energy profiles display a minimum at $\alpha \approx 40°$, while MP2 profiles have the minimum at α=0°, and the plateau at α=30° – 40°, rather than a minimum.

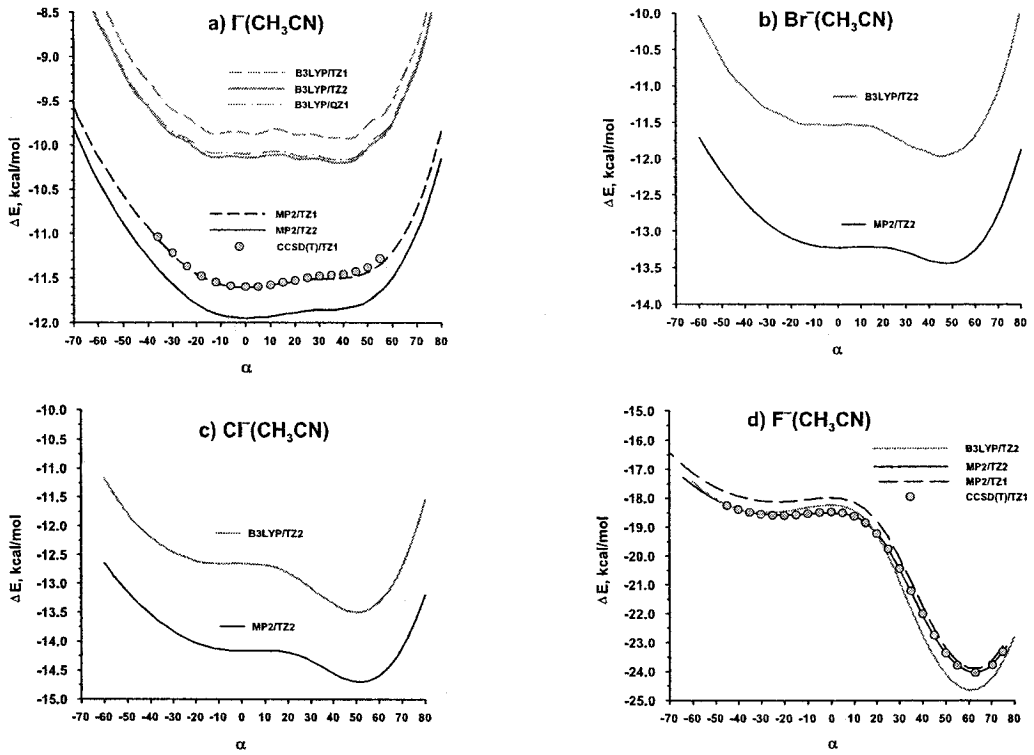

Figure 7. Potential energy profiles for the $X^-(CH_3CN)$ complexes in respect to the tilting along the angle α (Figure 6b), calculated at various levels of theory. Energies are given in kcal/mol relative to free acetonitrile and the halide

To address the discrepancy between the MP2 and DFT results, a CCSD(T)/TZ1 PES scan (Figure 7a) was performed. It matches very closely the MP2 profile with the same basis set, reproducing both the minimum at α=0° and the plateau at $\alpha \approx 40°$. Therefore, the global minimum appears to correspond to the linear structure, but due to the floppiness of the PES, the iodide anion may be almost uniformly distributed inside

the "pocket" of the methyl group (α=-10° – 50°) at non-zero temperatures, with only a slight preference for the linear structure.

In addition to B3LYP, we also performed PES scans with some other pure and hybrid DFT functionals and the Hartree-Fock (HF) method scans along the angle α, using the TZ2 basis set (*cf.* Figure 13 in Section III.7. Supporting information). The majority of the functionals provide a description, similar to B3LYP, but tend to give even more pronounced preference for the bent structure over the linear one (up to ca. 0.7 kcal/mol). On the other hand, HF calculations suggest the linear structure as the global minimum and do not reproduce the plateau at α=30° – 40°. Since hybrid DFT functionals (including B3LYP) contain a fraction of the HF exchange, most of them provide a more balanced description of the plateau region, compared to pure functionals. It is also interesting to note the spectacular failure of the new-generation meta-generalized gradient approximation (meta-GGA) exchange-correlation functional by van Voorhis and Scuseria[145] (VSXC): the PES calculated with this functional is "spiked" at α=0°, and the energy increases very rapidly as the iodide shifts from the acetonitrile symmetry axis. Thus, the iodide-acetonitrile complex appears to be an interesting system to benchmark various computational methods for description of the potential energy surfaces of intermolecular complexes.

We now turn our attention to the binding energies of the iodide-acetonitrile complex, presented in Table 5. The agreement between CCSD(T) and MP2 binding energies calculated with the same basis set is remarkable: the BSSE-corrected values differ by less than 0.2 kcal/mol, and CCSD(T) and CCSD(T)//MP2 binding energies are virtually the same. The BSSE-corrected D_0 obtained with the TZ2 basis set is in a very good agreement with the binding enthalpy averaged over seven available experimental values (11.4±0.9 kcal/mol),[146] and the agreement with the value reported by Hiraoka *et*

al.[65] (11.0±0.2 kcal/mol) is especially good. Calculations employing the TZ1 basis set tend to give lower binding energies (by ca. 1 kcal/mol). The error arising from the neglect of iodine core electron polarization under the effective core potential (ECP) approximation can be estimated using the core polarization potential (CPP)[97] approach, which corrects ECPs core-valence polarization effects.[147] Comparison of the CCSD(T)/TZ2 results with and without CPP shows that core-valence polarization effects tend to slightly stabilize the complex (by ca. 0.1 kcal/mol), but these effects appear to be marginal and can be neglected for the purposes of this work. Binding energies calculated with B3LYP/TZ1 are close to the CCSD(T)/TZ1 and MP2/TZ1 values. However, the B3LYP/TZ2 D_0 values are lower by ca. 1 kcal/mol than those predicted by MP2 or CCSD(T) and the experimental binding enthalpy. Further increase of the basis set does not really improve the binding energies calculated with B3LYP, as the B3LYP/TZ2 and B3LYP/QZ1 binding energies do not differ by more than 0.2 kcal/mol.

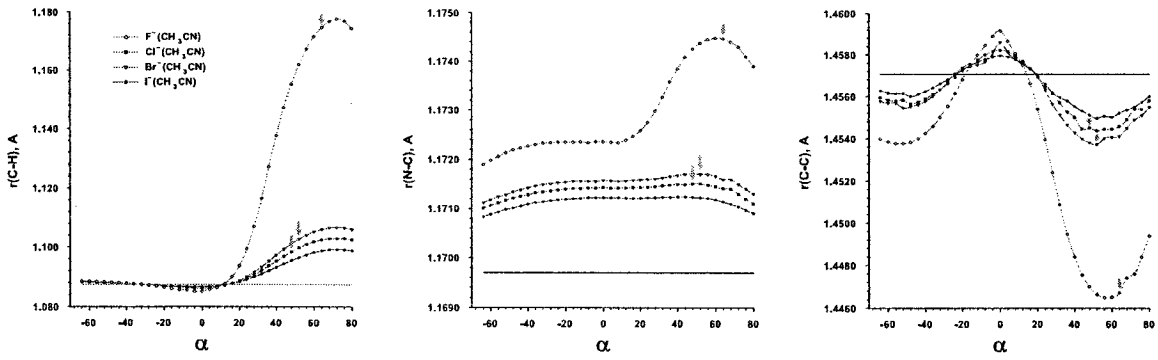

Figure 8. Evolution of the C–H, C–C, C–N bond lengths in respect to the tilting along the angle α (Figure 1b), calculated at the MP2/TZ2 level of theory.

The results of MP2 and CCSD(T) calculations with the TZ2 basis set point a very similar qualitative picture of the iodide-acetonitrile complex potential energy surface, and agree quantitatively with experimental data. Therefore, we adopted the CCSD(T)/TZ2//MP2/TZ2 scheme for further calculations of the complexes of

acetonitrile with halide ions. Results of the B3LYP calculations will be also reported for comparison.

Finally, we discuss the changes in the geometry and IR spectra of the acetonitrile molecule upon complexation with iodide. According to MP2/TZ2 calculations, the C–H bonds undergo a very small contraction by ca. 0.0007 Å, the C–C bond lengthens by about the same amount, and the largest geometry change happens to the remote part of the acetonitrile molecule: the C–N bond lengthens by 0.0016 Å (*cf.* Table 5, Figure 8). Accordingly, the harmonic vibrational frequencies (*cf.* Table 6) of the C–H stretches exhibit small blue shifts (by 9–17 cm^{-1}), and the C–C and C–N bond stretches undergo red shifts of ca. 15 cm^{-1}. The evolution of the bond lengths in the acetonitrile molecule upon tilting of the iodide off the CH_3CN symmetry axis is shown in Figure 8. When the I^- moiety moves towards one of the hydrogen atoms, the corresponding C–H bond starts elongating, becomes longer than in the free acetonitrile molecule at $\alpha > 10°$, and reaches a maximum of ca. 1.0991 Å (which is 0.0118 Å longer than in the monomer) for α=70°–75°. As for the C–C bond, its length drops down and reaches the minimum at 55°–65°, where it is contracted by 0.0020 Å with respect to the free CH_3CN molecule. The C–N distance does not depend much on the angle α, it is always longer than in free acetonitrile molecule by ca. 0.0015–0.0016 Å.

III.3.b.Bromide-acetonitrile and chloride-acetonitrile complexes

Unlike the iodide-acetonitrile complex, two minima exist on the MP2/TZ2 potential energy surfaces for the complexes of bromide and chloride with acetonitrile: a linear structure as in the case of iodide-acetonitrile, and a bent structure. The potential energy profiles with respect to tilting angle α in Figure 7b and Figure 7c suggest bent

structures as well pronounced global minima, whereas the PES around the linear-structures minima is rather flat. With MP2/TZ2 both linear and bent structures of bromide-acetonitrile and chloride-acetonitrile complexes exist as minima, while the linear structures are second-order saddle points with imaginary frequencies in the range of 10*i*–20*i* cm^{-1}, as was the case for iodide-acetonitrile complex, according to B3LYP/TZ2.

For the iodide-acetonitrile complex a plateau was observed at $\alpha \approx 40°$, which corresponds to a C–H···I (β) angle of ca. 140°; for the bent isomers of the bromide and chloride complexes the halide moves further away from the acetonitrile C_3 symmetry axis (α=47° and 52° respectively) and tends to align more with the C–H bond (β angle of 152° and 157°, respectively).

The binding energy differences between the bent and linear isomers of the bromide-acetonitrile and chloride-acetonitrile are very small (less than 0.5 kcal/mol). The inclusion of ZPE and BSSE corrections makes the structures practically isoenergetic, and sometimes even change the prediction of the most stable structure. At non-zero temperatures, the halide resides in a shallow well, from $\alpha \approx -30°$ to $\alpha \approx 70°$, with a slight preference for the bent configuration. Indeed, the calculated binding energies for the linear and bent structures are well within the range of experimental values (13 ± 1 and 14 ± 3 kcal/mol) based on averages of 7 and 12 experimental values for bromide-acetonitrile and chloride-acetonitrile complexes, respectively.[146] As was the case for the iodide-acetonitrile complex, the calculated binding energies are in excellent agreement with the experimental binding enthalpies reported by Hiraoka *et al.*[65] On the other hand, the recent experimental values by McMahon and co-workers[134] are 1–2 kcal/mol higher. B3LYP calculations seem to underestimate the binding energies by ca. 1.0–1.5 kcal/mol, as was the case for the iodide-acetonitrile complex.

It has been repeatedly shown[148-154] that the single-point correction for basis set superposition errors (BSSE) is often not sufficient to calculate correct intermolecular binding energies. The BSSE can significantly deform complex potential energy surfaces, leading to distorted complex geometries and, therefore, incorrect binding energies, in which case BSSE-corrected geometry optimizations and frequency calculations may be needed.[151,152] To test the effect of BSSE on the optimized geometries and final binding energies, we performed counterpoise (CP) corrected optimizations[100] of the linear and bent isomers of the chloride-acetonitrile complex. The resulting $D_{o/BSSE}$ values agree within 0.1 kcal/mol with the values obtained by CP-uncorrected optimizations. Not surprisingly, the distance between the chloride and the acetonitrile molecule slightly increases (by ca. 0.03 Å, Table 5) for both isomers. Overall, the distortion of the complex PES due to BSSE does not seem to be significant and the data obtained with non-BSSE-corrected optimizations appear to be fairly reliable.

Complexation with bromide and chloride distorts the acetonitrile molecule in the same way as for the iodide-acetonitrile complex, but the magnitude of the effect is slightly larger as the ion is smaller (*cf.* Figure 8). The linear structures are characterized by contraction of the C–H bonds by 0.0010 – 0.0012 Å and lengthening of the C–C bonds by ca. 0.0010 Å. For the bent structures, the situation is opposite: the C–H bonds, which interact with the halide ion, are significantly longer (by 0.010 – 0.015 Å) than in the free acetonitrile molecule, and the C–C bonds are slightly shorter (by ca. 0.0030 Å). The C–N bond length does not vary much with halide position, and it is always elongated by 0.017-0.0020 Å (*cf.* Figure 8). Like for the iodide-acetonitrile complex, a small *blue* shift (of ca. 20 cm^{-1}) is observed for C–H stretch of the linear isomers of the bromide-acetonitrile and chloride-acetonitrile complexes (*cf.* Table 6). The bent structures, on the other hand, demonstrate a substantial *red* shift of the C–H stretches (by 100-150 cm^{-1}). The shifts in BSSE-corrected vibrational frequencies are 5–20% smaller in magnitude,

and the distortion of the acetonitrile molecule upon complexation with the halide is smaller according to CP-corrected complex geometries.

III.3.c.Fluoride-acetonitrile complex

The fluoride-acetonitrile complex, unlike the complexes of chloride and bromide, appears to have only one minimum energy structure at all levels of theory employed – the bent structure. According to both MP2 and B3LYP harmonic frequency calculations the linear structure of C_{3v} symmetry is a second-order saddle point with imaginary frequencies around $50i$ cm^{-1}. These results are in very good agreement with those of recent calculations by Gonzales *et al.*,[131] performed with CCSD(T) and a number of DFT methods together with extended basis sets, and of early HF/3-21+G calculations by Hiraoka *et al.*[65] The potential energy profile with respect to tilt angle α (Figure 7d) shows that the bent structure corresponds to a fairly deep minimum (ca. 5 kcal/mol relative to the linear structure) at $\alpha \approx 65°$. Thus, in the series of "bent" complexes, the fluoride-acetonitrile cluster displays the largest deviation of the halide ion from the acetonitrile molecule C_3 symmetry axis, and the β (C–H···F) angle is very close to linear – ca. 172°. We also found an additional first-order saddle point (with imaginary frequency of $160i$ cm^{-1}) at $\alpha \approx -21°$, which apparently, corresponds to a transition structure between two equivalent bent energy minima, with the fluoride coordinated to either of two adjacent hydrogen atoms. No such structures were observed for other halide-acetonitrile complexes.

Two rather different experimental values have been reported in the literature for the binding enthalpy of the fluoride-acetonitrile complex: 24.5 ± 2.0 kcal/mol according to Hiraoka *et al.*[65] and 16.0 ± 2.0 kcal/mol according to Yamdagni and Kebarle.[155] Our calculations of the binding energy (*cf.* Table 5) are in very good agreement with the

former value, and with the CCSD(T)/aug-cc-pVTZ value of Gonzales *et al.* (25.1 kcal/mol).[131]

Not surprisingly, the distortion of the acetonitrile molecule upon complexation with fluoride is much more significant than with other halides. The most pronounced change is observed for the length of the C–H bond adjacent to the fluoride, which is extended by 0.3830 Å, according to MP2/TZ2 calculations. At the same time, the C–C bond is contracted by 0.0106 Å and the C–N bond lengthened by 0.0048 Å. These geometry changes are accompanied by changes in the IR spectra: a very large red shift (of ca. 1200 cm^{-1}) is observed for one of the C–H stretching vibrations (*cf.* Table 6). For the other vibrations, the frequency shifts are smaller (10–50 cm^{-1}), except for the CCN bending vibration, which undergoes a red frequency shift of ca. 85 cm^{-1}. As fluoride moves towards the acetonitrile C_3 symmetry axis, the adjacent C–H bond contracts and becomes shorter than in the free acetonitrile molecule for the linear structure, and the effect for the C–C bond is opposite (*cf.* Figure 8). The dependence of the C–N bond length on the angle α for fluoride-acetonitrile complex is somewhat different from that for other halide-acetonitrile complexes: a distinct maximum is observed around α=60°, which is very close to the optimal complex geometry, and when the fluoride moves towards the acetonitrile C_3 symmetry axis, the C–N bond length drops by ca. 0.0020 Å. For the other $X^-(CH_3CN)$ complexes the C–N bond length was not found to depend much on the halide position, and the maxima around α=50° are hardly noticeable.

III.4. Nature of bonding in acetonitrile-halide complexes

III.4.a.Geometry, vibrational frequencies and PES shape

For all $X^-(CH_3CN)$ complexes investigated in this work, the bent structures are found to be global minima, with the exception of iodide-acetonitrile complex. Geometrical features of the bent structures, *i.e.* the elongation of the acetonitrile C–H bond, suggest the existence of a conventional, red-shifting hydrogen bond between the halide and a hydrogen atom of the methyl group. The C–H bond elongation and red shift actually increase with increasing proton affinity (PA) of the halide (*cf.* Table 7). The C–H···X^- angle also shifts across the $Br^- \rightarrow F^-$ series towards 180°, which is the most favorable angle for the hydrogen bond (Table 5).[106,109] The calculated X^-···H distances for the bent isomers of the chloride and bromide complexes (~2.30 Å and ~2.50 Å) are close to these experimentally observed for the C–H···X^- hydrogen bonds in organic crystals (~2.40–2.65 Å and ~2.60–2.75 Å respectively).[108] It is not surprising that hydrogen bonds in gas phase complexes are systematically shorter, since there is no "damping" influence of the medium in that case.

The geometry of the linear structures, where the halide ion is aligned with the dipole moment of the CH_3CN moiety suggests that ion-dipole interaction is primarily responsible for the stabilization of these isomers. Note, that in this context we are referring to the interaction of halide ion with the dipole moment (static and induced) of acetonitrile molecule as *a whole*. Of course, the hydrogen bonding also includes the electrostatic and polarization components but it is more local (and more complex) in nature. Both ion-dipole and hydrogen bonding interactions have pronounced angular dependence. The ion-dipole interaction strength is proportional to the cosine of the angle between the dipole moment vector and the vector connecting the ion with the

dipole center of mass,[156] and therefore it will be maximal at α=0°. On the other hand, the hydrogen bond strength is at a maximum when the donor C–H bond and the halide are aligned (β=180°).[106,108,109] The competition between these two types of intermolecular interactions determine the shape of the acetonitrile-halide complex PES: as the halide shifts off the acetonitrile molecule C_3 symmetry axis, the ion-dipole interaction weakens, but the C–H···X^- angle becomes closer to 180° and hydrogen bonding comes into play. The flatness of the PES for the iodide, bromide and chloride complexes with respect to tilt angle α (Figure 7) suggests that the ion-dipole interaction and hydrogen bonding are comparable in strength. However, as the proton affinity of the halide increases up the halide series, the contribution of hydrogen bonding to the total interaction energy increases, and the angle β shifts towards 180°. In fluoride-acetonitrile, the fluoride moiety is practically aligned with the C–H bond, and the propensity for hydrogen bonding is so strong that the linear C_{3v} structure even ceases to correspond to a local minimum, unlike for other complexes, and becomes a second-order saddle point on the PES.

The potential energy curves in Figure 7 are clearly asymmetric: for the negative values of the angle α, which correspond to the halide situated in between two hydrogen atoms of the methyl group (*cf.* Figure 6), there is a steep increase in potential energy, in oppose to the positive values of α. Apparently, hydrogen bonding with two off-plane hydrogen atoms is relatively weak, and only in the case of fluoride-acetonitrile complex a shallow minimum is observed at $\alpha\approx$-21°. This structure, which appears to result from bifurcated hydrogen bonds, is a first-order saddle point corresponding to a transition structure for the fluoride ion shuttling motion between two neighboring hydrogen atoms.

Although the analysis of the geometry and the PES of the $X^-(CH_3CN)$ complexes provides a convincing evidence of the electrostatic, ion-dipole nature of the interactions

responsible for the linear isomers, some other interpretations have been proposed. For instance, Hobsa and Havlas[118] reported similar linear C_{3v} structures for a number of complexes of halide ions with mono-halomethanes CH_3X, since the calculated harmonic vibrational frequencies demonstrated blue shifts for the C–H stretching vibrations, and as in the present case for linear halide-acetonitrile complexes, the interaction in these complexes was ascribed to trifurcated $X^{-}\cdots H-C$ hydrogen bonds, with improper, blue-shifting character. On the other hand, Kraychko and Zeegers-Huyskens[128] argued that in these structures the angle β (C–H···X^-) is close to 90°, at which hydrogen bonding is known to vanish.[106,109] However, sole geometrical arguments may not be sufficient to account for intermolecular bonding in $X^-(CH_3CN)$ complexes, which warrants a more detailed analysis.

III.4.b. Atoms-in-Molecules (AIM) analysis

To gain further insight into the nature of bonding in the linear and bent isomers of the acetonitrile-halide complexes, the electronic density distribution in the $X^-(CH_3CN)$ complexes was analyzed within the framework of the quantum theory of Atoms-In-Molecules (AIM).[99] This approach is based on the topological analysis of the electronic density ρ(r), its gradient vector field ∇ρ(r) and its Laplacian $\nabla^2\rho(r)$. The analysis of ∇ρ(r) reveals various critical points (CPs) in the electronic density, as well as the paths of maximum electron density connecting nuclei in the molecule – atomic interaction lines (AIL) in general and bond paths (BP) for equilibrium geometries, and zero-flux surfaces dividing a molecule into regions of electronic density ascribed to different atoms – the interatomic surfaces (IAS). Integrating various properties over the atomic volumes separated from each other by IAS can provide important information such as atomic populations, total energy, volume, multipole moments, etc. The Laplacian

$\nabla^2\rho(r)$ can help reveal more subtle features in the topology of the charge density distribution, such as regions of charge concentration and depletion, providing an avenue to distinguish between covalent and ionic bonds and to identify lone pairs. AIM theory, which has been described in greater details elsewhere by Bader[99] and Popelier,[157] provides a rigorous approach to characterize the molecular structure, and helps recover qualitative bonding concepts of traditional chemistry from the results of quantum-chemical calculations and/or experimental electronic densities.

As it has been repeatedly shown,[99,111,158-167] AIM analysis can be a useful tool to investigate various intermolecular interactions, especially hydrogen bonds.[111,158-161,163,165-167] Based on the analysis of calculated electronic densities for a number of hydrogen-bonded complexes, Koch and Popelier[157,163,165] devised a set of AIM-based criteria which can be used to distinguish hydrogen bonds from other types of intermolecular interactions (most of these criteria were also discussed by Carroll and Bader[160] prior to the work of Koch and Popelier). The first and most important criterion is the correct topology of the electron density, which commands the existence of a bond path with associated bond critical point (BCP), connecting the hydrogen atom with the acceptor atom. The second and third criteria by Koch and Popelier specify the range of the values of the electron density ρ_{BCP} and its Laplacian $\nabla^2\rho_{BCP}$, at the BCP typical of hydrogen bonding – 0.002–0.04 e^-/a_0^3 and 0.02–0.15 e^-/a_0^5 (a_0 = 0.5292 Å), respectively. However, it should be noted that these ranges are based on the analysis of a few neutral complexes with fairly weak hydrogen bonds.[163] For stronger complexes involving charged or highly polar molecules, these limiting values are clearly inappropriate, since ρ_{BCP} can reach much larger values (up to 0.1 au) and $\nabla^2\rho_{BCP}$ can vary significantly, reaching even slightly negative values, for some very strong hydrogen bonds.[166,167]

In addition to the Laplacian of electron density $\nabla^2\rho_{BCP}$, Cremer and Kraka[168] proposed to use the total energy density at the BCP to discriminate between various

types of chemical bonding. The total energy density $H(r)$ is the sum of the potential $V(r)$ and kinetic $G(r)$ energy densities. These two components of $H(r)$ are related to the Laplacian of the electron density via the local virial theorem: $1/4\nabla^2\rho(r) = V(r) + 2G(r)$ (in atomic units).[99] Being a simple sum of the stabilizing potential and destabilizing kinetic energy densities, the total energy density at the BCP, H_{BCP}, were found to provide a more sensitive measure of the emerging covalent character of intra- and intermolecular bonds.[166-175] Using both the total energy density and the Laplacian of $\rho(r)$ at the BCP, Rozas *et al.*[167] proposed to classify hydrogen bonds according to their strength as: weak, with both $\nabla^2\rho_{BCP}$ and $H_{BCP} > 0$; medium, with $\nabla^2\rho_{BCP} > 0$, but $H_{BCP} < 0$; strong (or "quasi-covalent")[109] with both $\nabla^2\rho_{BCP}$ and $H_{BCP} < 0$. This AIM-based classification is consistent with the traditional categorization of HBs on the basis of binding energies.[107,167]

The next criterion of Koch and Popelier states, that the hydrogen and the acceptor atoms penetrate each other upon formation of the hydrogen bond. The penetration value for a given atom is calculated by subtracting its "non-bonded" radius from the "bonded" radius. In this context, a monomer "non-bonded" radius is approximated by the distance from a nucleus to a 0.001 au electron density contour in the direction of the hydrogen bond.[157,160] Atomic radii approximated this way are usually very close to the standard gas-phase van der Waals radii.[99] The "bonded" radius is the distance from a nucleus to the BCP of interest. The relative penetrations of the hydrogen and acceptor (base) atom can be related to the relative softness and hardness of the interacting species: the higher the penetration of the hydrogen by the base atom, the harder is the base and the softer is the acid (hydrogen bond donor).[160,163]

Finally, the last four criteria by Koch and Popelier are based on the integrated atomic properties of the hydrogen atom: compared to the monomer, upon formation of a hydrogen bond, the hydrogen atom loses negative charge and becomes energetically destabilized, and its dipolar polarization and atomic volume decrease as well. Recent

experimental studies of the charge density distribution in hydrogen-bonded complexes[176,170-175,177-179] gave more grounds to the hydrogen bond criteria by Koch and Popelier, which were obtained by analysis of calculated charge densities.

The interatomic surfaces have a very low curvature, which is typical for hydrogen bonds.[160] A very good correlation is observed between ρ_{BCP} and $\nabla^2\rho_{BCP}$ in the complex, and the proton affinities of the corresponding halide anions. As the proton affinity increases up the halide series, both parameters also increase. Even though the Laplacian value increases, the energy density becomes increasingly negative with halide proton affinity increase, a behavior, typical of HBs of medium strength. Indeed, the hydrogen bonds in the bent $X^-(CH_3CN)$ isomers can be classified as medium-strength, based on the energetic grounds ($12 < D_0 < 25$ kcal/mol,[107] *cf.* Table 5) and AIM analysis ($\nabla^2\rho_{BCP} > 0$, $H_{BCP} < 0$).[167]

Interestingly, the relative penetration of the halide by the hydrogen atom $\Delta r(X)$ is always significantly larger than the penetration of hydrogen by the halide $\Delta r(H)$, with the exception of the fluoride complex, for which these values almost equal (*cf.* Table 7). This suggests that the methyl group in the acetonitrile molecule acts as a hard hydrogen-bond donor, a surprising finding since the C–H bond is generally considered a soft acidic group.[160,180] The rest of the hydrogen bonding criteria are obviously fulfilled for the bent isomers (*cf.* Table 7) with an increase of the hydrogen-bonded character of these structures with increase of the halide proton affinity up the halide series.

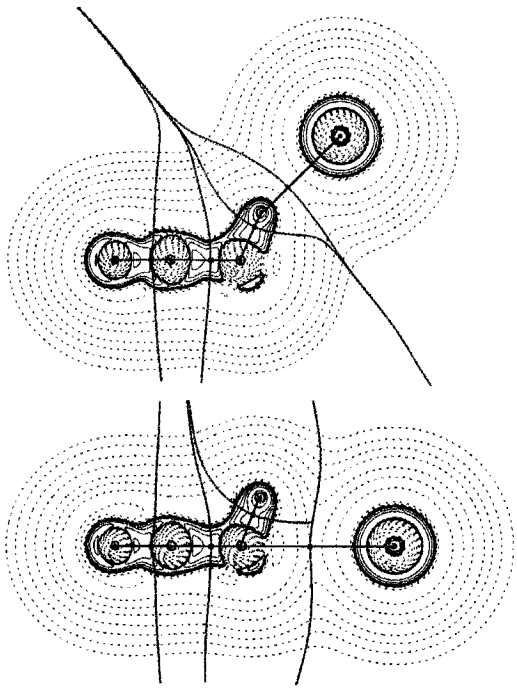

Figure 9. AIM plot for the bent and linear structures of the chloride-acetonitrile complex. Bond paths (purple) and inter-atomic surfaces (green) are super-imposed with the contour plots of the Laplacian of electron density $\nabla^2\rho$ (solid lines for $\nabla^2\rho < 0$, dashed lines for $\nabla^2\rho > 0$)

Table 3. AIM properties for the linear isomers of halide-acetonitrile complexes[a]

	$I^-(CH_3CN)$	$Br^-(CH_3CN)$	$Cl^-(CH_3CN)$	$F^-(CH_3CN)^b$
$\rho_{BCP(C-X)}$	0.007	0.009	0.010	0.016
$\nabla^2\rho_{BCP(C-X)}$	0.026	0.034	0.040	0.074
$H_{BPC(C-X)}$	1.4×10^{-3}	1.3×10^{-3}	1.5×10^{-3}	2.0×10^{-3}
q(X)	-0.956	-0.959	-0.962	-0.964

[a] Electronic density, the Lapalcian of the electronic density, energy density at the C–X bond critical points, and the atomic charges on halide. (All Values are in au, MP2/TZ2AE calculations)
[b] Second-order saddle point structure, included for comparison with other linear isomers

Charge transfer (CT) from the halide to acetonitrile also increases with the anion proton affinity, and reaches up to 0.1 electrons for the fluoride-acetonitrile complex.

Thus, the analysis of the electron density distribution with the AIM theory unequivocally supports the hydrogen-bonded nature of the bent $X^-(CH_3CN)$ complex.

In contrast to the bent isomers, the primary topological criterion for hydrogen bonding is not met with the linear $X^-(CH_3CN)$ structures. The intermolecular bond path does not connect the halide with any of the hydrogen atoms, but instead with the carbon atom of the methyl group, as can be seen from Figure 9. For all linear complexes, the values of the charge density and its Laplacian at the intermolecular BCP are typical of the van der Waals interactions,[164] and the electron density at the BCP(C–X) is at least twice as small as that for the BCP(H–X) in the corresponding bent structures. For the fluoride-acetonitrile, $\rho_{BCP(C-F)}$ is almost five times smaller than $\rho_{BCP(H-F)}$ (*cf.* Figure 9). However, the most striking difference between the linear and bent isomers is found in the atomic energy density. For the bent complexes H_{BCP} *decreases* with increasing proton affinity of the halide, which is consistent with increasing the (quasi)covalent character of the hydrogen bond.[166,167] On the other hand, for linear isomers the situation is opposite, as H_{BCP} slightly *increases* for linear structures with increased halide proton affinity. The degree of charge transfer from the halide to the acetonitrile molecule is also smaller than for the bent structures, and it *decreases* going up the halide series, the opposite trend to that observed for bent structures. Thus, the binding of halides to acetonitrile molecules is evidently due to interactions of the different nature for the linear and bent isomers of the $X^-(CH_3CN)$ complexes and the linear complexes are mostly held together by electrostatic (ion-dipole and polarization) interactions of the halide with the acetonitrile molecule as whole, and not trifurcated hydrogen bonds.

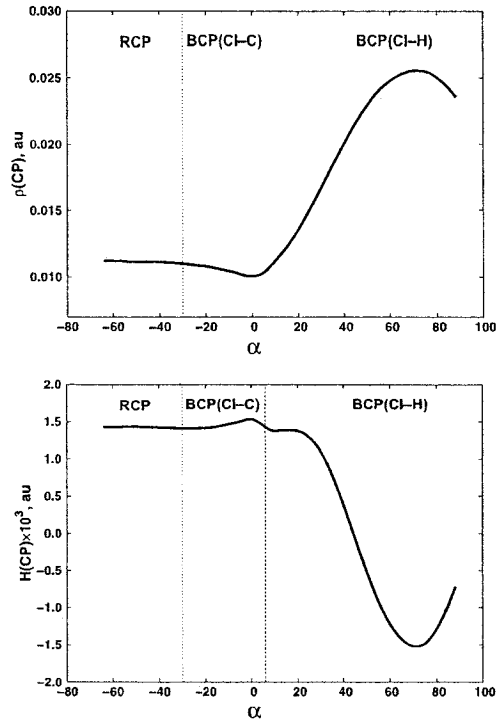

Figure 10. Evolution of the electronic density ρ and the energy density *H* at the critical point between the chloride and acetonitrile, and the nature of this critical point in respect to the tilting along the angle α (Figure 6b) calculated at the MP2/TZ2 level of theory (see also Figure 13 in Supporting information)

Traditional red-shifting and improper, blue-shifting hydrogen bonds are very similar in nature,[119,181,182] so the existence of blue-shifting HBs in the linear isomers of $X^-(CH_3CN)$ can be ruled out. Furthermore, linear halide-halomethane complexes $X^-(CH_3Y)$ are not likely to be hydrogen-bonded, as postulated earlier, given the fact that halomethanes have smaller gas-phase acidities than acetonitrile (gas-phase deprotonation enthalpies are: 365.2; 400.6; 392.2; 389.7; 379.4 kcal/mol, for CH_3CN, CH_3F, CH_3Cl, CH_3Br, CH_3I, respectively, Ref. 146), and are therefore less likely to be HB donors.

In order to examine how the nature of the ion-molecule interaction changes upon transformation of the linear structure into the bent one, Figure 10 displays the nature of the bond critical point between the halide and the acetonitrile molecule and the

corresponding atomic interaction line, and the evolution of the corresponding ρ_{BCP} and H_{BCP} for chloride-acetonitrile, as the chloride moves away from the acetonitrile C_3 symmetry axis in the C–C–H plane. The evolution of $\nabla^2\rho_{BCP}$, the chlorine atomic charge and the hydrogen charge, dipole moment, energy, and volume are given in Supporting information section (*cf.* Figure 14). The range of existence of a weak C–Cl bond appears to be very small, persisting only for $\alpha < 6°$, and further tilting of the chloride from the acetonitrile C_3 symmetry axis transforms the interaction into an H–Cl bond *via* a so-called conflict mechanism,[99,157] where the transition happens through an intermediate structure where the bond path from the chloride terminates at the BCP of the C–H bond. Remarkably, this transformation is accompanied by a change in C–H bond length: for $\alpha > 12°$ it becomes longer than that in the free CH_3CN molecule (*cf.* Figure 8), whereas for $\alpha < 12°$ it is shorter than in that of the free monomer. Therefore, when chloride becomes tilted by roughly 10° from the acetonitrile C_3 symmetry axis, it already forms a hydrogen bond with one of the hydrogen of the methyl group! As the angle α increases, the hydrogen bond interaction becomes stronger, as is evident from the increasing electron density at the chloride-hydrogen BCP (ρ_{BCP}) and the decreasing total energy density (H_{BCP}). At $\alpha \sim 45°$ H_{BCP} becomes negative, characteristic of a transition from a weak to medium-strength hydrogen bond. These parameters and other AIM parameters (provided in the supplementary information) evolve in the direction outlined by Koch and Popelier for hydrogen bonds with increase of the C–C–Cl tilt angle up to $\alpha \approx 75°$. At this point, hydrogen bonding in fact appears to be stronger than at the equilibrium bent complex geometry ($\alpha \approx 50°$), although this structure corresponds to a repulsive wall on the PES (*cf.* Figure 7c). Hence, the equilibrium bent structure is a result of a compromise between hydrogen bonding and ion-dipole interaction. The competition between these two modes of interaction of similar strength makes the PES flat, so that the PES does not

reflect the directionality, typical of hydrogen bonds. On the other hand, this directionality could be inferred from the evolution of the AIM parameters as a function of the angle α.

Negative values of the angle α correspond to the halide moving on the PES ridge between the two energy minima corresponding to equivalent bent structures (*cf.* Figure 6 and Figure 7). At $\alpha \approx -30°$ the C–Cl atomic interaction line (AIL) bifurcates, giving rise to two AILs connecting the halide with the BCPs of the two adjacent C–H bonds. Accordingly, the C–C bond critical point splits into two BCPs and a ring critical point (RCP). This topology appears to be highly unstable, and with a small shift of the halide moiety out of the C–C–H plane, one of these AILs disappears and another one forms to connect X^- to the closest hydrogen atom.

III.4.c.Polarization and charge transfer

To complement the AIM analysis of the electronic structure and bonding in halide-acetonitrile complexes, atomic point charges calculated with Natural Population Analysis (NPA)[141,183,184] and the electrostatic potential fit (ESP)[143,144] schemes are reported in Table 4. There is a generally good agreement between the NBO and ESP charges calculated for the halide and the adjacent hydrogen atom, and the corresponding AIM values (in Table 7 and Table 3). Increase of charge transfer from the halide to acetonitrile in the bent isomers with increase of the halide proton affinity is clearly demonstrated by all three approaches (AIM, NPA, and ESP), as so is the loss of negative charge of the hydrogen atom upon complexation. For linear isomers the degree of CT is smaller, in agreement with the AIM results, and does not seem to exhibit a strong dependence on the nature of the halide. The charges on the carbon and nitrogen atoms of the acetonitrile molecule differ slightly with the NBO and ESP schemes, but the general

trend points toward an increase of polarization with decrease of the halide radius. The dipole moment of the complexed CH_3CN provides a quantitative measure of the degree of the acetonitrile molecule polarization. As seen from Table 4, the calculated ESP dipole moment of the free acetonitrile molecule is in excellent agreement with its experimental counterpart of 3.92 D.[185] Upon complexation with halide, the acetonitrile molecule is significantly polarized, and the polarization increases with the ion size decrease (for the complex with fluoride the dipole moment of acetonitrile increases by more than 1.7 D), as was observed in our previous studies.[103]

Finally, to visualize the rearrangement of the electron density (due to polarization and CT) upon complex formation, the electron density difference diagrams,[187] obtained by subtracting the electron densities of the monomers (in the geometry of the complex) from that of the complex, are shown in Figure 11 for chloride-acetonitrile. The regions of space shown in blue represent regions of charge loss and those in red represent regions of charge gain. For the bent structure, one observes a pattern typical of hydrogen bonding: a rather compact zone of charge gain around the HB-acceptor atom, and an extended region of charge loss around the hydrogen atom, involved in the HB.[119,187,188]

The charge loss at the bridging hydrogen atom is in a good agreement with the atomic charges calculated with the AIM, NPA and ESP schemes (*cf.* Table 7, Table 3, and Table 4). The obvious charge gain of the halide seems to arise from polarization of the halide, and the more diffuse zone of charge loss is not visible with the isodensity value used for the density difference plots.

Table 4. Point charge distributions for the X-(CH_3CN) complexes.[a]

Charge type	N	C	C_M	H	H	X	μ^b
			CH_3CN				
NBO	-0.31	0.28	-0.68	0.24		-	-
ESP	-0.49	0.45	-0.47	0.17		-	3.92
			$I^-(CH_3CN)$ linear				
NBO	-0.39	0.30	-0.70	0.26		-0.98	-
ESP	-0.49	0.45	-0.56	0.19		-0.96	4.04
			$Br^-(CH_3CN)$ linear				
NBO	-0.39	0.30	-0.71	0.26		-0.98	-
ESP	-0.56	0.44	-0.48	0.19		-0.97	4.99
			$Cl^-(CH_3CN)$ linear				
NBO	-0.40	0.31	-0.71	0.26		-0.98	-
ESP	-0.57	0.43	-0.47	0.19		0.96	5.15
			$F^-(CH_3CN)$ linear				
NBO	-0.42	0.31	-0.71	0.28		-0.98	-
ESP	-0.58	0.40	-0.50	0.22		-0.95	5.56
			$Br^-(CH_3CN)$ bent				
NBO	-0.46	0.37	-0.67	0.31	0.21	-0.98	-
ESP	-0.57	0.46	-0.53	0.16	0.16	-0.96	4.92
			$Cl^-(CH_3CN)$ bent				
NBO	-0.40	0.31	-0.73	0.31	0.23	-0.95	-
ESP	-0.57	0.43	-0.43	0.27	0.12	-0.95	5.06
			$F^-(CH_3CN)$ bent				
NBO	-0.45	0.32	-0.79	0.37	0.21	-0.87	-
ESP	-0.62	0.48	-0.64	0.43	0.13	-0.90	5.69

[a] Point charges (q) in fractions of e

[b] Dipole moment of acetonitrile molecule extracted from point charges; the experimental value for free CH_3CN molecule is 3.924 D (from Ref. 186)

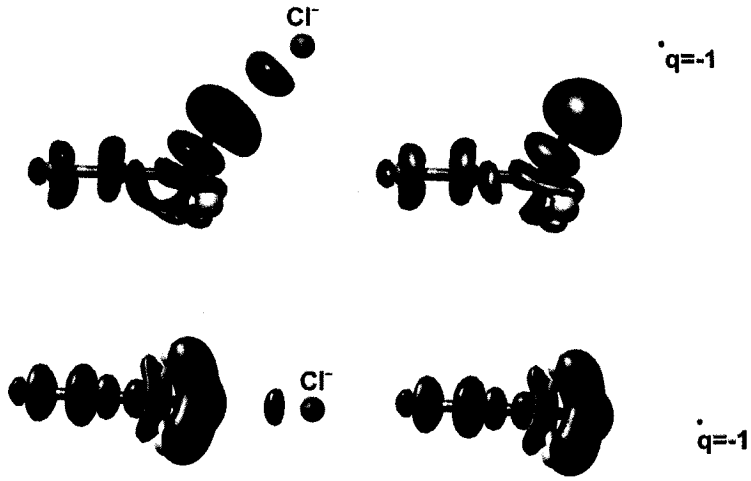

Figure 11. Electron density difference between the chloride-acetonitrile complex (bent and linear structures) and the non-interacting monomers calculated at the MP2/TZ2 level of theory. The regions in blue are characteristic of charge loss, and those in red of charge gain, the isodensity value is 0.002 au. The electron density difference where the chloride has been replaced by a point charge is shown on the right panel for comparison.

Since the net charge transferred from the proton acceptor (halide) is relatively small, the electron density difference diagrams are not very helpful to depict the CT effects, but rather useful to visualize polarization effects. For the linear structure, the similar alternating charge loss – charge gain pattern is observed, with a smaller region of charge gain for the halide, and a large region of charge loss for the hydrogen atoms of the CH_3 group. Further inspection of the charge difference diagrams reveals that the remote C≡N group of the acetonitrile molecule is polarized in a very similar way for both bent and linear structures, and in both cases, the picture remains practically unchanged with replacement of the halide by a point charge.

Hydrogen bonding is a complex phenomenon, and such interaction consists of several components of different nature and which one of these components prevails depend on the particular molecules involved and the medium they are placed in (gas phase, unpolar or polar solvent, etc.).[106,109] However, the electrostatic components, and

in particular the polarization component, are always among the most important ones.[156] In the case of gas-phase hydrogen-bonded acetonitrile-halide complexes, the polarization component appears to dominate, as is obvious from the comparison of the charge density difference plots with the actual halide and with a point charge (*cf.* Figure 11). However, the effects of overlap/penetration of the electronic clouds of the interacting molecules, which are usually referred to as charge-transfer (stabilizing) and exchange-repulsion (destabilizing) components, are rather subtle and not always straightforward to reveal and measure,[183] but at the same time they are very important, especially if we consider hydrogen bond formation as an incipient proton transfer reaction.[109]

The AIM and charge (re)distribution analyses confirm that the linear isomers of the $X^-(CH_3CN)$ complexes are the result of ion-dipole and polarization interactions of the anion with the acetonitrile molecule as a whole. The bent structures are mainly the result of hydrogen bonding, in which the polarization component also seems to play a major role. In fact, the ion-dipole interactions also plays a role in determining the bent complexes structure with chloride and bromide, resulting in "compromise" structures with "imperfect" C–H···X^- hydrogen-bond angles (<180°), as discussed above. On the other hand, the fluoride complex structure seems to be governed by hydrogen bonding.

III.4.d. Distortion of the CH_3CN molecule

We now turn our attention to the nature of the geometrical changes and the concomitant shifts of the vibrational frequencies of the acetonitrile molecule upon complexation with the halide. The elongation of the donor C–H bond in the hydrogen-bonded bent structures and the red shift of the corresponding stretching vibration is a very well known feature of hydrogen bonds, which has been rationalized by invoking purely electrostatic models (see for example Ref. 122) or charge-transfer arguments,

[namely, the interaction between a lone pair of the HB acceptor with the σ*(Y–H) orbital of the donor, Y=O, N, C, etc.[183]]. In the view of hydrogen bonding as an incipient proton transfer reaction,[108,109] the elongation of the hydrogen bond donor Y–H bond is also intuitively obvious. The origin of the contraction of the C–C bond, on the other hand, is less clear, and the latter is most probably due to the combination of polarization and charge-transfer effects. It should be noted that, for a number of strong hydrogen bonds of the type R–Y–H···X, there is a base, an analogous shortening of the R–Y bonds was observed experimentally.[108,189]

Whereas the hydrogen bond in the bent isomers has a rather complex character involving various electrostatic and charge-transfer effects, the linear structures are simply the result of ion-dipole and polarization interactions, and therefore the geometry distortion of the acetonitrile molecule in these structures (namely, C–H bond contraction, and C–C and C–N bonds elongation, *cf.* Figure 8 and Table 5) ought to have a straightforward electrostatic origin. Dannenberg and co-workers[124] have found that certain molecules like methane when exposed to a weak uniform bipolar electric field demonstrate C–H bond shortening. Hermansson[122] showed that, at large distances between interacting molecules, the Y–H bond of an HB-donor molecule contracts if the dipole moment of the molecule has a negative derivative with respect to the Y–H bond length ($\frac{d\mu}{dr_{Y-H}} < 0$). A similar argument can be used to rationalize the acetonitrile molecule distortion in the non-hydrogen-bonded linear complex. For instance, the derivative of the dipole moment of the free CH_3CN molecule with respect to the C–H bond length calculated with MP2/TZ2 is negative (-0.38 D/Å), whereas the derivatives with respect to the C–C and C–N bond lengths are positive (0.41 and 0.42 D/Å respectively). Thus, the dipole moment of the acetonitrile molecule increases with shortening of the C–H and lengthening of the C–C and C–N bonds. Therefore,

polarization of the nuclear backbone of the acetonitrile molecule in the electric field of the halide can account for the observed distortions of the bonds. The assignment of C–H bond contraction and associated C–H stretch blue shift to polarization is further supported by frequency calculations for the acetonitrile molecule in a weak electric field. Indeed, the C–H symmetric stretch frequency of the acetonitrile molecule in an electric field of 10 au (antiparallel to the CH_3CN dipole moment) exhibits a small blue shift of 0.6 cm^{-1}.

As seen earlier, from the charge density difference diagrams in Figure 10, the polarization patterns of the C≡N group are similar for both the linear and bent structures, and they hardly change upon substitution of the halide by a point charge. Thus, polarization effects seem to account for the elongation of the C–N bond in the bent structure as well.

To summarize, analysis of the geometry, vibrational frequencies, potential energy surfaces and the charge density distributions show that the complexes of halides with acetonitrile (and similar complexes with monosubstituted methanes YCH_3) involve two distinct types of intermolecular interactions – ion-dipole interactions and hydrogen bonding. The competition between these two types of interactions determines the shape of the complex PES, and the relative strength of these interactions determines which isomer – bent or linear – is most stable.

III.5. Methyl group as a hydrogen bond donor in complexes with halides

For most complexes investigated here, the hydrogen-bond and ion-dipole interaction energies are comparable (except for the fluoride-acetonitrile complex), which

leads to fairly flat potential energy surfaces. Since this balance is rather subtle, some small changes of the medium, the number of molecules in the cluster, or the nature of the interacting molecules may shift the preference from one interaction regime to another, an issue that is now addressed with a few examples.

III.5.a.Iodide-acetonitrile clusters

The structure of the complex formed by the iodide with acetonitrile has always been considered linear, governed by ion-dipole and polarization interactions,[61,63-65,126] as once again confirmed in this work. On the other hand, the "hydrogen-bonded plateau" is only 0.2 kcal/mol higher in energy, and should the conditions change even slightly, hydrogen bonding could come into play. Johnson and co-workers[61,64] investigated the complex of iodide with two acetonitrile molecules using photoelectron and absorption spectroscopy, and found strong evidence for the co-existence of two isomers of this cluster. These two complexes were ascribed to linear symmetric $NCCH_3\cdots I^-\cdots H_3CCN$ and asymmetric $NCCH_3\cdots NCCH_3\cdots I^-$ structures, postulated within the ion-dipole/polarization paradigm. In our recent quantum-chemical study[190] a new, hydrogen-bonded $I^-(CH_3CN)_2$ cluster structure was found with MP2/6-311++G(df,p), which is almost isoenergetic to the symmetric structure (19.3 and 20.0 kcal/mol respectively), where two perpendicular acetonitrile molecules form a hydrogen bond with iodide (*cf.* Figure 15 in Section III.7 Supporting information). Therefore, a simple addition of another acetonitrile molecule transforms the hydrogen-bonded region of the PES from a plateau to a minimum.

As the number of acetonitrile molecules around iodide increases, the importance of ion-dipole interaction would diminish, and for large $I^-(CH_3CN)_n$ clusters or for I^- solvated in liquid acetonitrile, hydrogen bonding is expected to be prevalent over ion-

dipole interactions. Indeed, in recent work by Mollner *et al.*,[129] the IR spectra of lithium iodide solutions in acetonitrile were reported to exhibit red-shifted absorption bands corresponding to the C–H stretching vibrations (2926 and 2980 vs. 2944 and 3004 cm^{-1} for pure acetonitrile, respectively), which were ascribed to the interaction of the acetonitrile molecules with iodide. Complementary quantum-chemical calculations by Mollner *et al.* for the symmetric isomer of the $I^-(CH_3CN)_2$ cluster, which was used as a model for solvated iodide in liquid acetonitrile, demonstrated a *blue* shift of the C–H stretching vibrations, as expected for the linear, ion-dipole bound complexes (*cf.* Table 6), and the authors[129] then argued that $I^-(CH_3CN)_2$ is too small a model for the iodide solvated in liquid acetonitrile. However, the hydrogen-bonded isomer of this cluster[190] does exhibit red-shifted C–H stretching vibrations (*cf.* Figure 15 in Section III.7 Supporting information), consistent with solution spectra.

To assess how the balance of ion-dipole interactions and hydrogen bonding changes for the complex of iodide and acetonitrile upon transition from the gas to liquid acetonitrile phase, single-point MP2/TZ2 calculations were performed for linear and bent (α=40°) iodide-acetonitrile with solvent effects accounted for by the continuum solvation model within the polarizable conductor approximation (CPCM).[191] Inclusion of solvation effects even in this very approximate fashion makes the bent, hydrogen-bonded structure slightly more stable (by ca. 0.15 kcal/mol) than the linear one. This supports the assignment of the red shift of the acetonitrile C–H stretching vibrations observed experimentally to hydrogen bonding between iodide and acetonitrile.[129]

III.5.b.Fluoride–monohalomethanes complexes

The propensity of fluoride to act as hydrogen-bond acceptor suggests the formation of bent complexes with many mono-substituted methanes, even those less acidic than acetonitrile. However, in a recent extensive computational study of a series of

complexes between halides and halo-substituted methanes,[128] the only minimum structures found with MP2/6-31+G(d,p) for the mono-chloromethane complexes with chloride and fluoride have linear C_{3v} symmetric configurations, similar to the linear isomers of the $X^-(CH_3CN)$ complexes reported in the present study. The existence of only one, linear isomer for the $F^-(CH_3Cl)$ complex seems surprising in light of the above discussion.

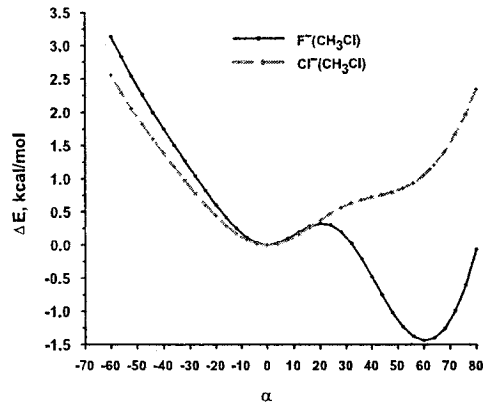

Figure 12. Potential energy profiles of the $X^-(CH_3Cl)$, complexes (X=F, Cl) in respect to the tilting along the angle α (Figure 1b), calculated at the MP2/TZ2 level of theory. Energies are given in kcal/mol relative to the energy of the linear structures (α=0)

To clarify the issue of the existence of bent isomers for complexes of chloride and fluoride with methyl-chloride MP2/TZ2 PES scans along the tilt angle α, are shown in Figure 12. The $Cl^-(CH_3Cl)$ complex indeed has only one energy minimum on the potential energy profile, which corresponds to a linear structure, but the hydrogen-bonding region (α=40°–60°) still manifests itself as a shoulder on the potential energy profile. Evidently, neither the chloride proton affinity, nor chloromethane acidity are sufficient to give rise to a hydrogen-bonded, bent structure. However, for the fluoride complex with chloromethane, the situation is opposite: the linear structure exists only as a local minimum, and the global minimum, which is ca. 1.5 kcal/mol lower in energy, is located around α=60° and thus corresponds to a bent structure [MP2/6-31+G(d,p)

calculations give very similar results]. This newly found global minimum for the $F^-(CH_3Cl)$ complex, and the aforementioned hydrogen-bonded isomer of the $I^-(CH_3CN)_2$ cluster,[190] serve as excellent examples that the possibility of hydrogen-bond formation between a methyl group and a halide should never be overlooked.

III.6. Summary and concluding remarks

By investigating a series of binary halide-acetonitrile complexes as a paradigm, it has been shown that complexes formed by halides and mono-substituted methane molecules may adopt two types of structural isomers, a bent or a linear structure. Whereas the geometry of the linear structures can be rationalized by electrostatic (ion-dipole) and polarization interactions between the halide and the acetonitrile molecule, the bent structures appear to result from a compromise between regular, red-shifting C–H···X^- hydrogen bonding and the ion-dipole/polarization interactions of the halide with the acetonitrile moiety as a whole. The stronger the proton affinity of the halide and higher the acidity of the substituted methane, the more the angle C–H···X^- approaches 180°, and the weaker the contribution of the ion-dipole interactions to the complex stabilization energy.

The hydrogen bonds in the bent structures can be classified as medium-strength, on the grounds of the complex binding energies and Atoms-In-Molecules (AIM) analysis and seem to be primarily due to electrostatic/polarization interactions. The shape of the complex PES is determined by a subtle interplay between the hydrogen bonding and ion-dipole interactions. When these two interactions have similar strength, the resulting PES is relatively flat with respect to tilting of the anion moiety off the YCH_3 symmetry axis. Due to this pronounced floppiness of the PES, subtle changes, such as the number of clustered molecules with the halide, the nature of one of the interacting species or the

medium can easily affect the balance between ion-dipole interactions and hydrogen bonding, making either the linear of bent structures more stable or distorting the geometry of the bent isomer. Therefore, for complexes of halides with mono-substituted methanes, one should never overlook the importance of both types, of ion-dipole and hydrogen bonding interactions, and thus the possible existence of therefore both types of linear and bent isomers.

Finally, on a technical note, MP2 and CCSD(T) calculations with triple-zeta quality basis sets appear to give very similar results for the binding energies, geometries and potential energy surfaces (PES) of the $X^-(YCH_3)_n$ binary complexes. The resulting binding energies are also in excellent agreement with experimental data. Thus, the MP2 method appears to be the method of choice for the investigations of these types of complexes, and larger clusters. DFT methods are found to underestimate the binding energies of the $X^-(CH_3Y)$ complexes, and to slightly overestimate the relative strength of the hydrogen bonds. Therefore, DFT methods are to be used with caution for calculations of complexes with weak hydrogen bonds, such has iodide-acetonitrile complex. Less surprising is the fact that the Hartee-Fock method is inappropriate for modeling $X^-(YCH_3)_n$ clusters, due to its inability to reproduce the hydrogen bonding component of the intermolecular interactions.

Table 5. Structural and Energetic Properties of X-(CH_3CN)[a]

										Binding energy			
		r_{C-N}	r_{C-C}	r_{C-H}	$r`_{C-H}$	r_{C-X}	r_{H-X}	α	β	D_e	D_0[b]	$D_{0/BSSE}$	ΔH°
CH_3CN													
CCSD(T)/TZ1		1.1633	1.4683	1.0943									
CCSD(T)/TZ2		1.1621	1.4660	1.0900									
MP2/TZ1		1.1703	1.4594	1.0914									
MP2/TZ2		1.1697	1.4571	1.0873									
B3LYP/TZ1		1.1512	1.4553	1.0918									
B3LYP/TZ2		1.1493	1.4542	1.0894									
B3LYP/QZ1		1.1510	1.4528	1.0887									
$I^-(CH_3CN)$													
CCSD(T)/TZ1	linear	1.1649	1.4697	1.0927		3.6990	3.4640	0.0	93.7	11.60	11.59	9.63	
CCSD(T)/TZ2	linear	1.1640	1.4676	1.0890		3.6313	3.3969	0.0	93.6	11.84	11.84	11.13	
CCSD(T)/$TZ2_{CPP}$[b]	linear									11.93	11.93		
CCSD(T)/TZ1//MP2/TZ1	linear									11.60	11.59	9.63	
CCSD(T)/TZ2//MP2/TZ2	linear									11.84	11.83	11.10	
MP2/TZ1	linear	1.1716	1.4599	1.0902		3.6854	3.4467	0.0	93.9	11.60	11.59	9.80	

										Binding energy			
		r_{C-N}	r_{C-C}	r_{C-H}	$r`_{C-H}$	r_{C-X}	r_{H-X}	α	β	D_e	D_o[b]	$D_{o/BSSE}$	ΔH°
MP2/TZ2	linear	1.1713	1.4578	1.0866		3.6154	3.3777	0.0	93.8	11.95	11.95	11.25	
B3LYP/TZ1	linear	1.1535	1.4555	1.0905		3.7839	3.5340	0.0	94.8	9.89	9.95	9.90	
	bent	1.1536	1.4533	1.0980	1.0917	3.8556	2.9136	40.7	143.9	9.95	9.83	9.79	
B3LYP/TZ2	linear	1.1517	1.4550	1.0882		3.7723	3.5249	0.0	94.6	10.15	10.21	10.16	
	bent	1.1519	1.4528	1.0957	1.0893	3.8373	2.9078	39.9	142.7	10.21	10.10	10.05	
B3LYP/QZ1	linear	1.1509	1.4550	1.0877		3.7715	3.5240	0.0	94.6	10.11	10.18		
	bent	1.1510	1.4528	1.0948	1.0887	3.8403	2.9206	39.1	141.7	10.17	10.08		
Expt													**11.4 ± 0.9[N]** **11.0 ± 0.2[H]**
$Br^-(CH_3CN)$													
CCSD(T)/TZ2//MP2/TZ2	linear									13.04	13.06	12.43	
	bent									13.18	13.04	12.10	
MP2/TZ2	linear	1.1714	1.4580	1.0863		3.3636	3.1352	0.0	92.6	13.22	13.24	12.61	
	bent	1.1715	1.4546	1.0980	1.0879	3.5039	2.4994	47.4	151.5	13.44	13.30	12.38	
B3LYP/TZ2	linear	1.1521	1.4550	1.0880		3.4997	3.2611	0.0	93.5	11.54	11.61	11.52	

										Binding energy			
		r_{C-N}	r_{C-C}	r_{C-H}	$r`_{C-H}$	r_{C-X}	r_{H-X}	α	β	D_e	D_o[b]	$D_{o/BSSE}$	ΔH°
	bent	1.1523	1.4518	1.1000	1.0896	3.5797	2.5874	45.5	149.6	11.97	11.86	11.77	
Expt													**13 ± 1** [N]
													12.9 ± 0.4 [H]
													14.3 ± 1.0 [M]
$Cl^-(CH_3CN)$													
CCSD(T)/TZ2//MP2/TZ2	linear									14.05	14.04	13.54	
	bent									14.47	14.29	13.51	
CCSD(T)/TZ2//MP2/TZ2cp[d]	linear									14.04	14.02	13.55	
	bent									14.47	14.32	13.60	
MP2/TZ2	linear	1.1716	1.4581	1.0861		3.1970	2.9755	0.0	91.7	14.16	14.15	13.64	
	bent	1.1717	1.4541	1.1024	1.0882	3.3382	2.2938	51.7	157.3	14.71	14.53	13.75	
MP2/TZ2cp[d]	linear	1.1715	1.4578	1.0862		3.2277	3.0048	0.0	91.8	14.15	14.13	13.64	
	bent	1.1717	1.4547	1.1007	1.0880	3.3670	2.3447	49.0	153.7	14.68	14.53	13.80	
B3LYP/TZ2	linear	1.1524	1.4547	1.0878		3.3058	3.0740	0.0	92.6	12.66	12.72	12.67	
	bent	1.1527	1.4510	1.1052	1.090	3.3848	2.3468	50.1	155.7	13.50	13.36	13.30	
Expt													**14 ± 3** [N]
													13.6 ± 0.5 [H]
													15.8 ± 1.0 [M]

		r_{C-N}	r_{C-C}	r_{C-H}	$r`_{C-H}$	r_{C-X}	r_{H-X}	α	β	Binding energy D_e	D_0[b]	$D_{0/BSSE}$	ΔH°
$F^-(CH_3CN)$													
CCSD(T)/TZ1	bent	1.1685	1.4595	1.1835	1.0981	2.6164	1.4393	62.3	172.7				
CCSD(T)/TZ2//MP2/TZ2	bent									24.40	25.09	24.00	
MP2/TZ2	bent	1.1745	1.4465	1.1743	1.0901	2.6390	1.4703	62.4	172.5	24.02	24.70	23.64	
B3LYP/TZ2	bent	1.1861	1.4409	1.0922	1.0922	2.6362	1.4576	61.0	171.3	24.65	25.46	25.20	
													24.5 ± 2.0[H]
													16.0 ± 2.0[K]

[a] D_e is the classical binding energy, D_0 and $D_{0/BSSE}$ the ZPE corrected binding energies without and with BSSE correction, ΔH° the experimental binding enthalpy (at T=200-400 K). Energies and enthalpies in kcal/mol, distances in Å and angles in °. Geometric parameters are defined in Figure 6

[b] For CCSD(T) values, ZPE corrections calculated with MP2

[c] Single-point calculation including a Core Polarization Potential for the ECP[97]

[d] Counterpoise-corrected geometry optimizations

[N] NIST recommended experimental binding enthalpy[146]

[H] Experimental binding enthalpy by Hiraoka and co-workers[65]

[K] Experimental binding enthalpy by Kebarle and co-workers[155]

[L] Experimental binding enthalpy by McMahon and co-workers[134]

Table 6. Frequencies of the acetonitrile vibrations and frequency shifts upon complexation with halides

	Sym	CH_3CN		Δω, linear structures				Sym	Δω, bent structures			
		ω_{expt}[b]	ω_{calc}	I⁻	Br⁻	Cl⁻	Cl^-_{CP}[c]		Br⁻	Cl⁻	Cl^-_{CP}[c]	F⁻
CH_3 d-stretch	e	3009	3188.6	9.4	12.8	15.7	14.4	A", a'	-10.2, -59.4	-11.0, -64.0	-8.3, -60.4	-36.5, -96.4
CH_3 s-stretch	a_1	2954	3095.4	13.6	18.1	21.8	20.5	A'	-110.3	-168.5	-141.2	-1177.2
CN stretch	a_1	2267	2209.0	-14.7	-16.2	-17.3	-16.7	A'	-15.1	-17.0	-16.6	-31.7
CH_3 d-deform	e	1448	1499.2	-27.9	-31.9	-34.3	-32.8	A", a'	-6.1, -20.6	-2.5, -20.4	-6.6, -21.2	18.0, -27.9
CH_3 s-deform	a_1	1385	1420.1	-41.8	-51.5	-56.4	-52.8	A'	-6.3	-0.9	-6.1	26.7
CH_3 rock	e	1041	1066.8	-34.8	-41.1	-44.9	-43.2	A", a'	3.5, -33.2	7.0, -31.7	4.8, -35.3	36.5, -50.7
CC stretch	a_1	920	934.6	-14.7	-16.4	-17.3	-16.3	A'	-2.7	-2.3	-3.7	9.3
CCN bend	e	362	358.8	15.4	15.8	17.1	17.5	A', a"	26.3, 22.2	32.2, 24.1	29.0, 23.3	85.5, 55.0

[a] Frequencies and shifts are cm^{-1}, MP2/TZ2 calculations
[b] Taken from the NIST database[192]
[b] Shifts calculated for the counterpoise-corrected MP2/TZ2 vibrational frequencies

Table 7. Experimental gas-phase proton affinities of the halide ions and AIM properties for the bent isomers of halide-acetonitrile clusters[a]

	CH_3CN	$I^-(CH_3CN)$ [a]	$Br^-(CH_3CN)$	$Cl^-(CH_3CN)$	$F^-(CH_3CN)$	Hydrogen Bond Criteria[b]
PA[b]		314.3	323.50	333.4	371.3	
$\rho_{BCP(H-X)}$		0.014	0.019	0.023	0.078	ρ at BCP > 0.002 au
$\nabla^2\rho_{BCP(H-X)}$		0.030	0.046	0.060	0.150	$\nabla^2\rho$ at BCP > 0.02 au for weak and medium HBs
$H_{BCP(H-X)}$		-1.2×10^{-4}	-1.3×10^{-4}	-6.5×10^{-4}	-2.9×10^{-2}	H at BCP > 0 for weak and < 0 for medium HBs
$\Delta r(H)$		0.42	0.52	0.56	0.90	Mutual penetration of H and cceptor atom ($\Delta r > 0$)
$\Delta r(X)$		0.73	0.75	0.78	0.92	
q(H)	0.079	0.132	0.196	0.224	0.416	Loss of negative charge on H atom
E(H)	-0.588	-0.549	-0.533	-0.520	-0.424	Energetic destabilization of H atom
μ(H)	0.148	0.136	0.124	0.114	0.042	Decrease of dipolar polarization of H
V(H)	45.93	40.30	35.05	32.53	19.21	Decrease of atomic volume of H
q(X)		-0.945	-0.947	-0.947	-0.909	

[a] PAs in kcal/mol, other values are in au, MP2/TZ2AE electronic densities
[b] Hydrogen bond criteria based on the AIM theory[163,167]
[c] Representative structure on the "hydrogen-bonded plateau" with α=40° (*cf.* Figure 6 and Figure 7), included for comparison with other bent isomers
[b] Experimental proton affinities of X^- (kcal/mol) from Ref. 146

III.7. Supporting information

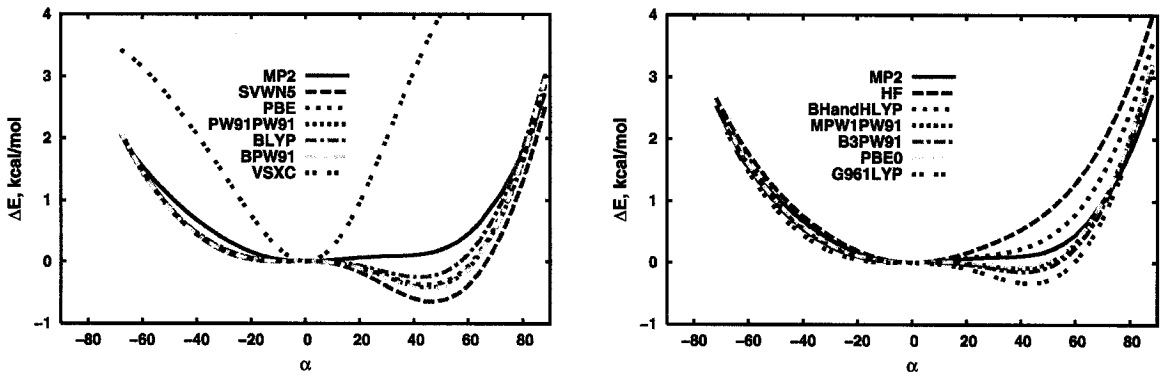

Figure 13. Potential energy profiles for the $I^-(CH_3CN)$ complex in respect to the tilting along the angle α (Figure 1b), calculated with various DFT methods and Hartree-Fock (HF) method. Energies are given in kcal/mol relative the energy of the linear structure (α=0°).

Pure DFT functionals used:

SVWN5: Slater exchange functional[193] in combination with Vosko, Wilk, and Nusair correlation functional (formula V)[194]

BLYP: Becke's 1988 exchange functional[195] in combination with correlation functional of Lee, Yang, and Parr[196]

PW91PW91: Exchange-correlation Perdew and Wang's 1991 functional[197]

BPW91: Becke's 1988 exchange functional[195] and Perdew and Wang's 1991 gradient-corrected correlation functional[197]

PBE: Exchange-correlation functional by Perdew, Burke and Ernzerhof[198]

VSXC: van Voorhis and Scuseria's exchange-correlation functional[145]

Hybrid DFT functionals used:

B3PW91: Becke Three Parameter Hybrid Functional[94] with Perdew and Wang's 1991 gradient-corrected correlation functional[197]

BHandHLYP: Half-and-half hybrid functional[100] defined as:

$$0.5*E_X^{HF} + 0.5*E_X^{LSDA} + 0.5*\Delta E_X^{Becke88} + E_C^{LYP}$$

G96LYP: Barone and Adamo's Becke-style one parameter functional[199] using Gill 1996 exchange[200] and LYP Correlation[196]

mPW1PW91: Barone and Adamo's Becke-style one parameter functional[201] using modified Perdew-Wang exchange and Perdew-Wang 91 correlation[197]

PBE0: Hybrid exchange-correlation functional by Perdew, Burke and Ernzerhof[198]

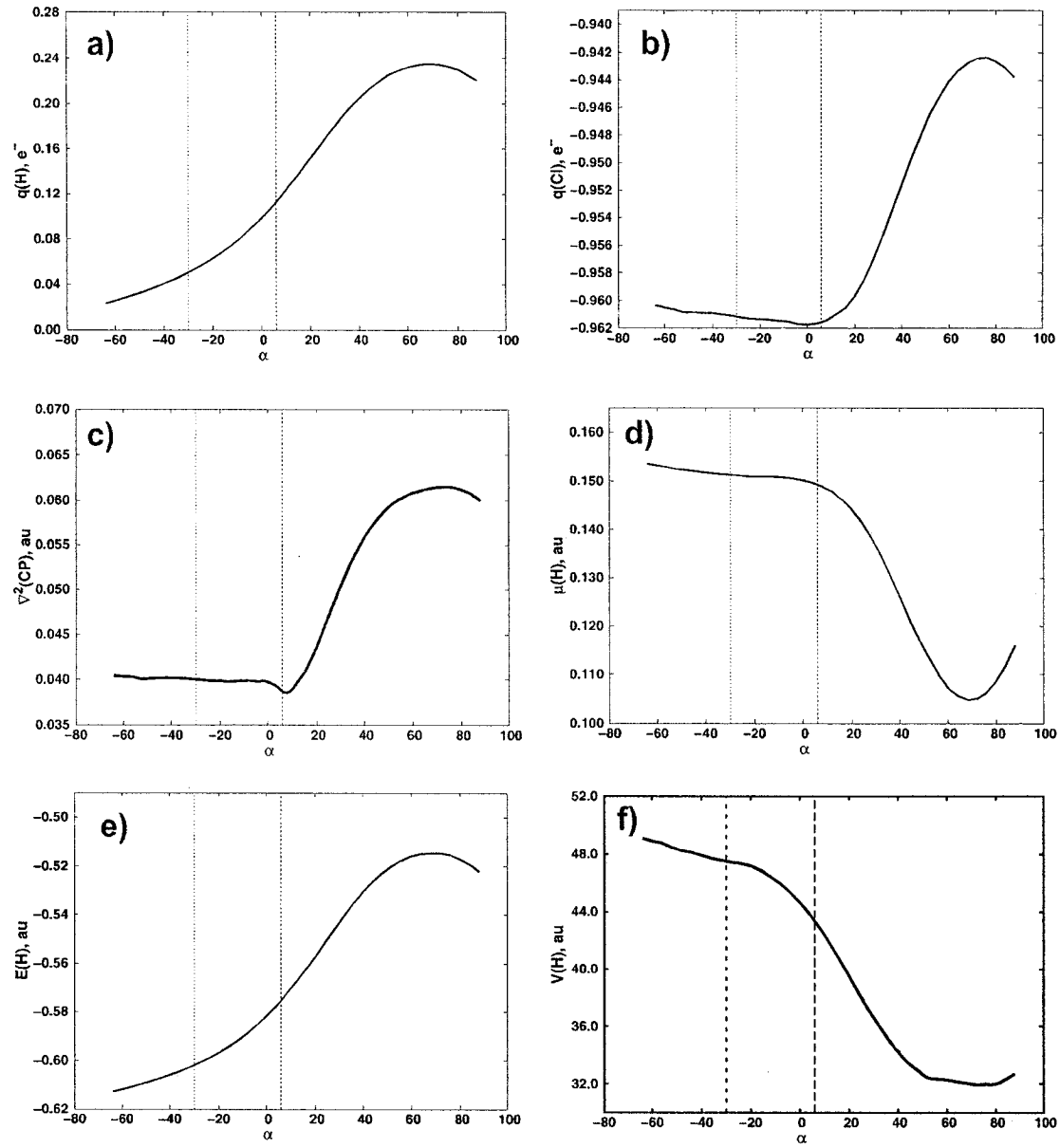

Figure 14. Dependence of various AIM parameters on the C–C···Cl⁻ tilt angle (α) for the Cl⁻(CH₃CN) complex (see also Figure 10 in the main text):

a) atomic charge of the H atom, adjacent to Cl⁻ moiety
b) atomic charge of the Cl atom
c) Laplacian at the intermolecular BCP between the Cl⁻ and CH_3CN
d) dipole moment of the H atom, adjacent to Cl⁻ moiety
e) energy of the H atom, adjacent to Cl⁻ moiety
f) volume of the H atom, adjacent to Cl⁻ moiety

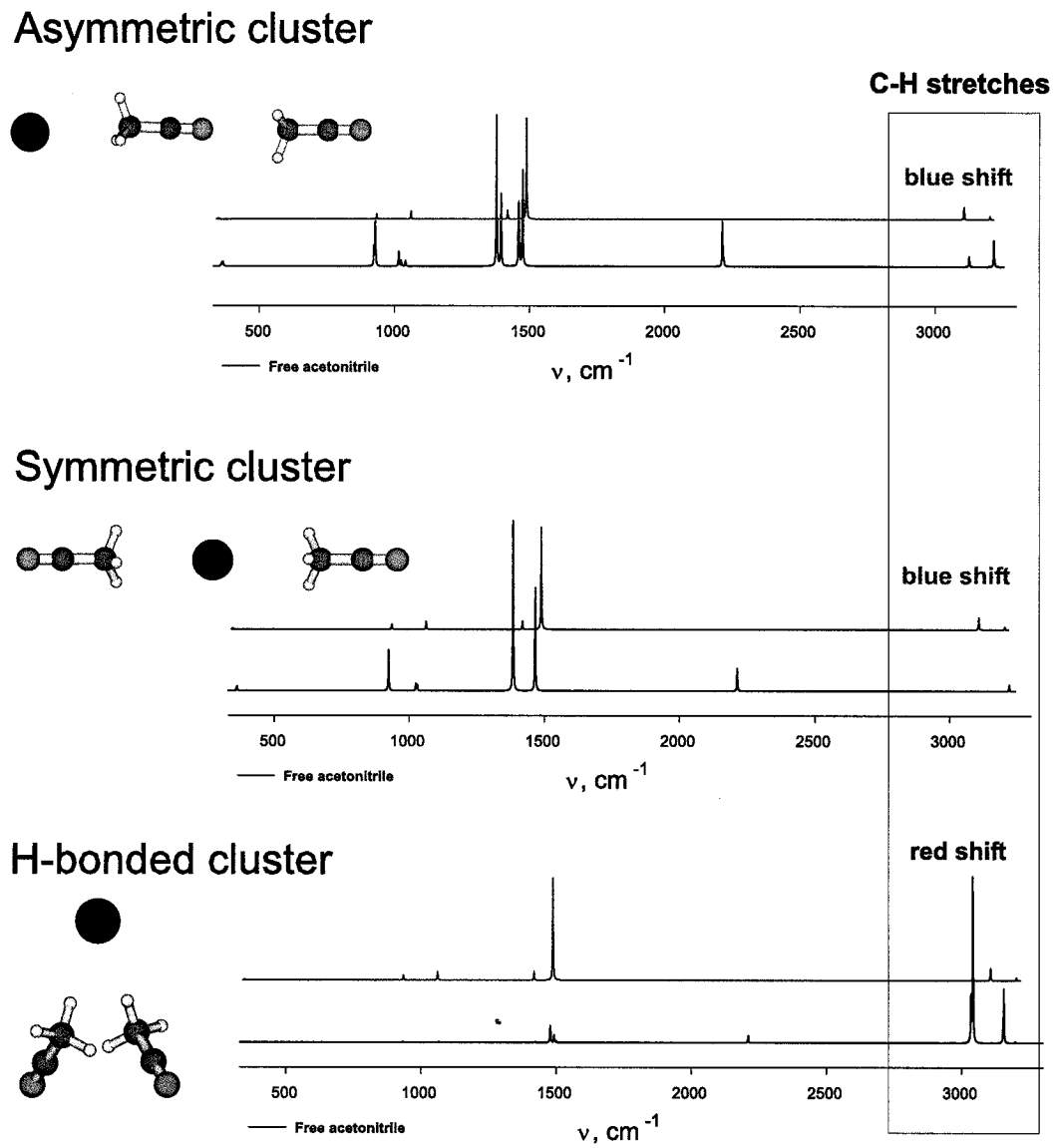

Figure 15. IR spectra of the $I^-(CH_3CN)_2$ cluster isomers, compared with the spectrum of free CH_3CN molecule, calculated at MP2/6-311++G(df,p) level (Timerghazin, Q. K.; Nguyen, T.-N.; Peslherbe, G. H. *J. Chem. Phys.* 2002, *116*, 6867-6870)

Cartesian coordinates in Å of the X-(CH_3CN) complexes calculated with MP2/TZ2 level

I-(CH3CN), linear
Charge = -1; multiplicity = 1
E(MP2)=-143.945901 Hartree

C	0.0000000	0.0000000	-3.6664024
C	0.0000000	0.0000000	-2.2085719
H	0.0000000	1.0129871	-1.8154386
H	-0.8772726	-0.5064935	-1.8154386
H	0.8772726	-0.5064935	-1.8154386
N	0.0000000	0.0000000	-4.8377014
I	0.0000000	0.0000000	1.4067938

Br-(CH3CN), linear
Charge = -1; multiplicity = 1
E(MP2)=-145.9167977 Hartree

N	0.0000000	0.0000000	-4.2392717
C	0.0000000	0.0000000	-3.0678523
C	0.0000000	0.0000000	-1.6098461
H	0.0000000	1.0115275	-1.2137725
H	0.8760085	-0.5057637	-1.2137725
H	-0.8760085	-0.5057637	-1.2137725
Br	0.0000000	0.0000000	1.7537831

Br-(CH3CN), bent
Charge = -1; multiplicity = 1
E(MP2)=-145.9171399 Hartree

N	-1.5831164	3.6275221	0.0000000
C	-1.5831164	2.4560208	0.0000000
C	-1.5831164	1.0014040	0.0000000
H	-0.5704543	0.5770288	0.0000000
H	-2.0972440	0.6338058	0.8855034
H	-2.0972440	0.6338058	-0.8855034
Br	0.9955473	-1.3709098	0.0000000

Cl-(CH3CN), linear
Charge = -1; multiplicity = 1
E(MP2)= -592.301544 Hartree

N	0.0000040	3.3587352	0.0000000
C	0.0000040	2.1871522	0.0000000
C	0.0000040	0.7285514	0.0000000
H	1.0105079	0.3308464	0.0000000
H	-0.5053260	0.3309934	0.8751879
H	-0.5053260	0.3309934	-0.8751879
Cl	0.0000040	-2.4704824	0.0000000

Cl-(CH3CN), bent
Charge = -1; multiplicity = 1
E(MP2)=-592.302407 Hartree

C	0.0000000	1.1623037	0.0000000
C	-1.4235699	1.4585002	0.0000000
N	-2.5668024	1.7152915	0.0000000
H	0.2140261	0.0808704	0.0000000
H	0.4612723	1.5944606	0.8858125
H	0.4612723	1.5944606	-0.8858125
Cl	1.4924944	-1.8236467	0.0000000

F-(CH3CN), bent
Charge = -1; multiplicity = 1
E(MP2)=-232.2735379 Hartree

C	0.0000000	0.8326479	0.0000000
C	-1.1836156	0.0010866	0.0000000
N	-2.1403284	-0.6802085	0.0000000
H	1.0015033	0.2194478	0.0000000
H	-0.0124199	1.4679304	0.8857829
H	-0.0124199	1.4679304	-0.8857829
F	2.3452588	-0.3773618	0.0000000

Chapter IV

Electrostatic interactions and spin-orbit coupling in iodine atom complexes: Accurate *ab initio* potential for the $Na^+\cdots I^\bullet$ complex

Published as: Qadir K. Timerghazin, Denise M. Koch, and Gilles H. Peslherbe, *Journal of Chemical Physics*, **124**, 034313 (2006)

IV.1. Introduction

Ab initio quantum-chemical characterization of open-shell intermolecular complexes has been a topic of intense research for the last few years.[202] Intrinsic properties of the open-shell systems, such as the existence of several low-lying electronic states, the importance of spin-orbit coupling effects and the anisotropy of the charge and spin density distributions, combined with a number of technical issues render computational studies of open-shell complexes rather non-trivial.[202] On the other hand, theoretical knowledge of the structure, thermodynamic stability and potential energy surfaces of the complexes and clusters formed by open-shell species is crucial in many fields of physical chemistry. Of particular interest are the complexes and clusters formed by halogen atoms and closed-shell solvent molecules, as they are typical photoionization products in photoelectron spectroscopy studies of the microsolvation of halide ions in solvent clusters.[203-217] The charge-transfer-to-solvent excited states of halide-solvent clusters also have a very similar (although more complex) nature: in this case, the photoexcited electron is ejected from the halide and trapped in a very diffuse dipole-bound orbital, resulting in formation of a cluster of a halogen atom and solvent molecules with a loosely attached dipole-bound electron.[64,69,217] The interpretation of the data obtained in these gas-phase photoionization or photoelectron spectroscopy experiments is highly dependent on the knowledge of the potential energy surfaces of the photoionized/excited products.

Another type of intermolecular complex with a halogen atom is encountered in studies of alkali halide photodissociation, which gained much attention since the seminal experimental work by Zewail and co-workers[218-223] on the real-time excited-state dynamics of these species. In these experiments, a pump laser pulse excites the alkali halide molecule (usually NaI) to the first A (Ω=0) excited state, which exhibits an

avoided crossing with the ground X (Ω=0) state. Both X and A states are formed by a combination of diabatic curves corresponding to pure ionic and covalent states. Before the avoided crossing region, the X state is mainly ionic, whereas it is mainly covalent beyond the avoided crossing region. The situation is reversed for the A state. As a result, the A state has a shallow well where the wavepacket produced by photoexcitation of the ground-state NaI may remain trapped. In experiments by Zewail and co-workers, the oscillatory motion of this wavepacket was probed by laser-induced fluorescence (LIF) of the sodium atom.[219-221] However, Engel and Metiu proposed that use of an ionizing probe pulse to monitor the time-evolution of the system would provide more detailed information about the excited-state dynamics, since the ionization potential is strongly dependent on the distance between the two atoms.[224] In subsequent experiments, Jouvet and co-workers successfully used a photoionization probe scheme to study the photodissociation dynamics of bare sodium iodide as well as that of $NaI(S)_n$ clusters (S = H_2O, NH_3, CH_3CN).[225-229] Photoionization of excited sodium iodide leads to the formation of the NaI^+ species, which can be regarded as the complex of a sodium cation and an iodine atom $Na^+\cdots I^\cdot$.

Knowledge of the potential energy curves for the $Na^+\cdots I^\cdot$ complex is necessary for a correct interpretation of pump-probe experiments with the photoionization probe scheme, and to perform reliable molecular dynamics simulations of these processes. However, no accurate experimental or theoretical studies of this complex have been reported to date. In a number of theoretical papers on NaI photodissociataion dynamics, simple empirical potentials for the $Na^+\cdots I^\cdot$ complex were employed. Engel and Metiu initially[224] used a potential which included an ion-induced dipole interaction (parameterized on the basis of the experimental estimate of the iodine atom polarizability) as the attractive part and a standard $1/R^8$ repulsion term. Subsequent work employed very similar potentials with minor modifications.[225,230-233] For instance,

polarization of the Na^+ moiety[225,231-233] and/or dispersion interactions[231-233] were also included in model potentials.

In addition to practical applications in molecular dynamics simulations of NaI photodissociation, the $Na^+\cdots I^\cdot$ complex is of general interest by itself, as a good model system to investigate intermolecular complexes formed by halogen atoms. Being a fairly small complex, it can be studied using high-level quantum chemistry methods. Spin-orbit interaction for the iodine atom is known to be significant, with an experimental splitting between the $^2P_{3/2}$ and $^2P_{1/2}$ levels of 0.943 eV = 21.74 kcal/mol. Thus, the $Na^+\cdots I^\cdot$ complex may also serve as a good model for detailed studies of the role of spin-orbit effects on the structure and stability of open-shell complexes at relatively high levels of quantum chemistry.

In this work, we present high-level *ab initio* quantum chemistry calculations of the sodium cation – iodine atom complex, discuss the nature of the bonding interactions and the role of spin-orbit effects, and report some spectroscopic properties for its low-lying states. The outline of this article is as follows. Computational methods are first detailed in section 2. The Λ-S potential curves of the $Na^+\cdots I^\cdot$ complex, without inclusion of spin-orbit coupling, are described in section 3, while the spin-orbit coupled potential curves are discussed in section 4. Complete Basis Set (CBS) extrapolations of the potential curves and spectroscopic properties of $Na^+\cdots I^\cdot$ are then presented in section 5, and model potentials describing these curves derived in section 6. Concluding remarks follow in section 7.

IV.2. Computational methods

The potential energy curves for the $Na^+\cdots I^\cdot$ complex were calculated with the internally-contracted multi-reference configuration interaction (MRCI)[234,235] method and

the spin-unrestricted open-shell coupled cluster method[236] with single and double excitations and perturbative triples correction[237] [UCCSD(T)]. The MRCI calculations used the Complete Active Space Self-Consistent Field[238,239] (CASSCF) reference wavefunction with the three 5*p* orbitals of iodine included in the active space, and energies were corrected with the multireference Davidson correction (MRCI+Q).[240-242] The UCCSD(T) calculations made use of the restricted open-shell Hartree-Fock (ROHF) reference wavefunction, and the resulting ROHF/UCCSD(T) method is further referred to as CCSD(T) for brevity. Although some spin contamination is allowed within this method, the deviation of $\langle S^2 \rangle$ from 0.75 never exceeded 0.002 in our calculations.

Basis sets from the correlation-consistent polarized core/valence cc-pVCxZ (x = D, T, Q) series were used for sodium,[243] while small-core relativistic pseudopotential (PP) correlation-consistent basis sets augmented with diffuse functions (aug-cc-pVxZ-PP, x=D, T, Q) recently developed by Peterson and co-workers[244,245] were used for iodine (and xenon). In the MRCI+Q and CCSD(T) calculations, the 5*s* and 5*p* orbitals of iodine and the 2*p* orbitals of sodium were included in the correlation space. Unfortunately, no correlation-consistent basis set has been reported for iodine with polarization functions for the 3*d* shell, so only the valence electrons of iodine were included in the correlation treatment. Since the 2*s* orbital energy of Na lies below that of the 3*d* orbitals of iodine, the Na 2*s* orbital was not included in the correlation space. The combination of the cc-pVCxZ basis set for Na and aug-cc-pVxZ-PP basis set for I will be further referred to simply as the xZ basis set (x = D, T, and Q).

Ab initio spin-orbit coupling calculations were performed with the interacting states method, using the effective one-electron spin-orbit (SO) operator included in the relativistic effective core potential of the iodine atom (see below).[244,245] Polarizabilities of the I atom were calculated with CCSD(T)/QZ and MRCI+Q/QZ by the finite-field method, using field strengths of ±0.005 au. Quadrupole moments were calculated

analytically with MRCI/QZ, and by the finite-field method with CCSD(T)/QZ, using field strengths of ±0.0001 au. Complete basis set (CBS) extrapolations of the total and relative energies, as well as internuclear equilibrium distances, were performed using the well-known mixed Gaussian/exponential formula of Dunning and Woon.[246] All *ab initio* calculations were performed with the MOLPRO package,[247] and spectroscopic constants were calculated from the potential curves using the LEVEL program.[248]

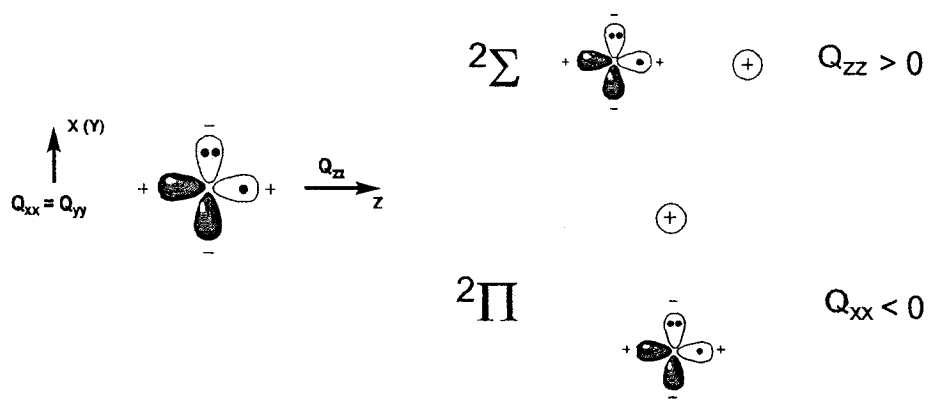

Figure 16. Components of the quadrupole moment of the iodine atom and their electrostatic interaction with the sodium cation

IV.3. Potential curves without spin-orbit interaction

There are two low-lying Λ-S states possible for the $Na^+\cdots I^\cdot$ complex, depending on the orientation of the half-filled 5*p* orbital of the iodine atom with respect to the interatomic axis: the $^2\Pi$ state, where the half-filled orbital is perpendicular to the Na–I axis and the $^2\Sigma$ state, where the half-filled 5*p* orbital is facing the Na^+ moiety, as depicted in Figure 16. Both MRCI+Q and CCSD(T) methods yield very similar potential curves for the $Na^+\cdots I^\cdot$ complex. In fact, for calculations with the QZ basis set, shown in Figure 17, the curves calculated by both methods essentially overlap. On the other hand, the $^2\Pi$ and $^2\Sigma$

potential curves are strikingly different: whereas the $^2\Pi$ potential exhibits a well-pronounced well with a depth of ca. 10 kcal/mol, the $^2\Sigma$ state is almost unbound. The $^2\Sigma$ potential exhibits a shallow minimum (<0.1 kcal/mol) at an interatomic distance of ca. 3.5 Å, which is separated from the long-tail region by a small barrier at ca. 5.0 Å, which is ≈0.1 kcal/mol higher than the asymptote. Similar anisotropy of the interaction, depending on the orientation of the half-filled 5*p* orbital of iodine towards the ion, has been reported previously for the $Ca^{2+}\cdots I^{\cdot}$ complex by Alekseev *et al.*,[249] but the $^2\Pi$ and $^2\Sigma$ states for this complex are much less different than for the $Na^{+}\cdots I^{\cdot}$ complex.

Table 8. Experimental and calculated polarizabilities and quadrupole moments of Xenon and Iodine atoms.[a]

	α_{xx}, α_{yy}	α_{zz}	α^b	Q_{xx}, Q_{yy}	Q_{zz}
Xe					
Expt.[c]			4.04		
CCSD(T)/QZ[245]	4.07	4.07	4.07		
I$^{\cdot}$					
Expt.[c]			5.35		
CCSD(T)/QZ	5.01	4.43	4.82	-0.36	0.71
MRCI+Q/QZ	4.90	4.48	4.76	-0.35	0.71

[a] Polarizabilities in Å^3, quadrupole moments in e·Å^2
[b] Isotropic polarizability. Calculated values are evaluated as $(\alpha_{xx} + \alpha_{yy} + \alpha_{zz})/3$ (*cf.* Ref. 250)
[c] From Ref. 186

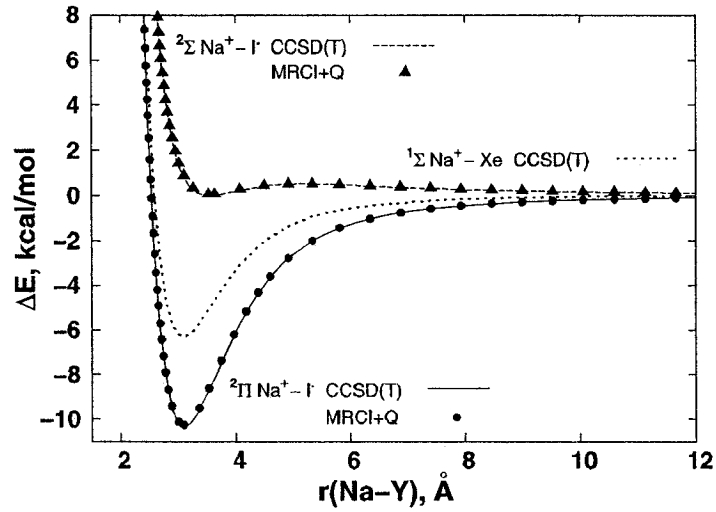

Figure 17. Potential energy curves without spin-orbit coupling for the $Na^+\cdots I^\cdot$ and $Na^+\cdots Xe$ complexes calculated with MRCI+Q/QZ and CCSD(T)/QZ.

If we compare the sodium cation – iodine atom potential curves with its closed-shell analogue, the $Na^+\cdots Xe$ complex, it is clear that the potential curve for the xenon complex lies roughly in between the $^2\Pi$ and $^2\Sigma$ potential curves of the iodine complex (*cf.* Figure 17), and the well depth of the $^2\Pi$ state of $Na^+\cdots I^\cdot$ is almost twice as much as that of $Na^+\cdots Xe$. However, the polarizabilites of the iodine and xenon atoms are very similar, as seen from Table 8. Therefore, the "ion + polarizable atom" model which has been employed previously[224,225,230-233] to describe the interaction of iodine with the sodium cation, does not seem very valid, as it would predict similar binding energies for the $Na^+\cdots I^\cdot$ and $Na^+\cdots Xe$ complexes.

The highly anisotropic character of the potential energy surfaces of open-shell complexes of halogen atoms, which stems from the anisotropy of the electronic and spin density distribution around the $X^\cdot$ moiety, is well known.[202,213,251-255] Since one of the 5*p* orbitals of iodine is half-filled, the iodine electron density distribution is not spherically symmetric, in contrast to that of the closed-shell Xe atom, which gives rise to a positive quadrupole moment aligned with this orbital, as sketched in Figure 16. For the $^2\Pi$ state,

the interaction of the quadrupole moment with the Na^+ ion is stabilizing, while it is destabilizing for the $^2\Sigma$ state. The drastic difference between the $^2\Pi$ and $^2\Sigma$ potential curves suggests that the ion-induced dipole and the ion-quadrupole interactions are of comparable magnitude. Therefore, it is absolutely necessary to include both types of interactions in a model potential describing the $Na^+\cdots I^\cdot$ complex. Indeed as shown in Figure 18, the long-tail portions of the $^2\Pi$ and $^2\Sigma$ potential curves are very well represented by a combination of ion – induced dipole and ion – quadrupole potential terms. For shorter sodium-iodine distances, the agreement deteriorates because short-range effects[254] become increasingly important. Fitted analytical expressions for the full $^2\Pi$ and $^2\Sigma$ potential curves will be presented in Section 6.

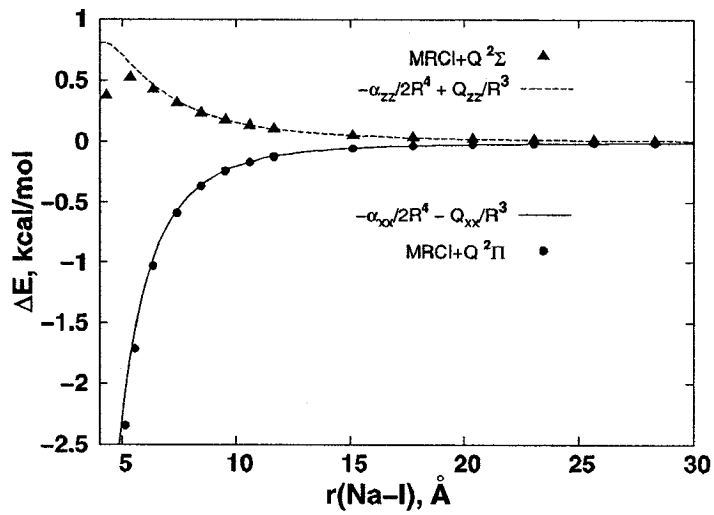

Figure 18. Long-tail portion of the $^2\Pi$ and $^2\Sigma$ potential curves for the $Na^+\cdots I^\cdot$ complex obtained from MRCI+Q/QZ calculations (points). Model curves made of ion-induced dipole and ion-quadrupole interaction terms are shown as lines. The polarizability and quadrupole moment of the iodine atom used for the model curves are obtained from *ab initio* calculations (*cf.* Table 8)

A detailed examination of the various interaction components for this system and similar metal cation – halogen atom complexes within the framework of intermolecular perturbation theory[256] would be very interesting, but this is beyond the scope of the

present article. Dispersion interactions apparently play a minor role in the stabilization of the complex, as the ROHF/QZ, CASSCF/QZ and CCSD/QZ curves are very similar to the CCSD(T)/QZ and MRCI+Q/QZ ones, and only slightly differ in the well depths. For instance, the ROHF/QZ and CASSCF/QZ ground-state binding energies are only 1 kcal/mol lower (9.31 kcal/mol) than the CCSD(T)/QZ value (10.35 kcal/mol), while the CCSD/QZ binding energy (10.24 kcal/mol) is within 0.1 kcal/mol of the CCSD(T) value. We note that the effect of the Davidson correction for MRCI calculations is relatively small: the MRCI/QZ binding energy (10.12 kcal/mol) is just 0.13 kcal/mol lower than the MRCI+Q/QZ value.

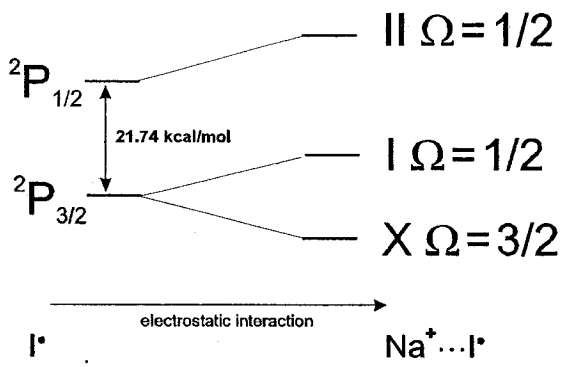

Figure 19. Splitting of the spin-orbit energy levels of the iodine atom in the electric field of the sodium cation. The value of the iodine $^2P_{1/2}$–$^2P_{3/2}$ spin-orbit splitting is taken from Ref. 257

IV.4. Spin-orbit potential curves

The spin-orbit coupling constant for the free iodine atom (0.94 eV)[257] is comparable in magnitude to the interaction energy of the $Na^+\cdots I^\bullet$ complex. Therefore, in order to obtain an adequate description of the potential curves for this complex, spin-orbit interaction effects must be taken into account. In the field of the sodium cation, the zero-field spin-orbit (SO) levels of $I^\bullet$ give rise to three spin-orbit states: one with Ω=3/2

and two with Ω=1/2 (*cf.* Figure 19).[258,259] While the Ω=3/2 state corresponds to the pure Hund case (a) $^2\Pi_{3/2}$ state, the two Ω=1/2 states result from the mixing of the Hund case (a) $^2\Pi_{1/2}$ and $^2\Sigma_{1/2}$ states. Since the spin-orbit coupling constant of the iodine atom is comparable in magnitude to the interaction energy of the complex, the situation for the $Na^+\cdots I^\bullet$ complex is much closer to Hund's case (c) rather than case (a) conditions. Thus, the projection of the total angular momentum on the internuclear axis Ω is the only good quantum number to describe the electronic states of $Na^+\cdots I^\bullet$. From now on, the spin-orbit coupled states will be labeled as X (Ω=3/2), I (Ω=1/2), and II (Ω=1/2).[259]

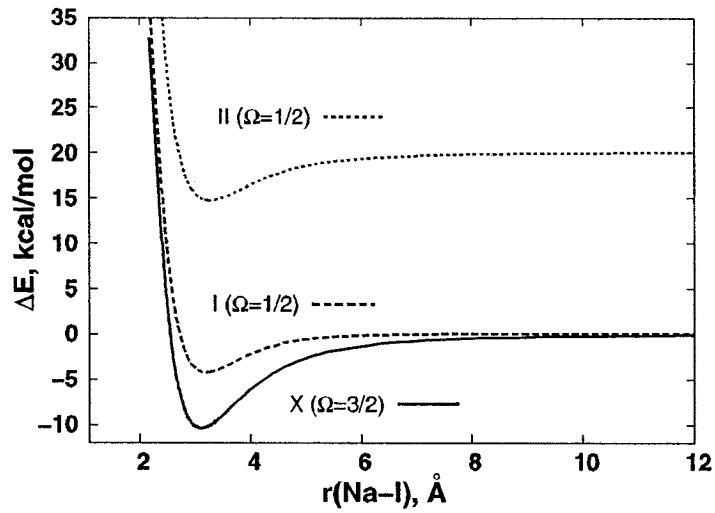

Figure 20. *Ab initio* (MRCI+Q/QZ) potential curves for the low-lying spin-orbit states of the $Na^+\cdots I^\bullet$ complex

In order to include spin-orbit effects in our *ab initio* calculations, we employed the effective one-electron spin-orbit operator from the relativistic pseudopotential for the iodine atom by Peterson and co-workers.[244,245] This effective SO operator $\hat{H}_{SO}$ was used to calculate the SO coupling elements with the MRCI method, and SO eigenstates were obtained by diagonalizing the $H_{el}+H_{SO}$ matrix with the diagonal elements (H_{el}) replaced by the MRCI+Q energy eigenvalues. Although the effective SO operator is used in parameterized form of the relativistic pseudopotential, this approach has proven to be

reliable for calculating spectroscopic and thermochemical properties (*e.g.* Refs. [260-262]). The resulting potential curves for the spin-orbit coupled states of the $Na^+\cdots I^\bullet$ complex are presented in Figure 20. As expected, the ground state does not change much with inclusion of spin-orbit interactions, since the X (Ω=3/2) state is in fact a pure $^2\Pi_{3/2}$ state which does not mix with other states. Indeed, the well depth of the X (Ω=3/2) potential is just slightly lower (by ca. 0.1 kcal/mol) than that of the $^2\Pi$ potential (*cf.* Table 9). The Ω=1/2 SO-coupled states represent a mixture of the $^2\Pi$ and $^2\Sigma$ states and, unlike the $^2\Sigma$ state, have well-pronounced minima with well depths in the 4.2–5.3 kcal/mol range (*cf.* Figure 20 and Table 9).

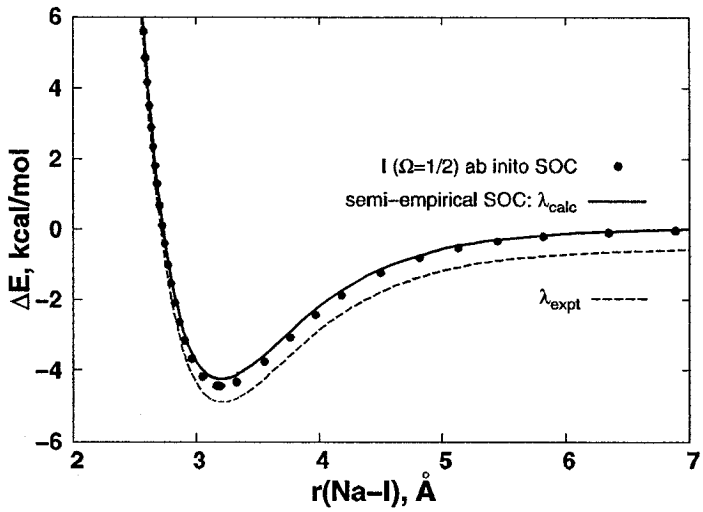

Figure 21. *Ab initio vs.* semi-empirical spin-orbit (SO) coupled curves for the I (Ω=1/2) state of the $Na^+\cdots I^\bullet$ complex. The *ab initio* curves are calculated with MRCI+Q/QZ, while the semi-empirical curves are calculated using $^2\Pi$ and $^2\Sigma$ potentials from MRCI+Q/QZ calculations with λ values for the free iodine atom obtained from experiment (λ_{expt}=7.25 kcal/mol) and MRCI/QZ calculation (λ_{calc}=6.69 kcal/mol)

For weak to medium-strength intermolecular complexes, the SO coupling matrix elements are not expected to differ drastically from the SO matrix elements for the non-interacting species. Consequently, it is possible to treat spin-orbit interactions via a

semi-empirical approach and avoid *ab initio* calculations of the SO matrix elements. In this widely used approach, the SO matrix elements are considered to be independent of the geometry of the complex and of the nature of the interacting states, and these matrix elements are evaluated for the isolated open-shell atom limit.[212,213,258,259,263-266] The full Hamiltonian including SO coupling for a particular Na–I distance r can thus be expressed in terms of the $^2\Pi$ and $^2\Sigma$ Λ-S states derived from *ab initio* calculations, and the spin-orbit coupling constant λ as:[213,258]

$$\hat{H}(r) = \begin{bmatrix} {}^2\Sigma(r) & \lambda & \lambda \\ \lambda & {}^2\Pi(r) & \lambda \\ \lambda & \lambda & {}^2\Pi(r) \end{bmatrix} \quad (1)$$

The coupling constant λ can be evaluated from the experimental SO coupling constant ξ of the free iodine atom: $\lambda=\xi/2=7.25$ kcal/mol, i.e. one third of the $^2P_{3/2}$–$^2P_{1/2}$ splitting.[213,259] Diagonalization of $\hat{H}(r)$ gives expressions for the SO coupled states in terms of the initial Λ-S states:[259,266]

$$X_{\Omega=3/2}(r) = {}^2\Pi(r) - \lambda \quad (2)$$

$$I_{\Omega=1/2}(r) = \frac{1}{2}\left\{{}^2\Sigma(r) + {}^2\Pi(r) + \lambda - \sqrt{[{}^2\Pi(r) - {}^2\Sigma(r)]^2 + 2\lambda[{}^2\Pi(r) - {}^2\Sigma(r)] + 9\lambda^2}\right\} \quad (3)$$

$$II_{\Omega=1/2}(r) = \frac{1}{2}\left\{{}^2\Sigma(r) + {}^2\Pi(r) + \lambda + \sqrt{[{}^2\Pi(r) - {}^2\Sigma(r)]^2 + 2\lambda[{}^2\Pi(r) - {}^2\Sigma(r)] + 9\lambda^2}\right\} \quad (4)$$

Eqs. (2)-(4) obviously reflect the fact that the X (Ω=3/2) state is a pure $^2\Pi$ state, just shifted down by λ, and that the I (Ω=1/2) and II (Ω=1/2) states are mixtures of the $^2\Pi$ and $^2\Sigma$ states. This semi-empirical scheme was successfully applied to a number of weakly bound complexes,[212,213,255,258,266] so it is of interest to assess the applicability of

this approach for the $Na^+\cdots I^\bullet$ complex, which has a relatively high ground-state binding energy.

Table 9. Internuclear equilibrium distances and binding energies for the $Na^+\cdots I^\bullet$ complex.[a]

State	Method	r_e	D_e [b]	D_0 [b]
$^2\Pi$	CCSD(T)/DZ	3.208	9.75	
	CCSD(T)/TZ	3.129	10.29	
	CCSD(T)/QZ	3.113	10.35	
	CCSD(T)/CBS_{dir} [c]	3.105	10.37	
	MRCI+Q/DZ	3.206	9.66	
	MRCI+Q/TZ	3.128	10.19	
	MRCI+Q/QZ	3.112	10.25	
	MRCI+Q/CBS_{indir} [d]	3.105	10.27	
	MRCI+Q/CBS_{dir}	3.104	10.28	
X (Ω=3/2)	MRCI+Q/DZ	3.204	9.78	
	MRCI+Q/TZ	3.127	10.31	
	MRCI+Q/QZ	3.111	10.36	
	MRCI+Q/CBS_{indir}	3.104	10.38	10.16[e]
	MRCI+Q/CBS_{dir}	3.103	10.37	
I (Ω=1/2)	MRCI+Q/DZ	3.325	3.45	
	MRCI+Q/TZ	3.216	4.24	
	MRCI+Q/QZ	3.199	4.24	
	MRCI+Q/CBS_{indir}	3.193	4.21	4.05[e]
	MRCI+Q/CBS_{dir}	3.191	4.21	
II (Ω=1/2)	MRCI+Q/DZ	3.435	4.38	
	MRCI+Q/TZ	3.291	5.25	
	MRCI+Q/QZ	3.272	5.30	
	MRCI+Q/CBS_{indir}	3.265	5.31	5.14[e]
	MRCI+Q/CBS_{dir}	3.264	5.31	

[a] Bond lengths in Å and binding energies in kcal/mol.
[b] Binding energies with (D_0) and without (D_e) zero-point vibrational energy correction.
[c] Obtained by direct complete basis set extrapolation of the property of interest (r_e or D_e).
[d] Obtained from CBS-extrapolated potential curves.
[e] The zero point vibrational energy corrections were calculated from the MRCI+Q/CBS curves with the LEVEL program.[248]

Figure 21 shows potential curves for the I (Ω=1/2) state obtained from the full *ab initio* calculations and by applying the semiempirical treatment of Eq. (3) to the *ab initio* $^2\Pi$ and $^2\Sigma$ curves. Very good agreement of the *ab initio* and semi-empirical treatments of the SO coupling can be observed, especially if one uses *ab initio* zero-field splittings for the iodine atom, which differ slightly from its experimental counterpart. If one uses the value of λ from *ab initio* calculations, the semi-empirical and *ab initio* curves practically coincide. Similar findings apply to the II (Ω=1/2) state (not shown).

Apparently, the spin-orbit coupling in $Na^+\cdots I^\bullet$ remains that of the free iodine atom even at fairly short interatomic distances, which suggests limited charge and spin delocalization from the $I^\bullet$ atom to the Na^+ moiety.[213] Thus, the use of the semi-empirical approach appears to be well justified for the treatment of medium-strength ionic complexes of halogen atoms.

IV.5. Complete basis set extrapolations of $Na^+\cdots I^\bullet$ properties

In order to obtain high-accuracy data from quantum chemistry calculations, data obtained from a set of calculations with a series of systematically convergent basis sets (such as the correlation-consistent basis set family) can be extrapolated to the complete basis set limit (CBS).[262,267-278] Out of several total and relative energy extrapolation formulas proposed in the literature, the mixed exponential/Gaussian function by Woon and Dunning has been found to give statistically the best performance for binding energy extrapolations:[274,279]

$$E(x) = E_{CBS} + Be^{-(x-1)} + Ce^{-(x-1)2} \qquad (5)$$

where x equals 2, 3, and 4 for calculations performed with the DZ, TZ, and QZ basis sets, respectively. For this three-point extrapolation, the resulting system of three equations with three unknowns can be solved to yield the CBS extrapolated energy:

$$E_{CBS}= \frac{E_{DZ}(e^{-7}-e^{-11}) + E_{TZ}(e^{-10}-e^{-4}) + E_{QZ}(e^{-3}-e^{-5})}{(e^{-7}-e^{-11}) + (e^{-10}-e^{-4}) + (e^{-3}-e^{-5})} \quad (6)$$

The CBS extrapolation can be applied directly to binding energies and other properties (even non-energetic ones, like internuclear equilibrium distances), or CBS extrapolated total energies of the $Na^{+}\cdots I^{\cdot}$ complex can be calculated at each point along the potential curve, and properties of the complex obtained indirectly from the extrapolated curves.[274,280] In this work, we used both direct (CBS_{dir}) and indirect (CBS_{indir}) complete basis set extrapolations.

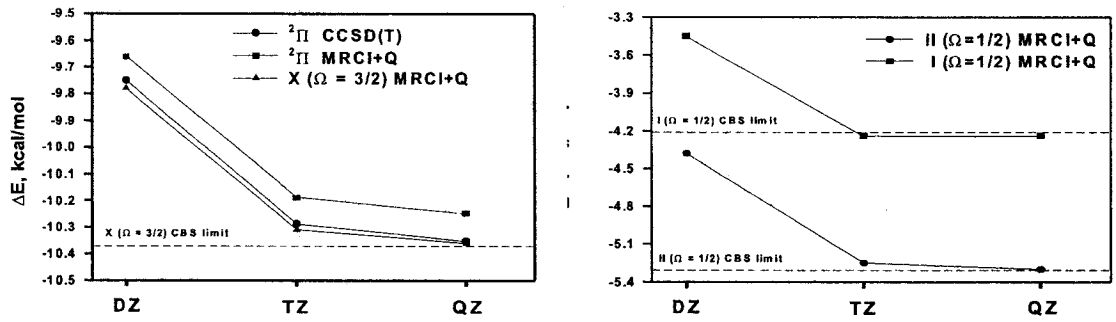

Figure 22. $Na^{+}\cdots I^{\cdot}$ complex formation energy ($\Delta E = -D_e$) *vs.* basis set size for different states

As immediately obvious from Table 9 or Figure 22, the ground-state binding energy of the $Na^{+}\cdots I^{\cdot}$ complex converges smoothly with increasing basis set size for both MRCI+Q and CCSD(T) methods. The MRCI+Q binding energies are slightly lower (by ca. 0.1 kcal/mol) than the CCSD(T)values for calculations with the DZ, TZ, QZ basis sets, and with CBS_{dir} extrapolation. As discussed earlier, the inclusion of spin-orbit coupling slightly stabilizes the complex, and the CBS_{dir} extrapolated binding energy for the X (Ω=3/2) state is 10.4 kcal/mol. For the upper spin-orbit coupled I (Ω=1/2) and II (Ω=1/2) states, the systematic increase in binding energy with basis set size is less pronounced. For the I (Ω=1/2) state, the binding energies calculated with the TZ and QZ

basis sets are equal, and the CBS_{dir} extrapolated value appears to be lower than the TZ and QZ values. Thus, since the binding energies for the Ω=1/2 states do not vary monotonously with basis set size, results of direct CBS extrapolation could be questionable and warrant comparison with those from indirect CBS extrapolation.

The CBS-extrapolated potential energy data generated from MRCI+Q calculations for the low-lying Λ-S and spin-orbit coupled states of the $Na^{+}\cdots I^{\cdot}$ complex are collected in Table 10, while the resulting CBS_{indir} binding energies and internuclear equilibrium distances are presented in Table 9. The binding energies found by direct and indirect CBS extrapolation appear to be in excellent agreement for the $^2\Pi$ state, as well as for all spin-orbit coupled states. For the $^2\Pi$ and X (Ω=3/2) states, the difference between the CBS_{dir} and CBS_{indir} binding energies does not exceed 0.01 kcal/mol. For the higher spin-orbit states the binding energies are virtually equal. Hence, both direct and indirect extrapolations for the I (Ω=1/2) state show a decrease of the CBS-extrapolated binding energies relative to the QZ and TZ values.

The non-monotonous behavior of the I (Ω=1/2) state binding energies with increasing basis set size can be understood, if one recalls that the Ω=1/2 spin-orbit coupled states are mixtures of $^2\Pi$ and $^2\Sigma$ Λ-S states, unlike the X (Ω=3/2) state which has pure $^2\Pi$ character. The internuclear distance at the $^2\Pi$ curve minimum corresponds to a repulsive region of the $^2\Sigma$ curve, and depending on the energy gap between those two parent states obtained with a given basis set, the well depth for the composite spin-orbit coupled states may increase or decrease. Indeed, the energy gap $E_{\Sigma-\Pi}$ between the $^2\Sigma$ and $^2\Pi$ states at the $^2\Pi$ state equilibrium geometry decreases when going from the DZ to the TZ basis set, and then slightly increases for the QZ basis set. As was shown by Haberland,[259] expressions (3) and (4) for the Ω=1/2 states can be approximated for the Hund's case (c) limit as:

$$I_{\Omega=1/2}(r) = \frac{2^2\Sigma(r) + {}^2\Pi(r)}{3} - \lambda \quad (7)$$

$$II_{\Omega=1/2}(r) = \frac{{}^2\Sigma(r) + 2^2\Pi(r)}{3} + 2\lambda \quad (8)$$

and therefore

$$I_{\Omega=1/2}(r) = {}^2\Pi(r) + \frac{2}{3}E_{\Sigma-\Pi}(r) - \lambda \quad (9)$$

$$II_{\Omega=1/2}(r) = {}^2\Pi(r) + \frac{1}{3}E_{\Sigma-\Pi}(r) + 2\lambda \quad (10)$$

Thus, since the increase of the $^2\Sigma-{}^2\Pi$ gap is not monotonous with basis set size, in contrast to the increase of the $^2\Pi$ curve well depth, the binding energy of the resulting I (Ω=1/2) state changes non-monotonously. The II (Ω=1/2) state has a higher $^2\Pi$ contribution, and is thus less affected by the $E_{\Sigma-\Pi}$ increase, which results in a monotonous increase of binding energy with basis set size for that state. Interestingly, not only the indirect, but also the simpler, direct CBS extrapolation scheme is able to capture the complex interplay between the $^2\Pi$ and $^2\Sigma$ components of the I (Ω=1/2) state with increasing basis set size. The CBS-extrapolated internuclear equilibrium distances obtained indirectly and directly are also found to be in very good agreement, with the CBS_{indir} values being systematically larger by 0.001–0.002 Å (*cf.* Table 9).

Table 10. Potential energy data for the $Na^+\cdots I^\cdot$ complex with and without inclusion of spin-orbit interaction.[a]

r(Na–I)	$^2\Sigma$	$^2\Pi$	X (Ω=3/2)	I (Ω=1/2)	II (Ω=1/2)
2.143	50.792	46.902	40.050	42.285	62.261
2.196	42.458	36.617	29.774	33.118	52.801
2.275	32.314	24.151	17.316	21.869	41.431
2.355	24.454	14.584	7.753	13.122	32.746
2.514	13.714	1.838	-4.989	1.283	21.097
2.540	12.413	0.347	-6.481	-0.122	19.710
2.567	11.224	-0.999	-7.827	-1.395	18.447
2.593	10.137	-2.212	-9.040	-2.547	17.300

r(Na–I)	$^2\Sigma$	$^2\Pi$	X (Ω=3/2)	I (Ω=1/2)	II (Ω=1/2)
2.619	9.145	-3.302	-10.131	-3.588	16.258
2.646	8.239	-4.280	-11.108	-4.526	15.314
2.672	7.413	-5.153	-11.981	-5.369	14.459
2.725	5.976	-6.620	-13.449	-6.802	12.987
2.778	4.787	-7.765	-14.595	-7.942	11.794
2.831	3.807	-8.639	-15.469	-8.835	10.834
2.916	2.594	-9.581	-16.411	-9.852	9.696
3.103	1.005	-10.275	-17.104	-10.852	8.411
3.104	0.999	-10.275	-17.104	-10.854	8.408
3.105	0.993	-10.275	-17.104	-10.856	8.404
3.106	0.988	-10.275	-17.104	-10.858	8.400
3.193	0.598	-10.169	-16.996	-10.941	8.198
3.197	0.583	-10.159	-16.986	-10.941	8.193
3.265	0.382	-9.956	-16.782	-10.900	8.152
3.270	0.369	-9.937	-16.763	-10.894	8.152
3.545	0.084	-8.563	-15.380	-10.246	8.584
3.757	0.129	-7.328	-14.137	-9.588	9.196
3.969	0.235	-6.164	-12.964	-8.971	9.842
4.180	0.341	-5.145	-11.936	-8.451	10.437
4.392	0.423	-4.288	-11.071	-8.034	10.953
4.710	0.500	-3.277	-10.050	-7.576	11.571
5.133	0.532	-2.331	-9.093	-7.190	12.154
5.821	0.492	-1.420	-8.172	-6.882	12.705
6.615	0.402	-0.877	-7.621	-6.751	13.020
7.408	0.319	-0.581	-7.321	-6.705	13.184
8.202	0.255	-0.404	-7.142	-6.690	13.278
8.996	0.205	-0.292	-7.027	-6.686	13.335
9.790	0.167	-0.217	-6.952	-6.687	13.371
10.584	0.137	-0.166	-6.900	-6.691	13.395
11.377	0.114	-0.130	-6.863	-6.695	13.412
12.171	0.095	-0.103	-6.835	-6.699	13.423
15.082	0.054	-0.050	-6.782	-6.710	13.445
17.727	0.034	-0.029	-6.760	-6.716	13.452
20.373	0.023	-0.019	-6.749	-6.720	13.456
23.019	0.017	-0.012	-6.743	-6.723	13.458
25.665	0.012	-0.009	-6.739	-6.725	13.459
28.311	0.009	-0.006	-6.737	-6.726	13.459

[a] Obtained with MRCI+Q/CBS, internuclear distances (r) in Å, and energies in kcal/mol relative to the $^2\Pi/^2\Sigma$ asymptote.

The inclusion of bond functions in the basis set has proven essential in determining accurate binding energies for weakly bound intermolecular complexes (see, for example, Ref. 281). However, as $Na^+\cdots I^\cdot$ is a fairly strong complex (D_o ~ 10 kcal/mol) with dominating electrostatic and polarization interactions, introduction of bond functions does not to have a significant effect on the ground-state binding energy, while it greatly increases the technical difficulty of the calculations. For instance, addition of bond functions to the basis set significantly increases the basis set superposition error (BSSE), which is quite difficult to deal with for open-shell systems with significant multi-reference character. In the case of $Na^+\cdots I^\cdot$, the BSSE is just 0.13 kcal/mol for CCSD(T)/QZ, and it is expected to become nearly zero in the CBS limit. Addition of (3*s*3*p*3*d*3*f*1*g*) bond functions leads to an order of magnitude increase in the BSSE (1.21 kcal/mol). In fact, the CCSD(T)/CBS NaI^+ binding energy (10.37 kcal/mol) is very close to the BSSE-corrected CCSD(T)/QZ+(3*s*3*p*3*d*3*f*1*g*) value (10.47 kcal/mol). While both approaches appear to give similar descriptions, the CBS treatment allows the calculation of accurate values for both CCSD(T) and MRCI+Q methods (with and without spin-orbit coupling). On the other hand, the counterpoise correction,[138] which is absolutely necessary when one uses basis sets augmented with bond functions, is hardly applicable for MRCI+Q calculations. We note that the CBS extrapolations presented here are in fact extrapolations to the infinite basis set cc-pVC∞Z(Na)/aug-cc-pV∞Z-PP(I) limit, and therefore do not remedy the possible intrinsic shortcomings of the basis sets series or of the computational procedure used, such as the exclusion of the iodine 3*d* electrons and the sodium 2*s* electrons from the correlation space.

Finally, the accurate CBS potential curves (*cf.* Table 10) obtained in this work can be used to compute a number of properties for the $Na^+\cdots I^\cdot$ complex, such as zero-point vibrational energy (ZPE) corrections to the binding energies (*cf.* Table 9). Inclusion of the ZPE decreases the binding energies by ca. 0.20 kcal/mol, and the ZPE-corrected

ground-state binding energy is 10.2 kcal/mol. Gas-phase vibrational and microwave spectroscopy is an indispensable tool for experimental studies of molecules and complexes.[282,283] A number of open-shell complexes have been investigated spectroscopically and their properties match very well with computed ones, thus bridging the gap between experimental and computational approaches. We used the CBS potential curves to calculate a number of rovibrational spectroscopic constants, which are collected in Table 11, hoping that these data will help guide future experimental studies of the $Na^{+}\cdots I^{\cdot}$ complex.

Table 11. Rovibrational spectroscopic parameters for the X, I, and II spin-orbit states of the $Na^{+}\cdots I^{\cdot}$ complex.[a,b]

Spin-orbit state	w_e	$w_e x_e$	v	E(v,0)-E(0,0))	$B_v \times 10^2$	$D_v \times 10^7$
X (Ω=3/2)	137.02	1.54	0	0.00	8.93	1.59
			1	132.83	8.82	1.66
			2	261.48	8.68	2.03
			3	380.84	8.46	2.32
I (Ω=1/2)	107.01	2.01	0	0.00	8.40	2.32
			1	99.21	8.20	2.73
			2	191.23	8.06	1.53
			3	289.31	8.08	1.91
II (Ω=1/2)	101.18	1.74	0	0.00	8.03	2.51
			1	89.43	7.86	2.05
			2	182.04	7.87	1.64
			3	277.69	7.66	4.11

[a] The notation for all parameters is taken from Ref. 250
[b] Calculated from the MRCI+Q/CBS curves (all values are in cm^{-1})

IV.6.$Na^{+}\cdots I^{\cdot}$ model potential energy curves

The determination of accurate potential energy curves for the $Na^{+}\cdots I^{\cdot}$ complex is not only interesting for understanding interactions involved in open-shell complexes, but also for molecular dynamics simulations of the photodissociation dynamics of NaI with a photoionization probe scheme. In previous computational studies, a single empirical potential has been employed to describe the $Na^{+}I$ probe state.[225,230,284] However, the present calculations suggest that both of the two lowest spin-orbit coupled states of the $Na^{+}\cdots I^{\cdot}$ complex X (Ω=3/2) and I (Ω=1/2) are accessible from the excited NaI A (Ω=0) state under typical conditions used in femtosecond spectroscopy experiments[225,226,228] [under the experimental conditions of Refs. [225,226,228], the II (Ω=1/2) state would not be accessible since its too high in energy]. Furthermore, according to the selection rules for photoionization of diatomic molecules reported by Xie and Zare,[285] transitions to both the $Na^{+}\cdots I^{\cdot}$ X (Ω=3/2) and I (Ω=1/2) states are allowed because $\Delta\Omega$ equals to 3/2 and 1/2, respectively.[285] In order to determine the relative importance of the transitions to the X (Ω=3/2) and I (Ω=1/2) states, one would need to perform accurate calculations of the photodetachment intensities from the NaI A (Ω=0) state to both the $Na^{+}\cdots I^{\cdot}$ X (Ω=3/2) and I (Ω=1/2) states. Unfortunately, the semi-empirical "atoms-in-molecule"[266] approach to photodetachment intensity calculations, which was successfully employed for weakly bound complexes[205,266,286,287] may not be applicable to the photoionization of excited NaI since the A (Ω=0) state has a rather complex nature and its properties can not be simply expressed as a combination of atomic properties.

Table 12. Model potential parameters.[a]

Fit parameters	$^2\Pi$ state	$^2\Sigma$ state
A (kcal/mol)	83340	71547
B (Å^{-1})	2.881	3.064
C (kcal/mol/Å^6)	7531	3728
α (Å^3)	5.02	4.53
Q (e·Å^2)	-0.34	0.72

[a] Obtained by fitting the functional form of Eq. (11) to CBS-extrapolated $^2\Pi$ and $^2\Sigma$ state potential energy data. The correlation coefficient (r^2) of the fits are 1.000 and 0.999 for the $^2\Pi$ and $^2\Sigma$ states, respectively.

Previous theoretical studies have employed various classical and/or semiempirical methods to simulate NaI photodissociation pump-probe experiments. It is therefore important to derive accurate analytical potentials of the experimentally accessible probe states for the purpose of these simulations. As discussed in Section 3, the long-range interactions for the $^2\Pi$ and $^2\Sigma$ states can be accurately modeled by an ion-induced dipole + ion-quadrupole potential of the form $-\alpha/2R^4 + Q/R^3$ (*cf.* Figure 18). The correct description of the entire potential curves would in principle require the use of sophisticated model potentials, which include higher-order multipole polarizabilities (quadrupolar, octapolar, etc.) as well as hyperpolarizabilities and a few dispersion terms.[254] However, even these complicated potential forms usually do not allow a perfect fit of experimental and/or *ab initio* data. Therefore, in order to derive a simple but accurate analytical potential for the low-lying $^2\Pi$ and $^2\Sigma$ electronic states of the $Na^+\cdots I^\bullet$ complex which takes into account the physical nature of the bonding interactions, we chose to describe the potential curves of the $^2\Pi$ and $^2\Sigma$ states with the potential form

$$V(R) = A\exp(-BR) - \frac{C}{R^6} - \frac{\alpha e^2}{2R^4} + \frac{Q e}{R^3} \qquad (11)$$

where the short-range interactions consist of a Born-Mayer repulsion term[288] and a London dispersion term,[289] and the long-range interactions are described by the ion-induced dipole and ion-quadrupole interaction terms mentioned earlier. Higher-order terms which are neglected in the potential are presumably compensated by a judicious choice of fitted parameters.

Fits to the CBS-extrapolated $^2\Pi$ and $^2\Sigma$ potential energy data of Table 10 were performed with a standard nonlinear regression technique,[290] and the spin-orbit coupled X and I states can simply be obtained from Eqs. (2) and (3), correlation coefficients larger than 0.999 were obtained in both fits and the resulting parameters are listed in Table 12. The α and Q parameters obtained from the fitting procedure (*cf.* Table 12) are very close to the iodine MRCI+Q/QZ polarizabilities and quadrupole moment (*cf.* Table 8). The slight variation in the fitted *vs.* high-level *ab initio* values stems from the use of CBS extrapolated data to fit model potentials. For instance, the (non-CBS extrapolated) MRCI+Q/QZ potential curves can be fitted exactly with α and Q parameters taken from MRCI+Q/QZ calculations for iodine (*cf.* Table 8). This suggests that the functional form of the Eq. (11) is adequate for describing the $Na^+\cdots I^\cdot$ potential curves and no higher order terms are necessary.

IV.7. Conclusions

High-level *ab initio* potential energy curves for the low-lying electronic states of the sodium cation – iodine atom ($Na^+\cdots I^\cdot$) complex were calculated, with and without inclusion of spin-orbit (SO) coupling effects using the MRCI+Q and CCSD(T) methods. The long tail of the potential energy for the electronic states without spin-orbit coupling is governed not only by ion-induced dipole interaction, as considered in previous work, but also by ion-quadrupole interactions, as the iodine atom has a relatively large

quadrupole moment. As a result, the $^2\Pi$ ground state, for which the ion-quadrupole interaction is stabilizing, is strongly bound, with a binding energy of ~10 kcal/mol, and the $^2\Sigma$ state, which is destabilized by ion-quadrupole interactions, is unbound. Spin-orbit coupling effects were treated both within *ab initio* and semi-empirical schemes. The semi-empirical approach, where SO-matrix elements are taken from the isolated iodine atom limit, was found to yield results in excellent agreement with full *ab initio* calculations. Inclusion of spin-orbit effects leaves the ground state practically unchanged, since the X (Ω=3/2) SO-coupled state has pure $^2\Pi$ character. On the other hand, the higher two Ω=1/2 SO states are mixtures of the $^2\Pi$ and $^2\Sigma$ states, and have binding energies that are roughly half of that of the ground state. Complete Basis Set (CBS) extrapolations were used to obtain accurate potential curves and binding energies for the low-lying electronic states of the $Na^+\cdots I^\cdot$ complex. The final estimate of the complex ground-state binding energy is 10.2 kcal/mol. The CBS-extrapolated potential curves were used to calculate spectroscopic rovibronic parameters to help guide future experimental investigations of the $Na^+\cdots I^\cdot$ complex, and served as the basis for parameterization of model potentials for future use in molecular dynamics simulations of NaI photodissociation/photoionization dynamics.

Chapter V

Photoexcitation and charge-transfer-to-solvent relaxation dynamics of the $I^-(CH_3CN)$ complex

Submitted as:

Qadir K. Timerghazin and Gilles H. Peslherbe, *Journal of Physical Chemistry A* (2006)

V.1. Introduction

Charge-transfer-to-solvent (CTTS) excited states constitute one of the most important features of the photochemistry of inorganic anions in polar solvent media.[49] CTTS photoexcitaion is characterized by ejection of the excess electron from the anion and its stabilization in a bound excited state arising from the interaction with the solvent electric field. The bulk CTTS excited state is believed to be very similar in nature to the solvated electron and, in fact, the latter can be easily produced from the former.[50,58,291] The nature of the CTTS states has been a topic of long-standing interest from both experimentalists and theoreticians,[49] and the ultra-fast excited electron and solvent dynamics following CTTS excitation have recently attracted considerable attention.[58,83,292-294] Whereas the gas-phase analogs of the solvated electron, *i.e.* small solvent cluster anions, have been known for a few decades,[26] the CTTS precursor states in finite anion-solvent clusters were only observed relatively recently.[295] Interestingly, just before the first experimental observations of CTTS states in clusters were reported,[60,61,68] Combariza *et al.* speculated, based on quantum-chemical calculations,[59] that CTTS states might potentially be observed only for very large halide-solvent clusters. However, Johnson and co-workers reported experimental observations of bound excited states just below the photodetachment threshold for a number of clusters formed by iodide and a few polar solvent molecules, including acetone, acetonitrile and water: $I^-(CH_3CN)_{1-2}$, $I^-(CH_3COCH_3)$ and $I^-(H_2O)_{1-4}$.[60,61,68] Similar to the bulk situation, where the relaxation of CTTS states leads to solvated electrons, the relaxation of the CTTS-precursor states in clusters was found to produce solvent cluster anions with high yields.[60,61]

Monitoring the dynamics of CTTS states in clusters can provide very important insight into the dynamics of the nascent solvated electron, and cluster studies provide a

unique opportunity to carry out the investigation at a truly microscopic level. Indeed, femtosecond photoelectron spectroscopy studies by Neumark and co-workers[34,69,70] have shown rich and interesting dynamics for the iodide-water clusters $I^-(H_2O)_n$ (n = 3–28), characterized by a small drop of the excited electron vertical detachment energy (VDE) in the first tens of femtoseconds, and subsequent slow increase of the VDE in the following tens of picoseconds. For larger clusters, the long-time evolution of the VDE is characterized by a slight drop of the VDE, which reaches a maximum around ~50 ps. On the theoretical side, the nature of CTTS photoexcitation has also been investigated by many, and excitation energies[88,89,296-299] and potential energy surfaces were calculated[72,296,300,301] using various quantum-chemical methods. Initially, Lehr *et al.* proposed[69,71] that the experimentally observed stabilization of the excited electron in $[I^-(H_2O)_n]^*$ clusters during CTTS relaxation is determined by the solvent cluster reorganization and that the iodine atom does not seem to play a significant role. This point of view was contested on the basis of static quantum-chemical calculations by Chen and Sheu[72,73], who claimed that the intriguing behavior of the excited electron vertical detachment energy could be explained by the departure of the neutral iodine atom which destabilizes the excited electron while in the cluster. Both of these solvent-driven and iodine-driven paradigms are correct to a certain extent, as suggested in our preliminary first-principles excited-state molecular dynamics (MD) study of the relaxation of photoexcited $I^-(H_2O)_3$ clusters (*cf.* Chapter VI and Ref. 302), which was confirmed recently by Kolaski *et al.*[303]

In most of the computational studies reported so far, the problem of the CTTS excited state relaxation mechanism was inferred from potential energy profiles.[72,296,300,301] However, the intrinsic floppiness and complexity of the potential energy surface of $I^-(H_2O)_n$ clusters lead to very complex relaxation dynamics, which can only be realistically modeled with full-scale MD simulations.[302] In this respect, the I^-

(CH_3CN) complex appears to be an excellent prototype system for computational studies of the photoexcitation and excited state dynamics of purely iodine-driven CTTS relaxation, since it contains only one, fairly rigid, solvent molecule. The small size and high symmetry of this binary complex also allow quantum-chemical calculations at relatively high levels of theory, and studies of such complex are very important for benchmarking various theoretical procedures that can be subsequently used for treatment of larger clusters.

In the present article, we report a quantum-chemical investigation of the CTTS states of the $I^-(CH_3CN)$ binary complex. The nature of photoexcitation and various components of the excitation energy are discussed, as well as the role of spin-orbit coupling. The potential energy profiles for the excited and ionized states are characterized, and an inexpensive, yet reliable procedure is devised to perform realistic first-principles excited-state MD simulations of the relaxation of photoexcited $I^-(CH_3CN)$. The outline of this article is as follows. The computational methods are overviewed in section 2. The static picture of the photoionization and photoexcitation of $I^-(CH_3CN)$ is presented in section 3, and the potential energy profiles of excited and ionized states are discussed in section 4. The dynamics of the excited state is then discussed in section 5. The concluding remarks follow in section 6.

V.2. Computational methods

The structure of the $I^-(CH_3CN)$ complex was optimized and its harmonic vibrational frequencies were calculated using second-order Møller-Plesset (MP2) perturbation theory.[91] The Dunning's correlation-consistent polarized double-zeta basis set augmented with diffuse functions (aug-cc-pVDZ) was used for the hydrogen, carbon and nitrogen atoms,[135] and the relativistic large-core ECP46MDF pseudopotential and

corresponding basis set by Stoll *et al.*[304] were used for the iodine atom. This basis set combination will be further referred to simply as the DZ basis set for brevity.

The excited and ionized states of the $I^-(CH_3CN)$ complex were calculated with multi-reference second-order perturbation theory (CASPT2)[305] using the state-average complete active space self-consistent field (CASSCF)[238,239] reference wavefunction. CASSCF calculations used a (6,4) active space consisting of three occupied 5*p*-orbitals of iodine and the lowest unoccupied orbital. For excited-state calculations the DZ basis set was further augmented by 8 diffuse *sp*-functions generated in an even-tempered manner from the average of the outmost *s*- and *p*-functions of the aug-cc-pVDZ basis set using the geometric progression ratio of 3.2,[41] resulting in an exponent of 1.9414×10^{-6} au for the most diffuse *sp*-basis function (*cf.* Section V.7, Supporting information). The augmented DZ basis set will be simply referred to as DZ+. In most calculations, the additional diffuse *sp*-functions were centered on the methyl group carbon atom. In a number of calculations, the "floating center" technique[306] was used, with the position of the diffuse center optimized with CASPT2 using numerical gradients.

Spin-orbit coupling calculations were performed with the interacting states method, using the effective one-electron spin-orbit (SO) operator included in the relativistic effective core potential of the iodine atom.[304] The CASPT2 energies of the lowest singlet and triplet electronic states were corrected on the basis of spin-orbit coupling (SOC) elements calculated with CASSCF. This approach is referred to as CASPT2-SOC.

For *ab initio* excited state-molecular dynamics simulations, the configuration interaction with single excitations (CIS)[92] method was used to calculate energy and analytical gradients at each step of the trajectories. The CIS calculations employed a small double-zeta quality basis set by Mitin *et al.* [307] augmented by a diffuse *s*-function for hydrogen and diffuse *sp*-functions for carbon and nitrogen.[308] For iodine, the large-

core effective core potential and corresponding basis set by Stevens *et al.*,[309] augmented by one diffuse *sp* shell,[310] was employed. In order to accommodate the dipole-bound electron, the basis set was further augmented by three additional diffuse *sp*-shells centered on the carbon atom of the methyl group and two *sp*-shells on the iodine atom. The diffuse exponents were generated from the outmost diffuse functions of the main basis set in an even-tempered manner using a 5.0 geometric progression factor. The resulting basis set will be further referred to as Min+.

Initial conditions for the excited-state molecular dynamics simulation were generated using the thermal Monte-Carlo sampling technique[311] implemented in the VENUS reaction dynamics program[312] on the ground-state HF/Min+ potential energy surface for T = 150 K. The constant-energy trajectories were propagated using dynamic reaction coordinate technique[313] employing velocity Verlet algorithm,[314] as implemented in GAMESS package,[101] with a time-step of 0.3 fs for up to 2 ps. The interfragment relative kinetic energy and the CH_3CN fragment rotational kinetic energy were calculated as implemented in VENUS program.[312]

All CASPT2 calculations were performed with the MOLPRO package,[102] HF and MP2 calculations were performed with the MOLPRO and GAMESS[101] packages, and all CIS calculations were performed with GAMESS.

V.3. Photoexcitation and photoionization of $I^-(CH_3CN)$

A general overview of photoionization and photoexcitaion for iodide in the gas phase and in clusters is illustrated in Figure 1. Free I^- does not possess bound excited states, and absorption of a photon with sufficient energy to overcome the ionization potential (IP) leads to photodetachment of the excess electron. Due to strong electrostatic and polarization interactions, complexation with one or more polar solvent

molecules significantly stabilizes the ion (typically, with anion binding energies D_{anion} larger than 10 kcal/mol or ~0.5 eV), whereas the stabilization by solvent molecule of the neutral iodine atom which forms upon photodetachment is rather small. This differential solvation leads to the well-known increase of the ionization potential of the solvated anion with an increasing number of solvent molecules in the cluster. If the solvent cluster possesses a dipole moment high enough ($\mu > 2.5$ D)[26] to bind the excess electron ejected from I^- upon photoexcitation, then a dipole-bound CTTS-precursor excited state can be formed, slightly lower in energy than the photodetachment limit (*cf.* Figure 23). Thus, the CTTS excitation energy is lower than the IP of iodide in the cluster ($IP_{cluster}$) by the excited electron vertical detachment energy (VDE). In small clusters this value is rather small (tens of meV), but the stabilization of the excited electron increases dramatically with cluster size and the CTTS excitation energy can be significantly lower than the IP in larger clusters. Thus, in order to quantitatively reproduce experimentally observed CTTS excitation energies, one must be able to reproduce various energy components, including the ionization potential of free iodide, the binding energies of iodide and neutral iodine to the solvent cluster and, finally, the stabilization energy of the dipole-bound excited/excess electron to the solvent molecule(s).

As immediately obvious from Figure 24, the excited-electron distribution in the photoexcited iodide-acetonitrile complex is very similar to the excess electron distribution in the dipole-bound acetonitrile anion, in agreement with previous studies.[89,298] However, in the case of the excited complex, the neutral iodine atom is seen to destabilize the dipole-bound electron, with an excited-electron distribution significantly more compact than the excess electron distribution in the CH_3CN^- anion. It is worth pointing out the importance of highly diffuse basis sets[26,41] for a reliable description of the CTTS-precursor states of iodide-solvent clusters: in our preliminary study,[298] the use of an insufficiently diffuse basis set provided a somewhat different

picture, with an artificially high excited electron density around the hydrogen atoms of the methyl group, which suggested stabilization of the excited electron in part be the interaction with local CH dipoles of the acetonitrile molecule.

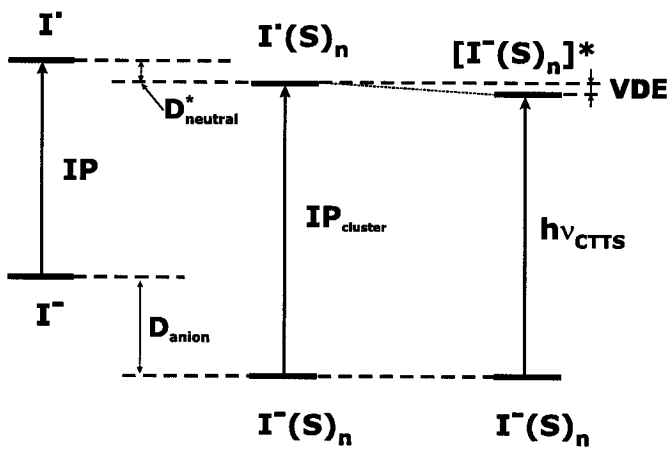

Figure 23. Photoionization and photoexcitation of free iodide and iodide-solvent clusters. $D^*_{neutral}$ is the vertical detachment energy of the $I^•(S)_n$ cluster in the equilibrium geometry of the $I^-(S)_n$ cluster

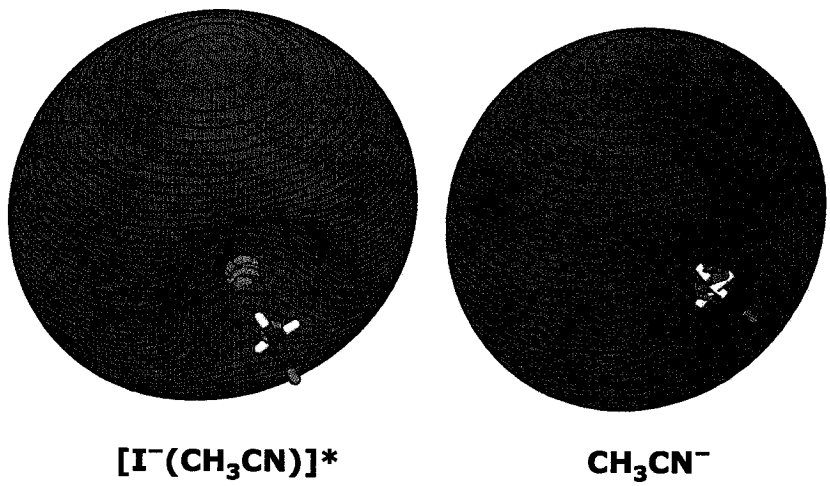

Figure 24. Distribution of the excited/excess electron in the excited iodide-acetonitrile complex and the dipole-bound acetonitrile anion (CASPT2/DZ+ natural orbitals, 0.0018 au and 0.0030 au isosurfaces, respectively)

Similarly to other intermolecular complexes formed by ^2P halogen atoms,[213,315] the interaction of the iodine atom formed upon photoionization/excitation of $I^-(CH_3CN)$ with the acetonitrile molecule is known to give rise to two possible electronic states which differ by the orientation of the half-filled $5p$-orbital towards the C_{3v} symmetry axis of the CH_3CN molecule. In the lower, doubly-degenerate 1^2E state, the half-filled p-orbital of iodine is perpendicular to the C_{3v} axis and, in the 1^2A state, with the half-filled p-orbital is aligned along the symmetry axis (the singlet and triplet CTTS excited states are 1^1E and 2^1A_1, respectively). However, since the interaction of the iodine atom with the acetonitrile molecule is relatively weak and significantly smaller than the spin-orbit coupling constant of the free iodine atom (0.94 eV),[257] a typical Hund case (c) situation arises, and the value of the total spin is not a good quantum number to describe the ionized and excited states of iodide-solvent clusters. The spin-orbit states of the iodine atom in the external field of polar molecules have been discussed in great detail elsewhere (*cf.* Chapter IV). Briefly, the spin-orbit mixing of the 1^1E and 2^1A_1 states of the ionized complex gives rise to three spin-orbit states, labeled *I*, *II* and *III* (*X* is used for the ground state of the $I^-(CH_3CN)$ complex, which is essentially 1^1A_1 state); the first two states correlate with the $^2P_{3/2}$ limit of the free iodine atom, whereas the third one correlates with the $^2P_{1/2}$ limit.[213,315] For a complex with cylindrical symmetry, such as $Na^+\cdots I^\bullet$ (*cf.* Chapter IV) or $I^\bullet(CH_3CN)$, one of the doubly degenerate states retains its character, whereas the other two spin-orbit states have mixed A_1 and E character. Since the spin quantum number is not a good quantum number for weak intermolecular complexes formed by iodine, the singlet and triplet CTTS excited states of iodide-solvent clusters are strongly mixed. Therefore, the lowest triplet excited state(s) are as good as an approximation to the actual (spin-orbit) excited CTTS states as the first singlet state(s). This further validates the "triplet approximation" approach employed by Bradforth and Jungwirth to model the CTTS states in water clusters and in the bulk.[297]

Table 13. Calculated and experimental binding energies and other properties relevant to the photoexcitation and photoionization of the $I^-(CH_3CN)$ complex[a]

	CASPT2/DZ+	CASPT2-SOC/DZ+	Expt.
$D_e[I^-(CH_3CN)]$	0.511	0.511	
$D_0[I^-(CH_3CN)]$	0.509 [b]	0.509 [b]	0.494 ± 0.040 [c]
$D_e^*[I^*(CH_3CN)]$	0.032 (1^2E)	0.032 (I)	
	0.021 (2^2A)	0.025 (II)	
		0.026 (III)	
VDE $[CH_3CN^-]$	11.0×10^{-3}		$(11 - 18) \times 10^{-3}$ [d]
$IP(I^-)$	2.979	2.674	3.059 [e]
$IP[I^-(CH_3CN)]$	3.470 ($1^1A_1 \rightarrow 1^2E$)	3.165 (X→I)	3.54, 4.48
	3.480 ($1^1A_1 \rightarrow 1^2A_1$)	3.171 (X→II)	
		4.084 (X→III)	
E_{CTTS}	3.463 ($1^1A_1 \rightarrow 1^1E$)	3.158 (X→I)	3.53, 4.47
	3.474 ($1^1A_1 \rightarrow 2^2A_1$)	3.164 (X→II)	
		4.078 (X→III)	
VDE $[I^-(CH_3CN)]^*$	6.7×10^{-3} (1^1E)	7.0×10^{-3} (I)	$\leq 10.0 \times 10^{-3}$
	5.9×10^{-3} (2^1A_1)	6.4×10^{-3} (II)	
	7.0×10^{-3} (1^3E)	6.7×10^{-3} (III)	
	6.3×10^{-3} (1^3A_1)		

[a] All values in eV
[b] Zero-point energy-corrected value with vibrational frequencies calculated with MP2/DZ
[c] Ref. 146
[d] Refs. 316 and 61
[e] Ref. 257

We now turn to more quantitative aspects of the photoionization and photoexcitaion of $I^-(CH_3CN)$. As we have recently demonstrated (*cf.* Chapter III),[317] *ab initio* (MP2) calculations predict binding energies for the binary halide-acetonitrile clusters in excellent agreement with experimental data. Indeed, the binding energy of the $I^-(CH_3CN)$ complex calculated with CASPT2/DZ+ of 0.51 eV (11.74kcal/mol) is well within the experimental range of 0.484±0.040 eV (*cf.* Table 13). Interestingly, the iodide-acetonitrile complex is the only complex in the $X^-(CH_3CN)$ series (X = F, Cl, Br, I)

which adopts a linear structure, resulting from solely ion-dipole interactions, as the global minimum-energy structure, while complexes formed with the other halides exhibit less symmetric, hydrogen-bonded minimum-energy structures (*cf.* Chapter III).[317] The calculated binding energy of the iodine atom to an acetonitrile molecule in the equilibrium geometry of the parent $I^-(CH_3CN)$ cluster, D_e^*, is relatively small (0.02-0.03 eV, or 0.5-0.7 kcal/mol, *cf.* Table 13). Thus, the shift of the ionization potential of iodide upon complexation with acetonitrile is practically equal to the $I^-(CH_3CN)$ binding energy D_{anion} (*cf.* Figure 23) and arises solely from ground-state stabilization of iodide by the acetonitrile polar solvent molecule.

The quantum-chemical treatment of systems with an extremely diffuse dipole-bound electron, such as the excited $I^-(CH_3CN)$ complex or the acetonitrile anion CH_3CN, presents certain technical problems.[26] As discussed above, the diffuse nature of the excited/excess electron dictates the use of extremely diffuse basis sets, which at the same time lead to severe convergence problems.[41] On the other hand, dispersion interactions are very important in the stabilization of the dipole-bound electron.[42,44,45,47] Thus, although the Hartree-Fock (HF) or complete active space self-consistent field (CASSCF) methods can provide a correct zeroth-order picture, inclusion of dynamic electron correlation is necessary to produce reliable VDEs for the dipole-bound electron. Inspection of Table 13 suggests that the CASPT2/DZ+ approach provides an adequate description of the dipole-bound electron binding energy for the acetonitrile anion, as the latter agrees well with experimental values and previously reported high-level *ab initio* calculations.[47]

The ionization potential of the free iodine atom is reproduced relatively well with CASPT2/DZ+, although introduction of spin-orbit coupling deteriorates the agreement, leading to significantly underestimated value for the IP (*cf.* Table 13). In fact, the ionization potential of iodide (or, in other words, the electron affinity of iodine) is known

to converge very slowly with the basis set size, and even calculations employing a pentuple-quality basis set aug-cc-pV5Z-PP still yield a slightly underestimated value.[245] Not surprisingly, the IP of $I^-(CH_3CN)$ complex is also underestimated with CASPT2-SOC/DZ+ by almost 0.4 eV. The spin-orbit non-corrected IP values are closer to experimental data, most likely due to a cancellation of errors. Although the absolute value of the IP for the iodide-acetonitrile complex is reproduced poorly, the calculated shift of the IP between the free and complexed iodide (0.44-0.49 eV) is very close to the one observed in experimental studies (0.48 eV).[61] Thus, the CASPT2-SOC/DZ+ calculations provide a correct quantitative picture of the photoexcitation and photoionization of the binary iodide-acetonitrile complex, if the systematic error due to the ionization potential of iodide is taken into account. The splitting between the 1^2E and 1^2A_1 ionized states of $I^-(CH_3CN)$ is found to be small (~0.01 eV), and even smaller for the lowest two spin-orbit states *I* and *II*, which may explain why it was not possible to resolve them in the experiment.[61]

Experimental data concerning the electron binding energy of the excited electron in the CTTS excited state of $I^-(CH_3CN)$ in the Franck-Condon region is rather uncertain, but photoneutral and photofragment action spectra suggest that the CTTS state lies *ca.* 10 meV below the IP.[61] Our calculations agree well with those experimental values, suggesting that the CTTS state is located 6-7 meV below the ionized state (*cf.* Table 13). Not surprisingly, the triplet excited states are *ca.* 0.5 meV more stable than the singlet ones, and the spin-orbit mixing of the singlet and triplet *E* and A_1 states leads to slightly higher VDEs.

To summarize, CASPT2 and CASPT2-SOC *ab initio* calculations with the highly diffuse DZ+ basis set provide a qualitatively and quantitatively correct description of the photoionization and photoexcitation of $I^-(CH_3CN)$ in the Franck-Condon region. However, a complete understanding of the subsequent CTTS relaxation process requires

knowledge of extended regions of the excited-state potential energy surface, to which we now turn our attention.

V.4. Potential energy curves for the ionized and excited states of $I^-(CH_3CN)$

Owing to the cylindrical symmetry of the $I^-(CH_3CN)$ complex, it is relatively easy to map the potential energy surfaces (PESs) of its ground, excited and ionized states. Although the ground-state PES is known to be rather flat with respect to tilting of the iodide off the acetonitrile symmetry C_3 axis and the iodine is relatively free to float in the "methyl pocket" at non-zero temperatures (*cf.* Chapter III), the most relevant coordinate for ionized and excited state relaxation dynamics in undoubtedly the C–I stretch coordinate along the C_3 axis (*cf.* Figure 25). Further, the rigidity of the acetonitrile molecule greatly facilitates the potential energy scans by keeping the acetonitrile geometry frozen during the scans. Figure 25 shows potential energy curves along the C–I stretch coordinate for the non-spin-orbit-coupled ionized and excited states of $I^-(CH_3CN)$ and the associated evolution of the excited electron VDE, while the Figure 26 shows the potential energy curves for the spin-orbit states and corresponding VDEs.

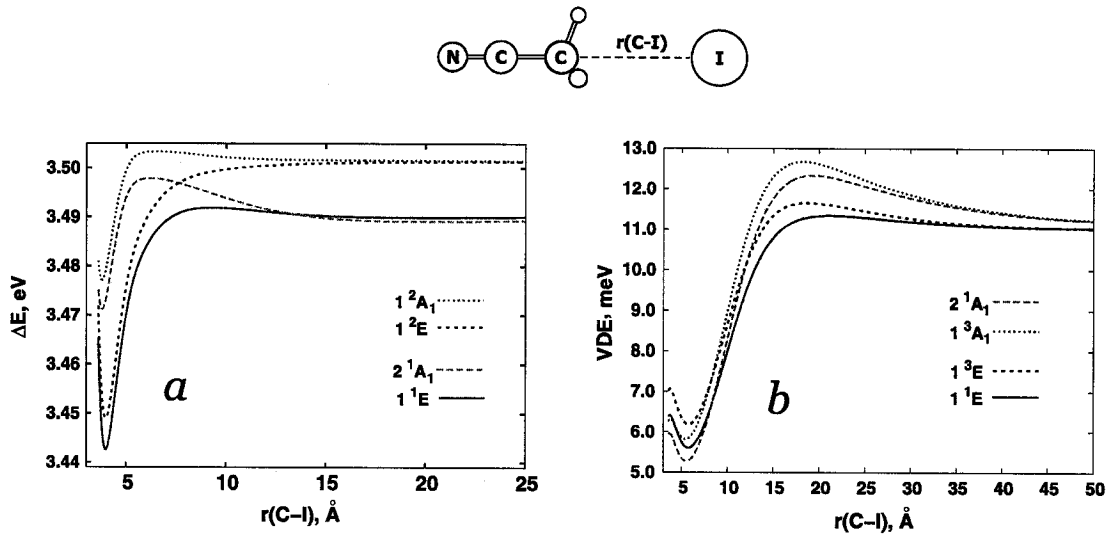

Figure 25. Potential energy curves (CASPT2/DZ+) for the non-spin-orbit-coupled singlet CTTS excited and ionized states (*a*) and excited electron vertical detachment energies (VDE) for the singlet and triplet excited states (*b*) of the $I^-(CH_3CN)$ complex along the C–I stretch coordinate. The equilibrium ground-state energy of $I^-(CH_3CN)$ defines the energy reference in (*a*) and the equilibrium C–I distance of $I^-(CH_3CN)$ corresponds to the onset of the curves.

Complexes formed with iodine involve a significantly anisotropic interaction of iodine with complexed molecule, depending on the orientation of the half-filled iodine 5*p*-orbital (*cf.* Chapter IV).[213,315] The anisotropy is related to the non-spherical distribution of the electron density of the iodine atom, giving rise to non-zero quadrupole moment and relatively large differences in the polarizability along different axes.[315] In the 1^2E state the interaction between acetonitrile and the iodine atom (located on the methyl group side) is relatively strong, with a potential well of *ca.* 50 meV (~1.2 kcal/mol) at a C–H distance of 3.98 Å (*cf.* Figure 25*a*). The well depth for the 1^2A_1 state is only 23 meV (~0.5 kcal/mol), but the potential energy minimum is located at shorter acetonitrile-iodine distance, with r(C–I) = 3.79 Å. The weaker interaction in the 1^2A_1 state can be explained by the destabilizing interaction of the iodine atom quadrupole

moment with the positive end of the acetonitrile molecular dipole, and the lower polarizability of the iodine atom along the half-filled *p*-orbital.

Generally, the potential curves for the CTTS excited states are similar to the corresponding ionized states, but 5-12 meV lower in energy (*cf.* Figure 25*a*). However, the E–A_1 anisotropy is somehow amplified: unlike the 1^1E state, the 2^1A_1 state has a distinct maximum at a C–I distance of *ca.* 6 Å which is *ca.* 6 meV above the dissociation limit. The well depths for both singlet excited states 45 and 16 meV (~1.1 and ~0.4 kcal/mol, respectively) are smaller than for the ionized counterparts. The triplet excited states 1^3E and 1^3A_1 (not shown) are very similar to the singlet CTTS states, but lie slightly lower by 1-1.5 meV. The dependence of the CTTS state VDEs on the C–I distance (*cf.* Figure 25*b*) exhibit a number of interesting features. As the distance between iodine and acetonitrile increases relative to the Franck-Condon region (the left onset of the curves), the VDE decreases and reaches a minimum around r(C–I)=5.5–5.8 Å depending on the state. After reaching the minimum, the VDE starts increasing and reaches a maximum around r(C–I)=18–21 Å, which corresponds to VDE values 0.3 – 1.5 meV higher than the VDE of the free CH_3CN^- dipole-bound anion. The VDE then decreases slowly, eventually converging to the free acetonitrile anion limit. It is worth pointing out that, even at an acetonitrile-iodine distance of 50 Å a small difference of *ca.* 0.2 meV between the VDEs is still observed for the singlet and triplet states, *i.e.* the dipole-bound electron still "feels" the presence of the iodine atom.

Since the excited dipole-bound electron distribution may change significantly depending on the position of the iodine atom, the diffuse basis set centered on the methyl group carbon atom may become inadequate for some regions of the potential energy surface. Hence, potential energy scans employing the "floating center" approach were also performed, where the position of the center of the 8 *sp*-diffuse functions used to describe the excited/excess electron was optimized at each point. The resulting

potential curves are essentially the same as shown in Figure 25*b*, with the VDEs slightly larger just by 1–2 meV.

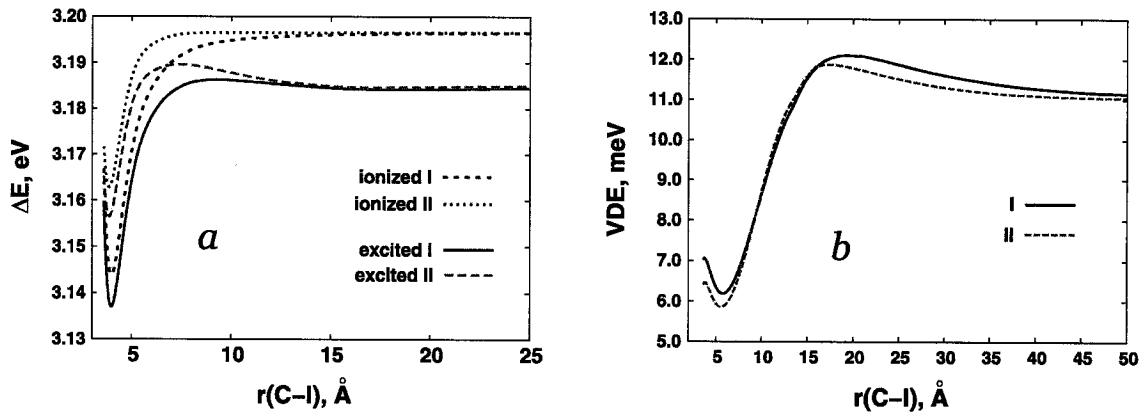

Figure 26. Potential energy curves (CASPT2-SOC/DZ+) for the lowest spin-orbit CTTS excited and ionized states (*a*) and excited electron vertical detachment energies (VDE) for the lowest excited states (*b*) of the $I^-(CH_3CN)$ complex along the C–I stretch coordinate. The equilibrium ground-state energy of $I^-(CH_3CN)$ defines the energy reference in (*a*) and the equilibrium C–I distance of $I^-(CH_3CN)$ corresponds to the onset of the curves.

The introduction of spin-orbit coupling does not significantly change the character of the potential curves for the ionized and excited states of the $I^-(CH_3CN)$ complex. The lower ionized and excited states (*I*) are practically identical to the corresponding 1^2E and $1^1E/1^3E$ states, but shifted down in energy by *ca.* 0.3 eV, since the *I* state has pure *E* parentage, similarly to other complexes of halogen atoms with cylindrical symmetry (*cf.* Chapter IV).[213,315] The *II* and *III* spin-orbit states (*cf.* Figure 26*a* where only *II* shown for clarity) have mixed *E* and A_1 character, and therefore exhibit deeper energy wells than the corresponding non-spin-orbit states of 33 and 29 meV (0.8 and 0.7 kcal/mol) for the ionized and excited states, respectively. The VDE dependence on the acetonitrile-iodine distance for the spin-orbit excited states (*cf.* Figure 26b) is also very similar to that for the non-spin-orbit-coupled case (Figure 25*b*).

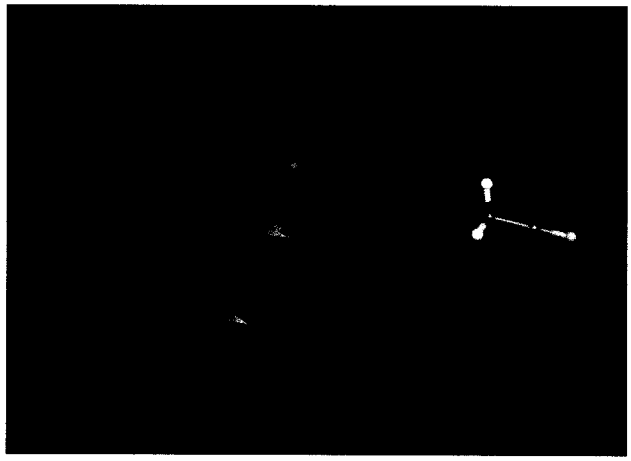

Figure 27. Distribution of the excited electron in the excited iodide-acetonitrile complex for r(C–I) = 6.6 Å (CASPT2/DZ+ natural orbital, shown with a 0.0020 au isosurface (only the lower half of the orbital is shown).

The dependence of the excited electron vertical detachment energy on the acetonitrile-iodine distance (*cf.* Figure 25*b* and Figure 26*b*) may already provide some insight into the "iodine-driven" relaxation of CTTS states in polar solvent clusters. The initial drop of the VDE around r(C–I)=6 Å can be attributed to the destabilization of the dipole-bound electron by the neutral iodine atom passing through the core of the dipole-bound electron distribution (*cf.* Figure 27), as was discussed in great detail by Chen and Sheu in the context of $I^-(H_2O)_n$ clusters.[72,89] However, the region where the excited electron is destabilized by iodine is relatively small and spans only ~10 Å. In fact, when the iodine atom is 15–25 Å away from acetonitrile, the excited electron appears to be stabilized by the the presence of iodine, as the VDE becomes larger than that for the free CH_3CN^-. As the iodine atom moves further away, the stabilization decreases and the VDE starts converging towards the free acetonitrile anion limit. We would like to point out the striking (but, possibly, coincidental) resemblance between the excited electron VDE dependence on the iodine-solvent distance presented in Figure 25*b* and Figure 26*b*, and the experimentally observed time-evolution of the VDE for the relaxation of CTTS

states of iodide-water clusters, very recently reported by Neumark and co-workers (Figures 5 and 6 of Ref. 70). In both cases, the VDE is characterized by initial sharp drop of the VDE, a subsequent rise to a maximum, followed by a small (and slow) decrease towards the asymptotic. Although the relaxation dynamics of excited $I^-(H_2O)_n$ clusters is a much more complex process, where the motion of water molecules plays an extremely important role, this resemblance suggests that the iodine-driven mechanism may, at least partially, explain the behavior of the observed VDEs in experimental studies of the dynamics of photoexcited iodide-water clusters.

The stabilizing role of the iodine atom observed in this work might be essential in order to rationalize the final, slow decrease of the VDE observed in experiments.[70] Hall and Adamowicz have reported a small stabilization of a dipole-bound electron, "sandwiched" between a polar molecule (uracil) and a polarizable rare-gas atom,[318] which might be attributed to dispersion interactions. The stabilization of the excited electron due to the presence of the iodine atom observed in this work (*ca.* 1–1.5 meV) is very similar to the value obtained by Hall and Adamowicz (*ca.* 1 meV) for the stabilization of the dipole-bound electron by He and Ne atoms, and may thus be attributed to dispersion interactions like in the rare-gas case. However, the stabilization energy is almost two orders of magnitude smaller than the final VDE shift observed by Neumark and co-workers for excited $I^-(H_2O)_n$ clusters (50 ± 20 meV).[70]This is possibly due to the much higher electron affinity of water clusters compared to acetonitrile, and therefore a more compact excess electron distribution, which may lead to stronger interactions with iodine. Indeed, Lee *et al.* reported an interaction energy between the iodine and a $(H_2O)_6^-$ cluster of *ca.* 20 meV,[301] a value that might be even larger for larger clusters. Potential energy scans can therefore provide valuable insight into the relaxation dynamics of the CTTS excited states of iodide-solvent clusters. However, even for a simple system such as the binary acetonitrile-iodide complex, simulations of the

real-time dynamics of CTTS relaxation are necessary in order to fully understand and characterize such processes.

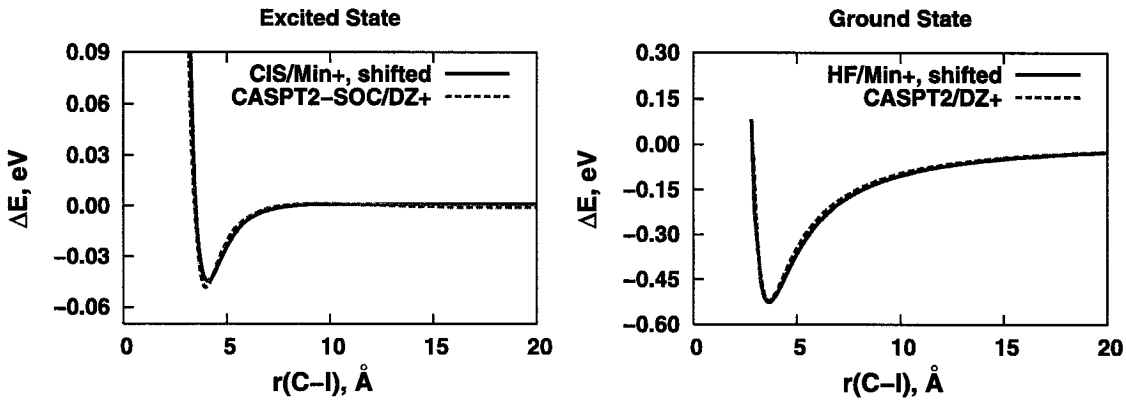

Figure 28. Comparison of the CASPT2-SOC/DZ+ and CIS/Min+ potential curves for the ground state and first excited state of the $I^-(CH_3CN)$ complex. The CIS and HF curves are shifted by -0.158 Å, and the asymptotic limit is set to zero for all curves

V.5. Dynamics of photoexcited $I^-(CH_3CN)$

V.5.a.Method validation

First-principles excited-state molecular dynamics simulations were shown to be necessary to understand the CTTS excited-state relaxation of iodide-solvent clusters,[302] as they provide a real-time dynamic picture which allows direct comparison with state-of-the-art ultra-fast photoelectron spectroscopy experiments. In this approach, the energy and atomic forces are calculated "on the fly" during the propagation of the atomic equations of motion by *ab initio* methods.[314] Unfortunately, molecular dynamics simulations employing high-level *ab initio* methods such as CASPT2 to calculate the energy and forces are not yet feasible. CTTS excited-state dynamics simulations are even more technically challenging, due to the highly diffuse nature of the dipole-bound electron, which leads to serious wavefunction convergence problems. The degenerate

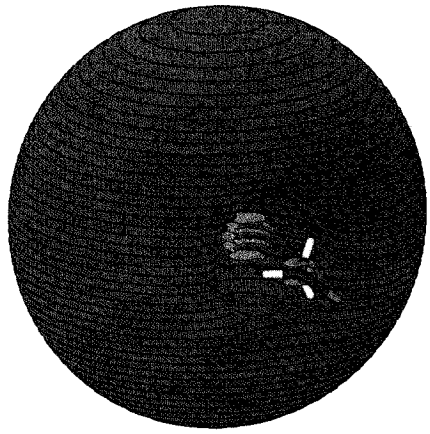

Figure 29. Distribution of the excited electron in the excited $I^-(CH_3CN)$ complex calculated with CIS/Min+ (0.0035 au isosurface)

Excited-state simulations starting from the ground-state equilibrium geometry of the iodide-acetonitrile complex and zero atomic velocities have shown that realistic thermal sampling of initial conditions is necessary for CTTS relaxation simulations. The excited-state well is deep enough (*ca.* 50 meV) to trap all trajectories originating from the Franck-Condon region if the $I^•$ and CH_3CN^- fragments have no initial kinetic energy. Therefore, the thermal Monte-Carlo sampling[311] available in the VENUS molecular dynamics code[312] was employed to generate a set of realistic thermal initial conditions for the ground-state $I^-(CH_3CN)$ complex, which were subsequently used for excited-state simulations. There is a wide uncertainty about the actual temperature of $I^-(CH_3CN)_n$ clusters generated in experiments. In our simulations the temperature of T=150K was chosen to generate initial conditions for the $I^-(CH_3CN)$ complex, as estimated from the Klots theory of the evaporative ensemble,[319] 128 trajectories were then propagated for 2 ps for acetonitrile clusters. Finally, the CIS/Min+ methodology appears to reproduce well the potential energy surface of the excited $I^-(CH_3CN)$ complex, and therefore must provide an adequate description of its relaxation dynamics. However, this model chemistry can not be used for the calculation of VDEs along trajectories, since it

significantly underestimates the dipole-bound electron vertical detachment energies (*ca.* 2–3 meV vs. 11 meV calculated CASPT2/DZ+). Therefore, single-point CASPT2/DZ+ calculations were performed at selected points along the CIS/Min+ trajectories (every 40 fs) to obtain a realistic picture of the VDE evolution during CTTS excited-state relaxation.

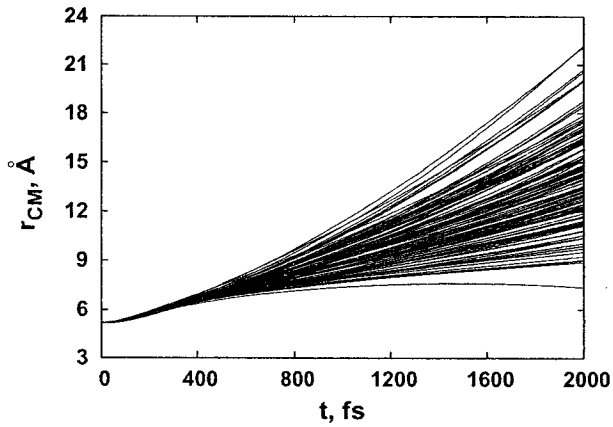

Figure 30. CTTS relaxation dynamics of the $I^-(CH_3CN)$ complex: evolution of the interfragment distance (measured as the distance between the fragment centres of mass, r_{CM})

V.5.b.CTTS relaxation dynamics

As can be seen from Figure 30, the relaxation of the CTTS excited state is generally characterized by reasonably fast dissociation of the complex into I• and CH_3CN^- fragments. By the end of the simulation time, the distance between iodine and acetonitrile is larger than 10 Å for most of the trajectories, the interfragment distance exceeds 20 Å for a few trajectories, and only one trajectory results in a complex loosely trapped in the excited-state potential well. These results are in good agreement with the experimental observation of the acetonitrile dipole-bound anion as the only negatively charged product of $[I^-(CH_3CN)]^*$ relaxation.[61] The evolution of the interfragment relative kinetic energy T_{rel}, shown in Figure 31*a*, is characterized by a rapid increase of the

relative kinetic energy during the first 100 fs, as complex reaches the bottom of the energy well on the excited state potential energy surface (*cf.* Figure 25*b*). As the system climbs out of the potential well, the trajectories start to differentiate: some complexes lose a significant amount of interfragment relative kinetic energy and the relative iodine-acetonitrile motion slows down, and some complexes keep gaining relative kinetic energy. All trajectories lead to dissociation (*cf.* Figure 30), except one for which the distance between the fragments starts decreasing after 1.2 ps. At the end of the simulation time (2 ps), the majority of the trajectories are characterized by a moderate interfragment relative kinetic energy (0.5–3 kcal/mol, Figure 31*c*), whereas a few trajectories gain up to 7 kcal/mol of T_{rel}, and about 20% result in very little T_{rel}.

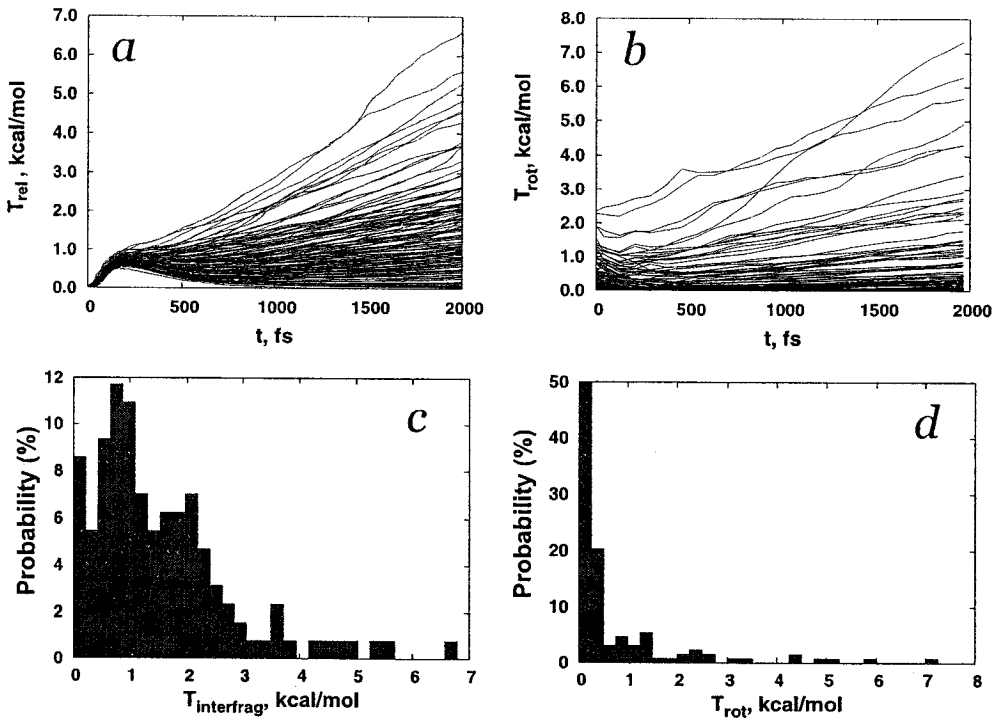

Figure 31. CTTS relaxation dynamics of the $I^-(CH_3CN)$ complex: evolution of the interfragment relative kinetic energy T_{rel} (*a*), rotational energy of the acetonitrile moiety T_{rot} (*b*, averaged over 75 fs); final distribution of T_{rel} (*c*) and T_{rot} (*d*)

The acetonitrile rotational energy, T_{rot}, is close to zero for almost half of the trajectories (*cf.* Figure 31*b* and *d*), and dissociation for these trajectories predominantly proceeds along the complex symmetry axis, on the potential energy surface that resembles the scans shown in Figure 26. On the other hand, if the acetonitrile moiety initially had substantial rotational energy, it gains even more rotational or orbital angular momentum during CTTS relaxation, and in some cases, the CH_3CN^- rotational energy reaches up to 7 kcal/mol at the end of the 2 ps simulation (*cf.* Figure 31*d*). To summarize, the relaxation of the photoexcited $I^-(CH_3CN)$ complex into iodine and the acetonitrile anion is a relatively fast process, the speed of which seems to depend on the initial conditions.

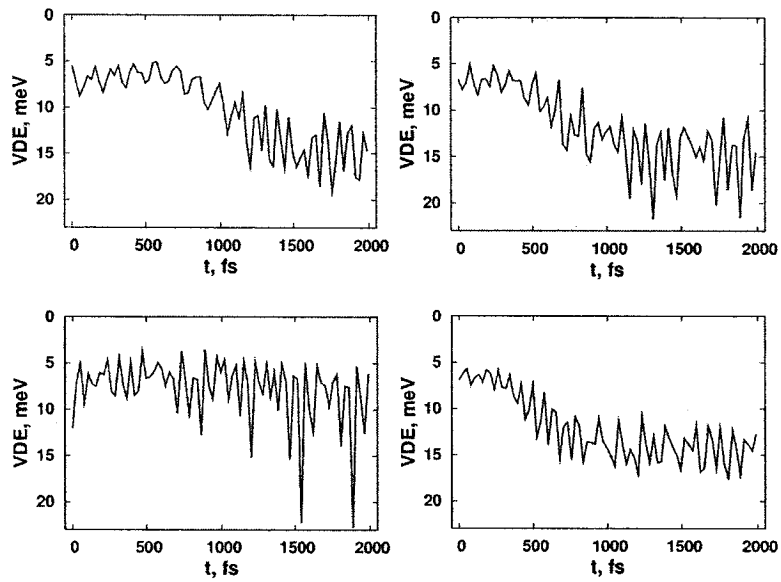

Figure 32. Evolution of the excited electron vertical detachment energy during CTTS relaxation of the excited $I^-(CH_3CN)$ complex for a few typical trajectories, calculated with CASPT2/DZ+ // CIS/Min+. The *y*-axis is inverted to mimic the evolution of the photoejected electron kinetic energy (E_{KE}=-VDE) in femtosecond photoelectron spectroscopy experiments (e.g. Ref. 69)

Individual VDE plots (*cf.* Figure 32) exhibit significant oscillations due to the vibrational and rotational motion of the acetonitrile anion. However, the evolution of the average VDE presented in Figure 33 is relatively smooth. It should be noted that the VDE calculated with CASPT2/DZ+ // CIS/Min+ along the CTTS relaxation trajectories can reach values significantly higher than the VDE of the free acetonitrile anion (*ca.* 11 meV). This can be explained partially by systematic overestimation of the excess electron binding energy calculated with CASPT2/DZ+ for the acetonitrile molecule optimized with CIS/Min+ (*ca.* 13.5 meV). Also, large oscillations of the VDE for some trajectories can be related to vibrational motion of the acetonitrile molecule, which may lead to significant increase or decrease of its dipole moment and thus the excess electron VDE, too.

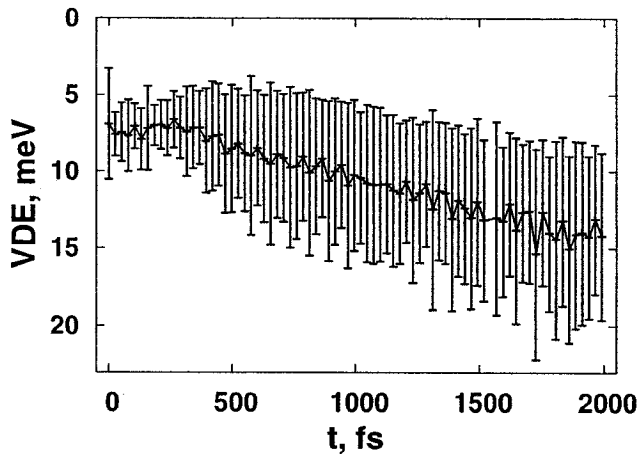

Figure 33. Average excited electron vertical detachment energy during CTTS relaxation of the excited $I^-(CH_3CN)$ complex, calculated with CASPT2/DZ+ // CIS/Min+. The VDE is averaged over 128 trajectories and the error bars represent a standard deviation. The *y*-axis is inverted to mimic the evolution of the photoejected electron kinetic energy (E_{KE}=-VDE) in femtosecond photoelectron spectroscopy experiments (e.g. Ref. 69)

The most interesting feature of the VDE evolution is the induction period up to 400 fs, during which the VDE remains relatively constant, around 6 meV, and the VDE

distribution is rather compact. This is reminiscent of the ~400–500 fs induction period observed by Lehr *et al.* in the CTTS relaxation of excited iodide-water clusters (*cf.* Figure 1 of Ref. 69). Following the induction period, the VDE starts increasing slowly and seems to stabilize around 1.7 ps (*cf.* Figure 33). The origin of the induction period in the VDE during CTTS relaxation of $I^-(CH_3CN)$ can be understood in light of the VDE dependence on the iodine-acetonitrile distance (*cf.* Figure 26). As can be seen from Figure 4, the lowest VDEs correspond to the excited-state potential energy well region, and the VDE rise roughly starts when the potential energy reaches a plateau (*cf.* Figure 26*b*). Since different trajectories with different initial conditions pass the minimum VDE region at slightly different times (*cf.* Figure 32), the average VDE value remains nearly constant during the first 300-400 fs. The initial drop of the VDE from the Franck-Condon region to the VDE minimum (*cf.* Figure 26*b*) is practically washed out in averaging over trajectories (*cf.* Figure 33). The maximum in the VDE (*cf.* Figure 26*b*) also does not seem to be reflected in the VDE time-evolution of Figure 33 for the same reason. It should be noted, that in experimental femtosecond spectroscopy studies[70] of iodide-water clusters, a distinct maximum of the VDE during CTTS relaxation is observed for larger clusters ($n \geq 9$), but not for the smaller clusters.[70]

The distribution of VDE values over the number of trajectories is rather disperse, due to the different relative positions of the $I^•$ and CH_3CN moieties and the vibrational distortion of the acetonitrile molecule which affects the binding of the excited electron. This emphasizes the importance of realistic molecular dynamics simulations that properly describe the evolution of the excited electron binding during the CTTS relaxation. As a note of caution, the current simulations included only 128 trajectories, and larger-scale simulations might possibly show sharper features of the VDE dynamics by providing more realistic averages.

The iodide-acetonitrile complex is a prototype system which presents a unique opportunity to investigate pure iodine-driven CTTS relaxation, unhindered by the rearrangement of solvent molecules in the cluster. Thus, it is rather surprising that the resulting evolution of the excited electron binding energy appears to have very similar features as that for CTTS relaxation in much more complex iodide-water clusters. Undoubtedly, the solvent rearrangement is one of the most important aspects of the $[I^-(H_2O)_n]^*$ relaxation process, and it would be rather naive to interpret the experimentally observed dynamics solely in terms of the iodine-driven mechanism. However, the present results indicate that the separation between the nascent solvent cluster anion and the iodine atom has a profound effect on the VDE of the excited electron during CTTS relaxation. Therefore, our results once again suggest that the rich and complex dynamics of photoexcited iodide-solvent clusters is a result of the synergy between the solvent- and iodine-driven mechanisms.

V.6. Summary and concluding remarks

In this paper, we presented a detailed investigation of the photoexcitation and photoionization of the binary iodide-acetonitrile complex using high-level *ab inito* methods. The calculations reproduce qualitative and quantitative aspects of the photoexcitation and photoionization of the $I^-(CH_3CN)$ complex, in excellent agreement with available experimental data, thus providing solid grounds for the computational investigation of the charge-transfer-to-solvent (CTTS) excited state relaxation processes. To this end, the potential energy curves for the ionized and CTTS excited states were calculated in order to unveil the dependence of the excited electron binding energy on the iodine-acetonitrile distance. It was found that, whereas the neutral iodine atom destabilizes the excited dipole-bound electron at short distances, it also can slightly

stabilize it at larger distances due to dispersion forces. An efficient two-level scheme for first-principles molecular dynamics simulations of the photoexcited $I^-(CH_3CN)$ complex was developed, which makes use of a lower-level economic model chemistry used to propagate the equations of motion along the trajectories, and a higher-level calculations to obtain the vertical detachment energy (VDE) of the excited electron. Extended excited state molecular dynamics simulations with realistic initial conditions were then performed for the CTTS relaxation dynamics of the iodide-acetonitrile complex. The resulting evolution of the excited electron vertical detachment energy shows features very similar to the experimental data for photoexcited iodide-water clusters, suggesting that the departing iodine atom may play an important role, in addition to the solvent dynamics, in the relaxation of the photoexcited $[I^-(H_2O)_n]^*$ clusters.

V.7. Supporting information

Extra diffuse exponents used in the DZ+ basis set

```
7.1207E-03
2.2046E-03
6.8253E-04
2.1131E-04
6.5421E-05
2.0254E-05
6.2706E-06
1.9414E-06
```

Cartesian coordinates for the $I^-(CH_3CN)$ complex optimized with MP2/DZ

```
Charge = -1; multiplicity = 1
E(MP2)= -143.83281184 Hartree
C          0.0000000000        0.0000000000       -3.8730950939
C          0.0000000000        0.0000000000       -2.4152644839
H          1.0129871700        0.0000000000       -2.0221310986
H         -0.5064935850       -0.8772726229       -2.0221310986
H         -0.5064935850        0.8772726229       -2.0221310986
N          0.0000000000        0.0000000000       -5.0443941539
I          0.0000000000        0.0000000000        1.2001015161
```

Chapter VI

Further insight into the relaxation dynamics of photoexcited $I^-(H_2O)_n$ clusters

Published as:

Qadir K. Timerghazin and Gilles H. Peslherbe, Journal of American Chemical Society, 125 (33), 9904-9905 (2003)

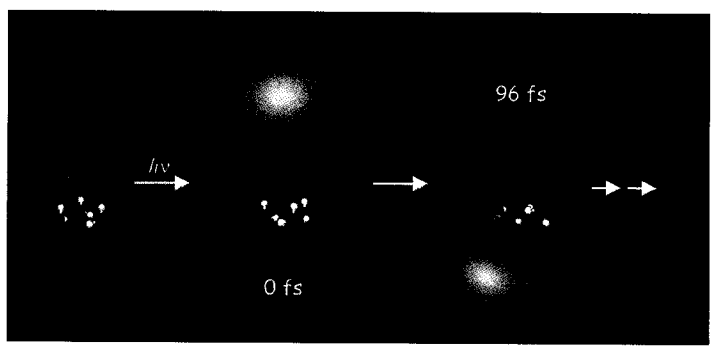

One of the fascinating features of anions dissolved in water, especially halides, is the possibility of photochemical transfer of an electron from the ion to the bulk solvent. The electron will be stabilized by the field of polar solvent molecules, giving rise to so-called charge-transfer-to-solvent (CTTS) excited states, which eventually lead to the solvated electron. In 1996, Johnson and co-workers were able to experimentally observe cluster analogs of the bulk CTTS states in clusters of iodide with one to four water molecules.[68] It was found that subsequent relaxation of the excited cluster may lead to the ejection of the neutral iodine atom and formation of a dipole-bound water cluster anion $(H_2O)_n^-$.

It is now well established that small to medium sized iodide-water clusters tend to have surface structures, where the iodide ion tends to sit at the surface of the hydrogen-bonded water network.[59,180] The cluster structures are governed by a combination of the interaction of the negatively charged I^- with the dipole moment of the entire water network, and the hydrogen-bonding interactions of the "dangling" hydrogen atoms with the iodide ion.[59] Upon photoexcitation, it was shown unambiguously that an electron from a I^- valence *p* orbital is transferred to a very diffuse solvent molecular orbital, where it is supported by the stabilizing interaction with the dipole moment of the solvent network, reflecting actual charge transfer to solvent.[89,298] As a matter of fact, the excited electron distribution in the excited state of iodide-solvent clusters in the Frank-Condon region has been found to be very similar to the electronic structure of the corresponding dipole-bound solvent cluster anions. The only significant difference between excited $[I^-(H_2O)_n]^*$ and $(H_2O)_n^-$ is the presence of the neutral iodine atom which destabilizes the excited electron. Moreover, the ion-dipole interactions, which kept the ion and solvent molecules together in the ground state, no longer exist in the excited state. Thus, profound structural changes are expected as the system relaxes after photoexcitation.

Neumark and co-workers applied femtosecond photoelectron spectroscopy techniques to study the relaxation dynamics of photoexcited $I^-(H_2O)_n$ clusters (n= 4–6), unveiling interesting dynamical characteristics of the excited electron in clusters of different sizes.[69] For the smallest cluster investigated $I^-(H_2O)_4$, the electron binding energy was found to remain constant throughout the measurement time window (2 ps), and the population of photoexcited clusters decayed exponentially because of the spontaneous ejection of the dipole-bound electron from the vibrationally excited water cluster. On the other hand, for $I^-(H_2O)_5$ and $I^-(H_2O)_6$, an induction period of *ca.* 500 fs was observed, during which the electron binding energy is constant, before it increases by ~0.3 eV, and the population of excited clusters start decaying until the end of observation time (2 ps). To rationalize their observations, Neumark and co-workers put forward the hypothesis that the rise in electron binding energy after the first 500 fs is due to reorganization of the water molecules in $I^-(H_2O)_5$ and $I^-(H_2O)_6$ clusters.[69,71] While the 4 water molecules in $I^-(H_2O)_4$ may not be able to rearrange and efficiently stabilize the excess electron transferred from iodide, 5 and 6 water molecules are known to bind an excess electron in a number of cluster configurations. Therefore, in the 500 fs following photoexcitation, the water molecules in $I^-(H_2O)_5$ and $I^-(H_2O)_6$ clusters are assumed to gain configurations which can support the excess electron much more efficiently than in the initial cluster configuration. This model is based solely on the consideration of solvent dynamics, neglecting the possible role of the neutral iodine atom formed by photoexcitation, and is hereafter referred to as the "solvent-driven" relaxation dynamics model. This model also accounts for the pronounced isotope effects observed, i.e. a longer induction period for $I^-(D_2O)_n$ than for $I^-(H_2O)_n$.[69,71]

Recently, Chen and Sheu proposed an alternative interpretation for the femtosecond experiments, based on quantum-chemical calculations, in which the stabilization of the excited electron is rationalized by the ejection of the neutral iodine

atom from the water cluster.[72,73] Quantum-chemical calculations show that the presence of the neutral iodine atom can considerably destabilize the excited electron in excited $I^-(H_2O)_n$ clusters, and thus as the iodine atom leaves the water cluster, the electron binding energy must increase significantly. According to this "iodine-driven" model of relaxation dynamics, a $I^-(H_2O)_4$ cluster would undergo iodine atom ejection on a very fast timescale, i.e. less than 100 fs, and only the dynamics of the $(H_2O)_4^-$ cluster product could be monitored. On the other hand, iodine would leave photoexcited $I^-(H_2O)_5$ and $I^-(H_2O)_6$ clusters more slowly, giving rise to the experimentally observed induction period. The main problem with the latter model is that it is based on static quantum-chemical calculations, which have the water cluster moiety frozen in the geometry of the cluster before photoexcitation. Excited-state quantum-chemical calculations of $I^-(H_2O)_4$ clusters by Vila and Jordan indeed showed that the excited state potential energy surface is repulsive along the hydrogen atom "flip" coordinate, which further supports the importance of solvent motion.[296]

None of the models proposed so far to interpret femtosecond experiments treats the relaxation of iodide-water clusters as a whole, neglecting either the role of the iodine atom or that of solvent reorganization. In the present Communication we report preliminary results from *ab initio* molecular dynamics simulations of $I^-(H_2O)_3$ relaxation. The electronic structure calculations were performed with the CASSCF technique,[239] as implemented in the MOLPRO program.[247] Computational details, including the active space and basis sets used,[41,91,296,310,320] as well as the molecular dynamics simulation procedure[314] are given in the Supporting Information section. In spite of its small size, $I^-(H_2O)_3$ possesses the crown-like structure characteristic of $I^-(H_2O)_n$ clusters with $n \leq 6$ and, even though there are no explicit experimental data on the relaxation dynamics for this cluster size, it can serve as a good model to gain some

insight into the general features of the excited-state time-evolution of larger $I^-(H_2O)_n$ species.

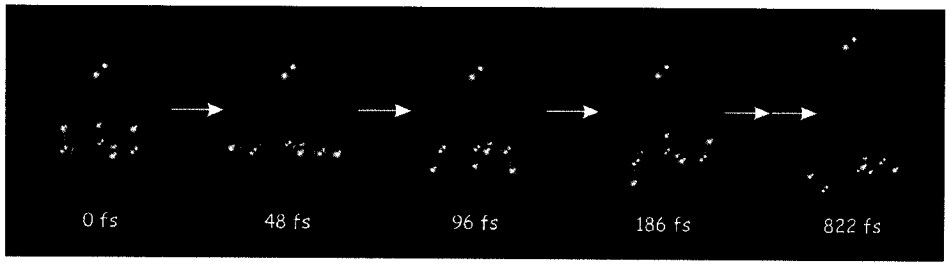

Figure 34. Snapshots of selected configurations along the trajectory of photoexcited $I^-(H_2O)_3$ relaxation

According to our simulations, the "dangling" hydrogen atoms which formed hydrogen bonds with iodide in the ground state, start moving away from the iodine atom, and in less than 50 fs the structure of the water cluster becomes almost flat (Figure 34, 48 fs), which is accompanied by a drop in the system potential energy. But because of the kinetic energy acquired, hydrogen atoms keep moving, until the water cluster moiety reaches an "inverted crown" structure (Figure 34, 96 fs). The latter structure is higher in energy than the "flat" structure, and the hydrogen atoms thus continue their oscillatory motion. In general, the relaxation process involves rapid oscillatory motion of the water molecules which results in abrupt oscillations in the system potential and kinetic energies (*cf.* Figure 35). After the first oscillation, the synchronicity of the water motion appears to be disrupted (Figure 34, 186 fs), as energy is transferred to other cluster vibrational modes, and the oxygen atoms and the hydrogen atoms which are involved in the water-water hydrogen bonding start gaining additional kinetic energy (*cf.* Figure 35). The water network undergoes deformations during the trajectory, and water-water hydrogen bonds break and form back and forth a few times. Meanwhile, the heavy iodine atom is slowly leaving the water cluster: the distance between iodine and the centre of mass of the $(H_2O)_3$ moiety reaches 6.3 Å in less than 900 fs (Figure 34, 822 fs), while it is

only 3.44 Å in the initial Frank-Condon geometry. As evident from Figure 35, the kinetic energy gained following photoexcitation appears mainly partitioned into the rotational and vibrational modes of water molecules.

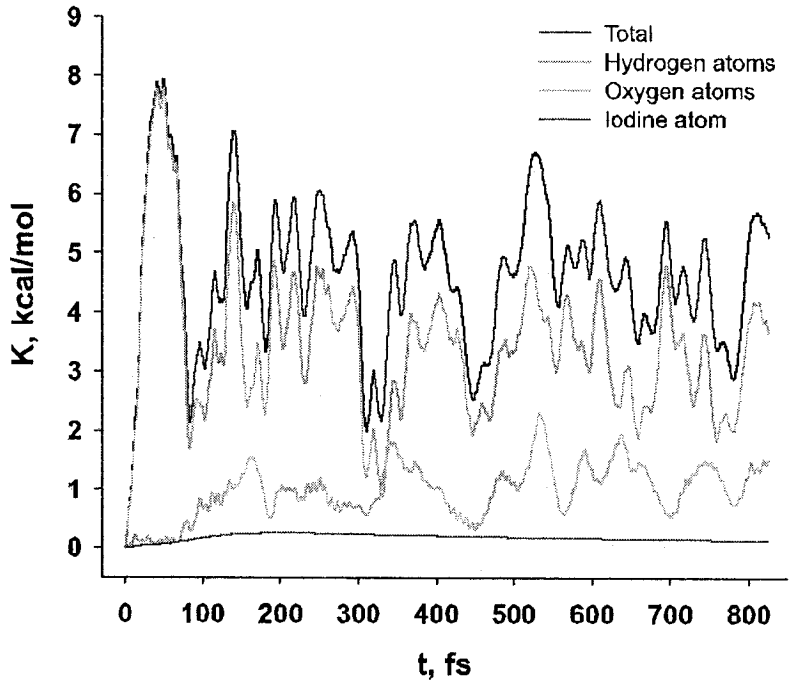

Figure 35. Time-evolution of the kinetic energy for the photoexcited $I^-(H_2O)_3$ cluster: total kinetic energy, kinetic energy of the iodine atom and kinetic energy of all oxygen and all hydrogen atoms

The main features of the relaxation of photoexcited iodide-water clusters that emerge from this preliminary study are the oscillatory motion of water molecules and the slow recoil motion of the neutral iodine atom. Rapid changes in the relative orientation of the water molecules that result from the interconversion of "crown" and "inverted crown" structures cause rapid changes in the total dipole moment of the $(H_2O)_n$ moiety, and in the excited electron distribution that follows the aggregate dipole. Thus, the binding energy of the excited electron must also undergo oscillatory changes along a given trajectory. However, in the femtosecond experiments of Neumark and co-workers, the measured electron binding energy is changing quite smoothly.[69] This may be

explained by the fact that at finite experimental temperatures, ground-state $I^-(H_2O)_n$ clusters exist in various configurations and isomers. The observed experimental signal is an average over the whole ensemble of possible initial cluster structures, which may lead to observed smooth changes in ensemble-averaged electron binding energies. A large number of trajectories, starting with many different initial cluster configurations, will thus be needed to make a thorough connection with experiment for larger clusters. However, the present simulations already suggest that the relaxation of photoexcited $I^-(H_2O)_n$ clusters is a complex process, where both the role of iodine and solvent motion must be included in order to fully rationalize experimental observations.[69] While the rapid motion of water molecules observed in our simulations clearly supports the "solvent-driven" model of relaxation dynamics, the role of iodine motion may also be critical in determining the time-evolution of the electron binding energy following photoexcitation, which is consistent with the "iodine-driven" model of cluster relaxation dynamics.

VI.1. Appendix: computational details

Ground and excited state electronic structure calculations were carried out using the state-averaged Complete Active Space Self-Consistent Field (CASSCF) formalism,[239] with the active space consisting of two *p* orbitals of the iodine atom – which are doubly occupied in the ground state – and the lowest unoccupied orbital – which accommodates the excited electron upon photoexcitation. Inclusion of the highest two *p* orbitals of iodide was necessary to insure fast convergence of the CASSCF calculation at the beginning of the simulation when the system is nearly symmetric and the two *p* orbitals are nearly degenerate. With the (2,2) CAS that was employed in Ref. 6, the excited-state wavefunction oscillates between two nearly degenerate solutions, which significantly deteriorates the convergence. We have also tested CASSCF calculations with (6,4) and

(6,6) active spaces and found that the results were practically the same as with the (4,3) CAS which we used in our molecular dynamics simulations.

The basis set used in this work is based on the standard 6-31+G(d,p) basis set by Pople and co-workers,[91] which was used in its original form for hydrogen and oxygen atoms. For iodine, we used the LANL2DZ effective core potential (ECP) basis set by Hay and Wadt,[320] augmented by d-polarization functions with the optimized exponents of Check *et al.*[310] Further, a special set of uncontracted Gaussian basis functions, with diffuse exponents, was added to allow for a proper description of the dipole-bound excited electron. In contrast to static quantum chemical calculations of dipole-bound cluster anions $(H_2O)_n^-$ or dipole-bound $[I^-(H_2O)_n]^*$ excited states,[41,296] the *ab initio* molecular dynamics simulations demand an even more diffuse basis set, which can describe the excited electron along the whole trajectory, where the cluster structure can change dramatically during the relaxation process. In order to construct a diffuse basis set, flexible enough for dynamical calculations, we added a number of diffuse *sp*-shells centered on the iodine atom, with exponents α_{sp}= 3.0800×10^{-2}, 4.4000×10^{-3}, and 6.2857×10^{-4}. Two *sp*-shells with exponents α_{sp}= 3.6000×10^{-2}, 5.1429×10^{-3} and one s-shell with exponent $\alpha_s=7.3469\times10^{-4}$ were also centered on each of the three "dangling" hydrogen atoms, *i.e.* those that are not involved in water-water hydrogen bonding in the cluster. All quantum-chemical calculations were performed with the MOLPRO suite of *ab initio* programs.[247] The molecular dynamics simulation was initiated with the cluster in its ground state minimum energy structure with no kinetic energy, and the classical equations of motion were propagated for all atoms with the velocity Verlet algorithm, with energy and gradient calculated at each time step by the quantum-chemical procedure just described.[314] A time-step of 0.3 fs was used, and the trajectories were propagated for up to 900 fs.

Chapter VII

A theoretical study of the dipole-bound and valence-bound acetonitrile anions

Submitted as:

Qadir K. Timerghazin and Gilles H. Peslherbe, *Physical Chemistry Chemical Physics* (2006)

VII.1. Introduction

The interaction of a free electron with a neutral molecule is one of the most fundamental processes in chemistry. In many cases, an additional (or excess) electron can be accommodated in an empty or half-filled valence orbital of the accepting molecule, giving rise to a so-called valence-bound (VB) anion. However, if the molecule which accepts an electron does not have a suitable valence orbital, but possesses a sufficiently high multipole (dipole, quadrupole, etc.) moment, the excess electron can be loosely trapped in the electric field exerted by the molecule, thus producing a so-called multipole-bound anion.[26,321,322] Dipole-bound (DB) anions are the most abundant among the multipole-bound anions, although a number of quadrupole-bound anions have also been reported in the literature.[322-324] The most interesting situation arises when the dipole moment of the electron-acceptor molecule is high enough to trap an electron in its field and, at the same time, the molecule possesses a low-lying empty valence orbital which can also accommodate the excess electron.

Mutual interconversion of the dipole- and valence-bound states of molecular anions is a very important yet complex process.[75,80,325,326] This topic has recently attracted considerable attention since the trapping of low-energy electrons by biochemically-relevant molecules in dipole-bound states, with subsequent transformation of the dipole-bound anions into valence-bound radical anions may be an important step in the radiation damage of DNA and RNA molecules.[77,326,327] The excess negative charge distribution in valence-bound anions is much more compact than that of dipole-bound anions, so the balance between the dipole-bound and valence-bound anionic states can be significantly altered by the medium. One of the most profound examples of medium effects on the balance between the dipole- and valence-bound forms of the molecular anions is the excess electron binding by acetonitrile molecules.

The dipole-binding of an excess electron by acetonitrile molecule and clusters in the gas phase has been studied extensively;[42,61,328,329] in fact the acetonitrile dipole–bound anion was among the first dipole-bound anions to be observed experimentally.[24] The CH_3CN^- anion can be efficiently produced by Rydberg electron transfer[24,316] or by relaxation of charge-transfer-to-solvent (CTTS) excited states of the binary iodide-acetonitrile complex $I^-(CH_3CN)$,[61] and the binding energy of the excess electron to the neutral molecule (or, in other words, the anion ionization potential) is about 10–20 meV.[47,61,316] Johnson and co-workers have also synthesized the acetonitrile dimer anion $(CH_3CN)_2^-$ by photoexcitation and CTTS relaxation of the ternary iodide-acetonitrile cluster $I^-(CH_3CN)_2$, and postulated a resulting linear head-to-tail structure $NCCH_3\cdots NCCH_3^-$.[61] Experimental observations of larger acetonitrile anion clusters have also been reported.[330,331]

The lowest unfilled valence π^*(C–N) orbitals of acetonitrile are significantly higher in energy (by *ca.* 2.8 eV) than the dipole-bound orbital,[332] and the valence-bound CH_3CN^- anion exists in the gas phase only as a metastable anion in an unbound state.[329,332] On the other hand, experimental studies of γ- or X-ray irradiated solid[333,334] and liquid[335,336] acetonitrile strongly suggest that, in a polar medium, the CH_3CN molecules can bind excess electrons into valence orbitals, thus forming valence-bound radical anions. In the early works of Williams and co-workers[333,337] and the recent work of Shkrob and co-workers,[334] EPR and UV-vis spectroscopies were used to study solid acetonitrile treated with γ or X radiation. It was shown that, depending on the crystal structure, two distinct species can be produced: a dimeric form of the acetonitrile radical anion $(CH_3CN)_2^{\bullet-}$ was found in α-acetonitrile, whereas monomeric acetonitrile radical anions CH_3CN^- were found in β-acetonitrile. Recent work by Shkrob *et al.*[335] and Xia *et al.*[336] showed that, in liquid acetonitrile, an excess electron may exist in two forms: the dimer radical anion (as in solid acetonitrile) and the classical solvated electron. The

latter exists as a separate entity in the solvent cavity stabilized by the aggregate field of the solvent, and can be considered as a condensed-phase analog of the dipole-bound electron. In liquid acetonitrile, both these two forms — the valence-bound anion and the solvated electron — exist as a result of a dynamic equilibrium. On the other hand, the $CH_3CN^{\bullet -}$ monomer anion seems to react readily with a neutral CH_3CN molecule to form the dimer anion, thus $CH_3CN^{\bullet -}$ can only be observed in solid β-acetonitrile, whose crystal structure precludes dimerization.[333,334]

Until very recently, it was accepted that gas-phase acetonitrile clusters $(CH_3CN)_n$ can bind an electron only in the dipole-bound/solvated electron manner. However, in the recent photoelectron spectroscopy study of Mitsui *et al.*[331] it was shown that the valence-bound state starts to emerge in the clusters as small as $(CH_3CN)_{11}^-$. According to these experiments, the dipole-bound and valence-bound forms coexist for clusters with n = 11 – 100; however, for clusters with $n \geq 13$ the valence-bound form prevails.[331] There is also some indirect evidence for the existence of valence-bound acetonitrile anions in small solvent clusters. For example, Balaj *et al.*[338] reported that a neutral acetonitrile molecule inside water cluster anions undergoes a hydrogen atom addition reaction. The proposed reaction mechanism[338] involves transfer of the excess electron to the acetonitrile molecule and subsequent reaction of the valence-bound $CH_3CN^{\bullet -}$ radical anion with a water molecule. Thus, recent experimental results suggest that even very limited solvation seems to be able to stabilize valence-bound acetonitrile anions, and that these species may play a much more important role than previously thought.

According to the early EPR spectroscopy studies,[333] the dimer anion appears to have a symmetric structure with the spin density mostly localized on the nitrogen atoms (*ca.* 75 %), and to a lesser extent on the cyanide carbons (*ca.* 25%). Williams and co-workers proposed that, in $(CH_3CN)_2^{\bullet -}$, the two acetonitrile moieties are oriented in an antiparallel fashion with the excess electron residing in a delocalized molecular orbital

formed by the combination of two π^*(C–N) orbitals. Whereas the acetonitrile moieties in the dimer anion were considered to remain linear, for the monomer anion CH_3CN^-, the C–C–N angle was estimated to be 130°. In the case of the monomer anion, the spin density is also concentrated mainly on the nitrogen atom (*ca.* 55%).

In the recent works by Shkrob *et al.*[334] and Xia *et al.*,[336] the first quantum chemical calculations of the acetonitrile radical anions were reported. According to density-functional theory (DFT) calculations with double-zeta quality basis sets (3-21G to 6-31++G**), the acetonitrile molecules possess a bent geometry, with a C–C–N angle of 127°–135° in both the monomer and dimer anions. The distance between the two cyanide carbon atoms appears to be relatively short (1.6 – 1.8 Å), which suggests a "pseudo-bond".[334] Whereas calculations predict the valence-bound dimer anion to be kinetically stable even in the gas phase, a stationary point on the potential energy surface (PES) can only be found for the valence-bound monomer $CH_3CN^{\bullet-}$ in a polar solvent represented by continuum solvation models.

No in-depth investigations of the peculiar electronic structure of the valence-bound acetonitrile anions have been reported to date, and the information about the dipole-bound dimer anions is also pretty scarce. For instance, the nature of the C–C "pseudo-bond" in the valence-bound dimer anion is quite intriguing, but it has not been well characterized experimentally or computationally. The changes in the electron density distribution in the acetonitrile molecule(s) upon addition of an excess electron to the valence orbitals and solvent effects on the electronic structure have also not been addressed yet. Moreover, the wavefunction of the open-shell valence-bound acetonitrile radical anions is expected to possess high multi-reference character; however, only single-determinant unrestricted DFT and second-order Møller-Plesset (UMP2) perturbation theory calculations have been reported so far for these systems. In these unrestricted single-determinant calculations, the spin contamination can be a serious

problem, especially in the case of UMP2 calculations. On the other hand, the dipole-bound anions can be well described by single-reference *ab initio* calculations, but such calculations require very diffuse basis sets and an extensive treatment of electron correlation to correctly describe the excess electron binding.

In this work, we report a quantum-chemical investigation of the structure, excess electron binding and relative stability of the dipole-bound and valence bound acetonitrile anions $(CH_3CN)_n^-$ (n = 1, 2). In order to gain some insight into the electronic structure of the acetonitrile anions, a topological analysis of the electron density was used within the framework of the quantum theory of Atoms in Molecules (QT AIM).[99,157] The outline of this article is as follows. The computational methodology is first described in Section 2. The structure, stability and topology of the electron density distribution of the dipole-bound acetonitrile dimer anions are presented in Section 3, while Section 4 is devoted to the molecular and electronic structure of the valence-bound acetonitrile monomer and dimer anions in the gas phase and in liquid acetonitrile. Concluding remarks follow in Section 6.

VII.2. Computational methods

The geometry of dipole-bound and neutral acetonitrile dimer anions was optimized with unrestricted second-order Møller-Plesset (UMP2) theory,[91] and single-point energies were calculated with unrestricted coupled clusters with single and double excitations (UCCSD).[339] The Dunning-Hay split valence polarized (SVP) basis set augmented with diffuse functions (SVP+) was used for all atoms,[340] except for the methyl group carbons, for which the SVP basis set was augmented with 2*s* and 2*p* Rydberg functions[340] and additional 2*s* and 2*p* functions with exponents obtained in an even-tempered manner from those of the initial Rydberg functions (the smallest exponent is

2.6×10^{-4} au). For brevity, this basis set will be referred to as SVP+R. Also, a somewhat larger augmented double-zeta correlation-consistent basis set by Dunning[135] has been used with additional 3*s* and 3*p* diffuse functions on the methyl group carbon atoms (the exponents used: 5.625×10^{-2}, 1.125×10^{-2} and 0.225×10^{-2});[47] this basis set will be referred to as aVDZ+R. The thermodynamic properties of the dipole-bound and neutral acetonitrile dimer anions were calculated under the rigid-rotor/harmonic-oscillator approximation using harmonic frequencies calculated with UMP2/ SVP.

The valence-bound acetonitrile dimer anion is an open-shell molecule with the excess electron delocalized over the valence orbitals of the two parent acetonitrile molecules, which have a highly distorted geometry compared to that of the free acetonitrile molecule. Thus, single-reference unrestricted *ab initio* methods do not seem to be applicable in this case: indeed, unrestricted Hartree-Fock (UHF) calculations give highly spin-contaminated wavefunction with $\langle S^2 \rangle > 0.95$, which renders unreliable the results obtained from post-Hartree-Fock correlation treatments (e.g. perturbation theory) which use the UHF wavefunction as a reference. The complicated electronic structure of the valence-bound acetonitrile anions thus dictates the use of mutli-configurational *ab inito* methods. On the other hand, dipole-bound anions can be reliably described by single-reference post-Hartree-Fock methodologies, but they require an extensive treatment of electron correlation preferably with coupled-clusters methodologies. It is worth noting that DFT methods are generally not suitable for description of systems with a dipole-bound electron.[26] Thus, the proper description of the dipole- and valence-bound acetonitrile anions requires using different computational methodologies, similarly to the approach Gutsev and Barlett used for the nitromethane anions.[76]

In this work, we have applied the complete active space self-consistent field[238,239,341] (CASSCF) method for calculations of the valence-bound acetonitrile anions.

For the dimer anion, the active space included four doubly occupied orbitals, the singly occupied orbital, and three virtual orbitals, thus yielding a (9,8) active space. In the case of the valence-bound acetonitrile monomer anion a (7,7) active space was used. The shapes and occupancies of the active space orbitals are given in Figure 42 and Figure 43 of Supporting information section. In order to improve the CASSCF results by including dynamic electron correlation, we employed the second-order multireference perturbation theory[305,342] (CASPT2) with the CASSCF reference wavefunction just described. Both the CASSCF and CASPT2 calculations employed the Dunning-Hay polarized split valence basis set augmented with diffuse functions (SVP+).[340] Additionally, DFT calculations were performed with PBEO functional.[198] Unrestricted density-functional theory methods will also be used, as are they known to perform relatively well for open-shell molecules with nearly multi-configurational character.[343,344] PBEO calculations employed an augmented polarization-consistent basis set (aug-pc-1) recently developed by Jensen and specifically designed for DFT calculations.[345-348]

UMP2 and UCCSD calculations were performed with the Gaussian 03 program package,[349] and gas-phase CASSCF and CASPT2 calculations were performed with the MOLPRO[102] suite of *ab initio* programs, while all PBEO calculations were performed with the Gaussian 98 package.[100] Solvent effects were included using the conductor-like polarizable continuum model (CPCM) by Barone and Cossi,[350,351] as implemented in Gaussian 98 for PBEo calculations, and in Gaussian 03[349] for CASSCF calculations. The topology of the electron density distribution was analyzed with the AIMPAC program package,[140] using electron densities obtained from CCSD, CASSCF and PBEO calculations.

VII.3. Dipole-bound acetonitrile dimer anions

The dipole-bound acetonitrile monomer anion has been extensively studied (*cf.* Ref. 47 and Chapter V), and therefore we concentrate in this work on the structure and stability of the acetonitrile dimer anions. Numerous computational studies[352-357] suggest that there are two possible isomers for the neutral acetonitrile dimer: a cyclic structure with antiparallel orientation of the dipoles and a collinear, head-to-tail structure:

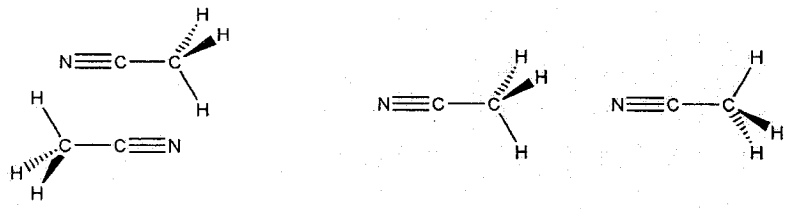

cyclic collinear

The more stable cyclic dimer, with the binding energy of 5–6 kcal/mol,[355] has a net zero dipole moment and can not bind an electron in a dipole-bound fashion, which explains why Rydberg electron transfer experiments failed to produce acetonitrile dimer anions by attaching an electron to a neutral dimer.[66] On the other hand, the higher-energy collinear isomer, with a binding energy of *ca.* 3 kcal/mol, has a substantial dipole moment of *ca.* 8.5 D,[355] and certainly can give rise to a dipole-bound acetonitrile dipole anion. Indeed, one of the two possible isomers of the dipole-bound acetonitrile dimer anion found in this work clearly originates from electron attachment to the collinear acetonitrile dimer, as shown in Figure 36. The excess electron distribution in this collinear isomer of the acetonitrile dimer anion is very similar to the dipole-bound anion of acetonitrile (*cf.* Figure 24). However due to its larger dipole moment, the collinear acetonitrile dimer has a much larger excess electron vertical detachment energy (VDE) – 102 meV according to UCCSD/aVDZ+R//UMP2/SVP+R, *vs.* 10–12 meV for the acetonitrile monomer (*cf.* Chapter V and Refs. [47,61,316]).

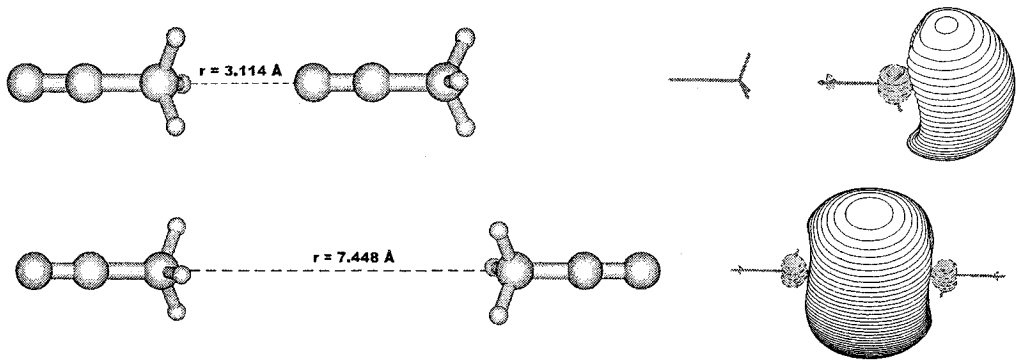

Figure 36. Structures (with relevant geometrical parameters) of the dipole-bound acetonitrile anions and corresponding excess electron distributions (CCSD singly occupied natural orbitals, 0.011 au isosurfaces)

On the other hand, the structure of the second isomer of the acetonitrile dimer anion shown in Figure 36 is drastically different from that of the neutral acetonitrile dimers, and is characterized by two acetonitrile monomers facing each other, with the excess electron "sandwiched" in between the acetonitrile methyl groups. Unlike the collinear head-to-tail isomer, this head-to-head isomer can only exist due to the presence of the excess electron, which is screening the repulsive interaction between the acetonitrile dipoles. Removal of the excess electron would lead to highly repulsive $NCCH_3\cdots H_3CCN$ interactions that will result in dissociation. Therefore, it is not surprising that the VDE for the second dimer anion (155 meV, calculated with UCCSD/aVDZ+R // UMP2/SVP+R) is significantly larger than for the collinear head-to-tail isomer. A number of similar cluster anions with the excess electron trapped between molecular dipoles have been recently predicted.[48,318,358-361] These structures were referred to as having an "internally suspended electron",[318,358] a "solvated electron",[48] or an "e⁻-bond".[360] Combined experimental and computational investigation by Gutowski *et al.* have provided compelling evidence that the hydrogen fluoride trimer anions $(HF)_3^-$ may exist in two forms at finite temperature in the gas phase: a chain dipole-bound isomer $FH\cdots FH\cdots FH^-$ and a "solvated electron" structure $HF(e^-)HF\cdots HF$, where the excess

electron is trapped between a hydrogen fluoride molecule and a hydrogen fluoride dimer.[48] It is worth noting that the competition between the surface and internal solvation of the excess electron in water cluster anions is a matter of on-going dispute.[33,35-37,362,363] The possible existence of the two isomers of the acetonitrile cluster anion raises several important questions, regarding the relative stability of these isomers at finite temperature, and as to which isomer was produced experimentally via photodissociation of the $I^-(CH_3CN)_2$ cluster. It is also of interest to investigate the intermolecular bonding between the acetonitrile molecules via an "e^--bond" in detail.

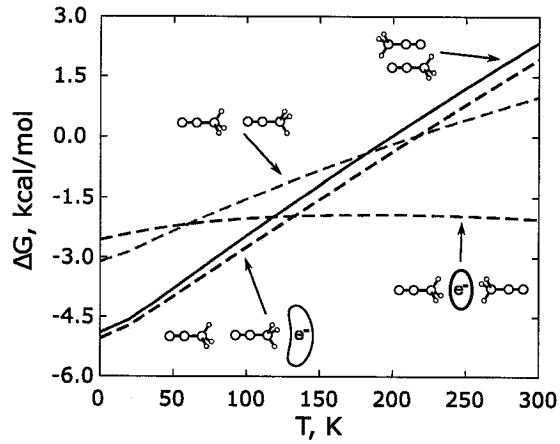

Figure 37. Temperature dependence of the relative Gibbs free energies of the neutral acetonitrile dimers and dimer anions. The free energy difference is that of the free acetonitrile molecules and a free electron in the case of anions

We first turn our attention to the relative stability of the neutral and anionic acetonitrile dimers in the gas phase. Figure 37 displays the temperature dependence of the Gibbs free energy for these species, relative to the free energy of the dissociated species. At 0 K, the most stable form of the acetonitrile dimer is the collinear head-to-tail dipole-bound anion, whereas the head-to-head dimer anion is the least stable of all neutral and anionic acetonitrile dimers. However, all of these dimers are stable with respect to dissociation. On the other hand, as temperature increases, the thermodynamic

stability of both neutral dimers and of the collinear head-to-tail anion rapidly decreases, whereas changes in the stability of the head-to-head anion structure are negligible. This is mainly due to the vibrational contribution to the entropy, which is significantly larger for dimers with relatively stiff, direct acetonitrile-acetonitrile intermolecular interactions, compared to that for the head-to-head dimer anion, where the acetonitrile moieties are bound via the excess electron cloud, resulting in a very flat potential energy surface. As a matter of fact, the latter species is the only acetonitrile dimer which appears to be stable at temperatures above 250 K. A very similar temperature dependence of the relative stability of the classical dipole-bound and "solvated electron" isomers of the hydrogen fluoride trimer anion have been reported by Gutowski *et al.*[48] Although the free energy temperature profiles shown in Figure 37 are obtained under the rigid-rotor/harmonic oscillator approximation and thus do not account for anharmonicity of the potential energy surface, they still provide insight into the thermal stability of the acetonitrile dimer anions and suggest that, at non-zero temperatures, the "solvated-electron" isomer of the acetonitrile dimer anion may coexist with the collinear head-to-tail isomer and even become the predominant dimer anion structure.

As discussed above, the dipole-bound acetonitrile anion can not be produced by attachment of an excess electron to a neutral acetonitrile dimer. However, it can be prepared by photoexcitation and CTTS relaxation of the ternary iodide-acetonitrile complex $I^-(CH_3CN)_2$, as it shown by Johnson and co-workers,[66] who postulated that this acetonitrile dimer anion has a collinear head-to-tail structure, based on the structure of the parent iodide-acetonitrile cluster. Our recent computational results[190] suggest that the collinear isomer of the ternary iodide-acetonitrile complex with the asymmetrically solvated iodide is less stable than the symmetrically solvated structure, similar to the head-to-head acetonitrile dimer anion, and the novel hydrogen-bonded isomer (*cf.* Figure 15). It is not clear how the relaxation of the CTTS excited states of either of the

low-energy isomers of the $I^-(CH_3CN)_2$ clusters can lead to formation of the acetonitrile dimer anion, and which isomer of the latter is being formed. Clearly, only extensive molecular dynamics simulations of the CTTS excited-state relaxation dynamics can help clarify this problem.

Another interesting issue is the intermolecular bonding in the "solvated-electron" acetonitrile dimer anion isomer, and, more generally, the topological characteristics of the charge density distribution in the acetonitrile cluster anions. We thus applied quantum theory of Atoms in Molecules (AIM) to gain a better understanding of the electronic structure and chemical bonding in the dipole-bound acetonitrile dimers.

The AIM theory is based on the topological analysis of the total electron density $\rho(r)$ in the molecule, its derivatives – the gradient $\nabla\rho(r)$ and Laplacian $\nabla^2\rho(r)$, as well as a number of related functions, such as the energy density $H(r)$ and its components. The theoretical basis and the key applications of AIM theory are discussed in great detail in monographs by Bader[99] and Popelier.[157] Briefly, the analysis of the charge density gradient and Laplacian allows finding critical points, which correspond to maxima, minima and saddle points in the $\rho(r)$ distribution. Local maxima, or attractors, of the charge density usually correspond to atomic nuclei (nuclear critical points). Two nuclear critical points can be connected by a gradient path (bond path) which is indicative of chemical bonding between the two atoms, and corresponds to the line of maximum charge density between two nuclei. The point of minimum charge density along a bond path is a first-order critical point, called bond critical point (BCP). The properties of the BCP can be used to characterize the nature of chemical bonding between two atoms. Zero-flux surfaces perpendicular to the bond paths at the BCP separate the atoms from each other in molecules and are therefore usually called interatomic surfaces (IAS). Integration over the atomic volume yields a number of atomic properties (*e.g.* charge, volume, energy and its components) which are transferable between molecules to a

certain extent. The Laplacian of the charge density provides a way to identify regions of charge concentration ($\nabla^2\rho < 0$) and depletion ($\nabla^2\rho > 0$), allowing distinguish between covalent and ionic bonds and identify lone pairs, which are a local minima of $\nabla^2\rho$. Thus, AIM theory provides a solid theoretical footing to interpret electron densities in terms of classical chemical concepts, such as atoms, molecules or chemical bonds. And Figure 38 presents the resulting AIM plots for the dipole-bound acetonitrile dimers, showing the map of the Laplacian of charge density, bond paths and interatomic surfaces.

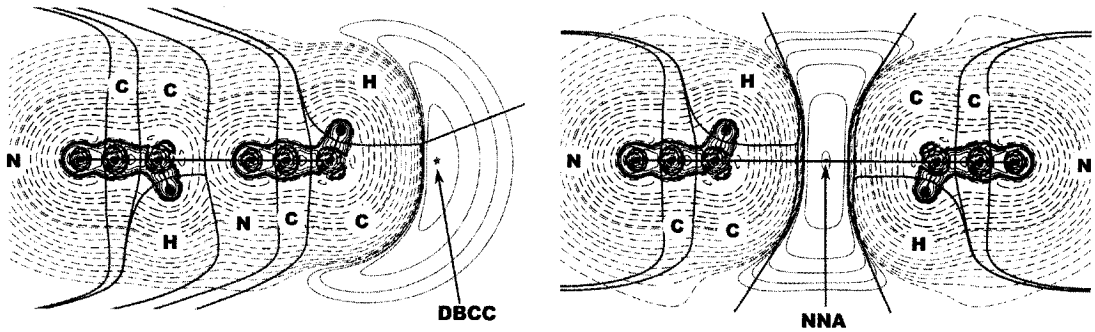

a) collinear head-to-tail **b) "solvated electron" head-to-head**

Figure 38. AIM plots for the dipole-bound acetonitrile dimer anions. Bond paths (purple) and inter-atomic surfaces (green) are super-imposed with the contour plots of the Laplacian of electron density $\nabla^2\rho$ (solid lines for $\nabla^2\rho < 0$, dashed lines for $\nabla^2\rho > 0$)

Table 14. AIM properties of relevant critical points for the acetonitrile dimer anions[a]

Isomer	Critical point	ρ	$\nabla^2\rho$	*G*	*G*/ρ	*H*
Collinear	DBCC	1.57×10^{-4}	-1.24×10^{-5}	7.05×10^{-7}	4.50×10^{-3}	-3.80×10^{-6}
Head-to-head	NNA	3.20×10^{-4}	-4.06×10^{-5}	8.60×10^{-7}	2.70×10^{-3}	-1.10×10^{-5}
	BCP(C–NNA)	3.00×10^{-4}	5.40×10^{-5}	1.72×10^{-5}	5.70×10^{-2}	-3.70×10^{-6}

[a] Electron density (ρ), the Laplacian of the electron density ($\nabla^2\rho$), kinetic energy density (G), kinetic energy density per electron (G/ρ), and the total energy density (H). All values (in atomic units), are calculated from CCSD/SVP+R // UMP2/SVP+R electron densities.

As perturbations of the electronic structure in acetonitrile molecules upon dimerization and/or excess electron dipole-binding are marginal,[48,355] we concentrate on the features directly related to the excess electron binding. As can be seen from Figure 38, the dipole-bound electron in the collinear head-to-tail isomer gives rise to a very diffuse region of charge concentration in the non-bonded region of the acetonitrile molecule, far away from the region of valence shell charge concentration (VSCC) representative of covalent bonding. This "dipole-bound" charge concentration (DBCC), which spreads over the atomic volumes of the hydrogen atoms of the methyl group, is very similar to the diffuse charge concentrations found by Bader and co-workers for Rydberg excited states of ammonia.[364] The local minimum of the Laplacian for the DBCC is situated at 3.60 Å from the carbon atom of the methyl group (*cf.* Figure 38), and the properties of this critical point (presented in Table 14) can be used to characterize the dipole-bound electron from the point of view of AIM theory. The DBCC critical point is characterized, not surprisingly, by a low electron density and a low negative value of the Laplacian. The kinetic energy of the dipole-bound electron, which can be expressed by the kinetic energy per electron $G(r)/\rho(r)$ at the critical point, is also very low, *ca.* 5×10^{-3},

and typical of loosely bound, diffuse electron distributions,[365] and dipole-bound electrons in particular.[26]

The electron density distribution for the "solvated electron" head-to-head isomer of the acetonitrile dimer anion is characterized by a very similar charge concentration region in between the acetonitrile molecules (*cf.* Figure 38). However, in this case, the excess electron gives rise not only to the regions of DBCC and the corresponding local minimum of the Laplacian of the electron density, but also to a local maximum of the electron density, which is connected to the carbon atoms of the acetonitrile molecules via bond paths, and the region of charge concentration is separated from the carbon and hydrogen atoms by interatomic surfaces. The region of charge concentration with a maximum in the electron density, separated from the other atoms in the molecule by interatomic surfaces, correspond to a topological atom in AIM theory. Thus, the excess electron in the head-to-head isomer of the acetonitrile dimer anion gives rise to a pseudo-atom of electron density, and exists as a separate topological entity, separating the acetonitrile molecules from each other and binding them together via an "e^--bond".

The maxima, or attractors, of electron density are typically found at atomic nuclei. Attractors of electron density without the corresponding nucleus – non-nuclear attractors (NNA) – are fairly uncommon, and only have been reported for a few systems, which include some metal clusters and solids,[366,367] solid lithium fluoride[365] with crystal defects (*F*-centers) and some alumosilicates.[368] The properties of the non-nuclear attractor and the bond critical points connecting it to the carbon atoms are presented in Table 14. The electron density at the NNA is almost twice that at the CC critical point for the collinear isomer, and the Laplacian of $\rho(r)$ has a more negative value, consistent with the tighter binding of the excess electron in the "solvated-electron" isomer. Remarkably, the value of the kinetic energy per electron at the NNA is lower than that of the CC critical point in the collinear isomer, even though the excess electron is more confined in

the "solvated-electron" structure. The prevalence of stabilizing factors, represented by the potential energy, over destabilizing factors, which can be related to the kinetic energy, is also reflected in the larger negative value of the total energy at the NNA. The BCPs connecting the NNA with acetonitrile molecules are situated outside of the dipole-bound charge concentration and therefore characterized by positive values of the Laplacian. The value of the electron density at the BCPs is not much lower than that at the NNA, which suggests that the distribution of $\rho(r)$ is rather flat for the pseudo-atom formed by the excess electron, similar to the electron density distribution found for pseudo-atoms related to crystal defects.[365] Integration of the charge density over the pseudo-atom volume gives a charge of -0.53 e, *i.e.* only half of the excess electron is located inside the pseudo-atom (with a volume of *ca.* 4.6×10^3 Å^3). Not surprisingly, the average kinetic energy per electron for the excess electron pseudo-atom is low ($G/\rho=8.60 \times 10^{-3}$ au), similar to pseudo-atoms corresponding to that of crystal defects.[365] Our on-going work[369] suggests that the existence of non-nuclear attractors of electron density and the corresponding pseudo-atoms is typical of the electron density distributions in polar solvent cluster anions where the excess electron is confined in between solvent molecules.

To summarize, *ab inito* calculations suggest that the acetonitrile dimer anion has two possible isomers. The first isomer is characterized by a collinear head-to-tail orientation of the acetonitrile molecules and trapping of the excess electron in the field of the resulting cluster dipole outside the cluster. The second isomer has the excess electron trapped in between the acetonitrile molecules, which are oriented in a head-to-head fashion and screened from each other by the excess electron cloud ("solvated-electron" isomer). Although the latter isomer is less stable at low temperatures (< 200 K), it becomes more stable at higher temperatures due to entropic factors which favor less rigid structures. Topologically, the excess electron in the acetonitrile dimer anion is

characterized by a very diffuse region of charge concentration, and in the case of the "solvated-electron" isomer, a non-nuclear electron density maximum and a corresponding pseudo-atom as well.

The interaction of an excess electron with two acetonitrile molecules can lead to formation of cluster anions with very interesting structural, thermodynamic and topological properties. However, dipole-binding is not the only way the excess electron can interact with acetonitrile molecules. As mentioned earlier, acetonitrile molecules may also form anions by accepting an electron in a valence orbital. We now turn our attention to these valence-bound acetonitrile anions.

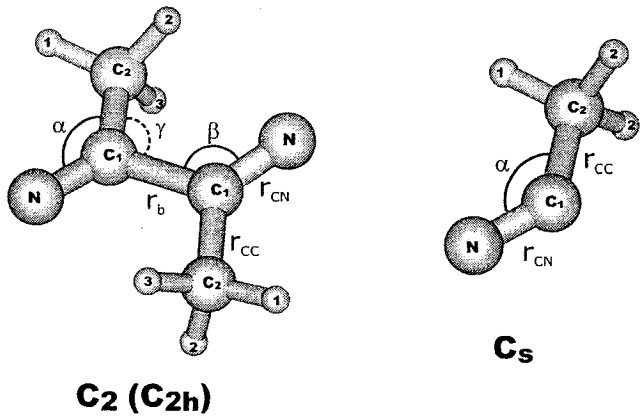

Figure 39. Structures of the valence-bound acetonitrile dimer and monomer anions. Geometrical parameters for these structures are collected in Table 15

VII.4. Valence-bound acetonitrile dimer and monomer anions

We will discuss the structure of the valence-bound dimer anion because it is in many aspects more well-behaved system than the monomer. It can be easily calculated for the gas phase, without using continuum solvation models and therefore can be a good system to study the application of various methods. Figure 39 displays the structure of

the acetonitrile valence-bound acetonitrile dimer anion and Table 15 lists selected geometrical parameters and the excess vertical electron binding energies (or ionization potentials) calculated with various model chemistries. CASSCF/SVP+ calculations produce a geometry for $(CH_3CN)_2^{\bullet-}$ generally similar to that previously reported on the basis of DFT calculations.[335,336] The valence-bound dimer anion possesses a structure similar to that of the neutral head-to-tail acetonitrile dimer, with the bent acetonitrile moieties connected at the cyanide carbon atoms. However, CASSCF predicts bridging C–C bond somewhat longer (r_b is 2.05 *vs.* 1.6–1.8 Å for the neutral head-to-tail acetonitrile dimer) and the excess electron vertical detachment energy is negative, implying that the valence-bound state of the acetonitrile dimer anion is unbound. Inclusion of dynamic correlation with CASTP2 leads to a much shorter bridging C–C bond and a positive VDE (*cf.* Table 15), which highlights the importance of dynamic electron correlation for the description of valence-bound acetonitrile anions. The PBEO/aug-pc-1 results are in reasonable agreement with those of CASPT2 calculations, although the VDE value is almost twice as large. Even though the molecular spin is not exactly defined in DFT (the wavefunction is not an eigenfunction of the spin operator), it is worth noting that unrestricted PBEO calculations yield results unaffected by spin contamination ($\langle S^2 \rangle \approx 0.76$). Multi-configurational *ab initio* calculations (CASSCF and CASPT2) predict the cyanide carbon atoms to be slightly pyramidal, thus leading to a slightly non-planar structure with C_2 symmetry, whereas DFT calculations suggest a planar C_{2h} structure. The valence-bound acetonitrile dimer anion in the gas phase is predicted by CASPT2 and PBEO to be higher in energy than the neutral collinear head-to-tail acetonitrile dimer by *ca.* 25 and 17 kcal/mol (or 0.74 and 1.08 eV) respectively (ZPE-corrected energies). Thus, CASPT2 and unrestricted PBEO calculations seem to provide generally consistent description of the valence-bound acetonitrile anions. In addition, the PBEO method appears to be a reasonable alternative to the computationally expensive CASPT2

approach. It also allows exploration of the bulk solvation effects with continuum solvation models, which are not yet developed for the CASPT2 method.

Table 15. Vertical detachment energies and selected geometrical parameters for the valence bound acetonitrile anions[a]

	Method	VDE	r_b	r_{CN}	r_{CC}	α	β	γ	d(N-C-C-N)	d(C-C-C-C)
$(CH_3CN)_2^{\bullet-}$	CASSCF	-1.24	2.054	1.215	1.507	134.4	121.5	104.2	177.0	176.5
	CASPT2	1.03	1.668	1.256	1.522	127.8	122.2	110.0	171.2	170.5
	PBEO	1.88	1.668	1.230	1.511	128.4	121.5	110.1	180.0	180.0
$(CH_3CN)_2^{\bullet-}$ [b]	CASSCF	1.17	2.010	1.217	1.507	134.0	120.3	105.7	179.6	179.1
	PBEO	3.97	1.662	1.231	1.506	128.5	120.9	110.7	167.7	168.2
$CH_3CN^{\bullet-}$ [b]	CASSCF	0.77		1.238	1.529	132.1				
	PBEO	2.19		1.213	1.507	133.1				
CH_3CN	CASSCF			1.176	1.476	180.0				
	CASPT2			1.180	1.472	180.0				
	PBEO			1.156	1.451	180.0				

[a] VDE in eV, bond lengths in Å and angles in degrees
[b] Solvation effects included using the CPCM continuum solvation model of refs. [350,351]

Solvation in liquid acetonitrile, modeled using the CPCM[350,351] continuum solvation methodology, does not seem to significantly alter the geometry of the acetonitrile radical dimer anion calculated with CASSCF and PBEO (*cf.* Table 15), the most important changes being a shortening of the bridging C–C bond length r_b, and a slight pyramidalization of the cyanide carbon atoms in the case of PBEO. However, the solvation has a profound effect on the excess electron binding, as the VDE increases by 2.1–2.4 eV. In contrast to the gas phase, in solvent the valence-bound acetonitrile dimer anion is lower in energy than the neutral head-to-tail acetonitrile dimer by *ca.* 32

kcal/mol as predicted by PBEO/aug-pc-1 CPCM calculations (including solvation free energy).

Inclusion of solvation effects also allows calculation of the valence-bound acetonitrile monomer anion, whose structure resembles that of one monomer in the dimer anion, as can be seen in Figure 39. Similar to the dimer, the monomer anion is bent at the cyanide carbon atom and has a positive VDE. On the other hand, it does not appear to exist in the gas phase, unlike the dimer, which appears to be kinetically stable even in the absence of solvation. Gas-phase single-point calculations for the monomer anion at the equilibrium geometry of the solvated species suggest that the excess electron is not valence- but rather dipole-bound. Thus, the dimeric form seems to be the most stable form of the valence-bound acetonitrile anion, and the valence-bound isomers of the acetonitrile cluster anions $(CH_3CN)_n^-$ observed experimentally[331] are likely to be made up of an acetonitrile dimer radical anion clustered with neutral acetonitrile molecules: $[(CH_3CN)_2^{\bullet-}(CH_3CN)_{n-2}]$.

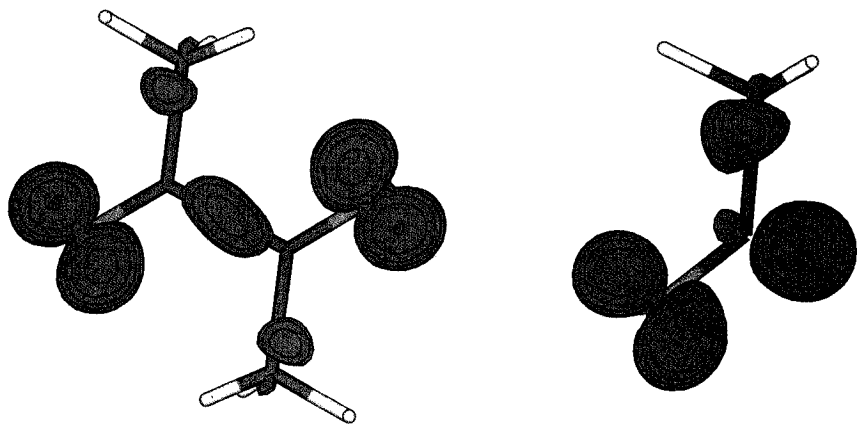

Figure 40. Spin density plots for the solvated monomer and dimer acetonitrile anions calculated with PBEO/aug-pc-1 (0.01 au isosurface)

We now turn our attention to the electronic structure of the valence-bound acetonitrile anions. The α, β and γ angles at the cyanide carbon atom (*cf.* Figure 39) are

all close to 120°, which suggests that the carbon changes its hybridization state from *sp* to sp^2 upon addition of an electron, also consistent with the elongation of the carbon-nitrogen bond. The re-hybridization of the cyanide carbon means that one of the carbon-nitrogen π-bonds disappears or, at least, becomes significantly weaker. Inspection of the unpaired spin density plots shown in Figure 40 reveals a strong delocalization of the excess electron over the acetonitrile molecule(s). For both the dimer and monomer anions, the majority of the excess electron density seems to be located at the nitrogen atoms, and around the cyanide carbon atoms (in between the cyanide carbon atoms for the dimer). The typical *p*-orbital shape of the spin density around the nitrogen atoms and, to a lesser extent around the cyanide carbon atoms, suggests that the excess electron resides, at least partially, in the N–C π*-orbital. Although these qualitative observations provide useful insight into the electronic structure rearrangements due to the addition of the excess electron, analysis of the electron density topology within the framework of the AIM theory allows a more quantitative characterization of these rearrangements.

The AIM plots for the valence-bound acetonitrile dimer and monomer anions are shown in Figure 41, while the properties of the relevant bond critical points are listed in Table 16, the integrated properties of the topological atoms are presented in Table 17, and the properties of the relevant valence-shell charge concentrations (minima in the Laplacian of the electron density) are collected in Table 18. The most important conclusion which arises from inspection of the AIM plots and the properties of the BCP for the bridging bond between the cyanide carbon atoms in the dimer is that this bond, although relatively weak (the estimated bond order is *ca.* 0.63), possesses a clear covalent character. Indeed, the charge concentrations are shared between the carbon atoms (*cf.* Figure 41), which is supported by the negative value of the Laplacian of the electron density at the BCP (*cf.* Table 14).

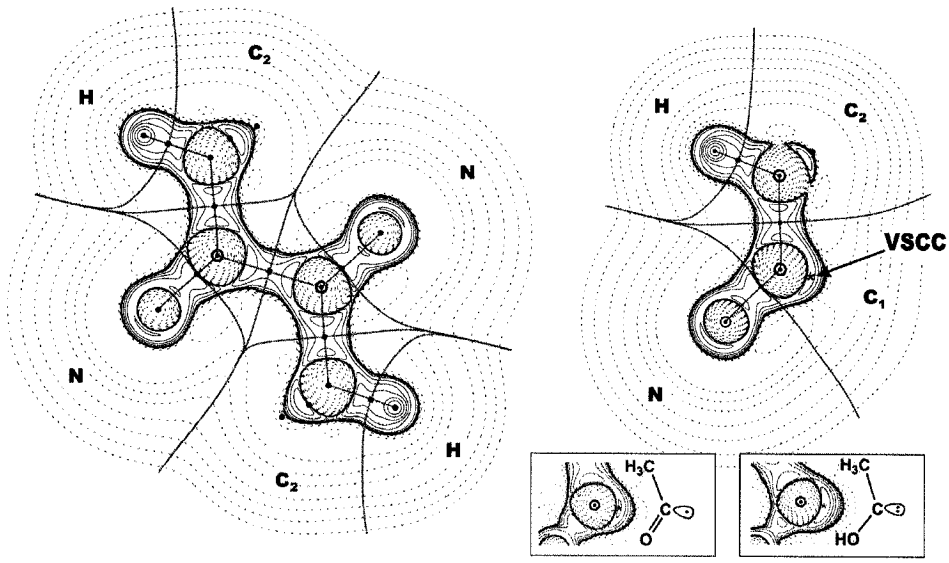

Figure 41. AIM plots for the valence-bound dimer and monomer acetonitrile anions. Bond paths (purple) and inter-atomic surfaces (green) are super-imposed with the contour plots of the Laplacian of electron density $\nabla^2\rho$ (solid lines for $\nabla^2\rho < 0$, dashed lines for $\nabla^2\rho > 0$). Insets show contour plots of the Laplacian of the electron density with valence shell charge concentrations at carbon atoms in model carbon-centered radicals and carbenes

Another important observation is that the carbon-nitrogen bond partially loses its triple-bond character, as can be seen from the ellipticity value at the BCP (ε=0.153), which is almost half the ellipticity value for the C=C double bond (ε=0.345). The ellipticity is related to the anisotropy of the electron density distribution around the BCP in the plane perpendicular to the bond path.[99] Near-zero ellipticity corresponds to a highly isotropic density distributions typical of single and triple bonds (*e.g.* the C≡N bond in acetonitrile), whereas double bonds typically have significantly higher ellipticity values at the BCPs. Thus, one of the acetonitrile carbon-nitrogen π bonds seems to be weakened upon formation of the acetonitrile valence-bound dimer anion, in agreement with the bent C–C–N structure mentioned earlier (Figure 39).

Table 16. AIM properties of selected bond critical points for the valence-bound acetonitrile anions and the acetonitrile molecule [a]

	BCP[b]	ρ	$\nabla^2\rho$	ε	Bond order[c]
$(CH_3CN)_2^{\bullet-}$	C_1–C_1	0.176	-0.235	0.057	0.63
	C_1–C_2	0.245	-0.512		1.01
	C_1–N	0.422	-0.657	0.153	
$(CH_3CN)_2$ [e]	C_1–C_1	0.158	-0.149	0.022	0.56
	C_1–C_2	0.238	-0.488		0.97
	C_1–N	0.424	-0.551	0.128	
$(CH_3CN)_2^{\bullet-}$ [d]	C_1–C_1	0.178	-0.244	0.054	0.64
	C_1–C_2	0.248	-0.523		1.04
	C_1–N	0.421	-0.665	0.140	
$CH_3CN^{\bullet-}$ [d]	C_1–C_2	0.241	-0.483		0.99
	C_1–N	0.429	-0.338	0.020	
CH_3CN	C_1–C_2	0.265	-0.621		1.16
	C_1–N	0.472	0.256	0.000	
CH_3CN [d]	C_1–C_2	0.266	-0.629		1.17
	C_1–N	0.472	0.212	0.000	

[a] Electron density (ρ), the Laplacian of the electron density ($\nabla^2\rho$), ellipticity (ε) of the carbon-nitrogen and the bridging carbon-carbon bonds, and the estimated bond orders for carbon-carbon bonds. Calculated based on PBEO/aug-pc-1 electron densities (all values are in atomic units)
[b] Atom labels are given in Figure 39
[c] Bond orders are estimated using the *bond order* = $\exp[A(\rho_{BCP} - B)]$ formula[99] parameterized on the basis of PBEO/aug-pc-1 ρ_{BCP} values for ethane, ethene and ethylene (0.2421, 0.3443, and 0.4023 au, respectively)
[d] Solvation effects included using the CPCM continuum solvation model of refs. [350,351]
[e] "Vertical neutral" dimer in the equilibrium geometry of the anion

Interestingly, the properties of the BCPs for the valence-bound acetonitrile dimer anion do not change significantly upon solvation (*cf.* Table 16). Moreover, even in the "vertical neutral" structure obtained by removal of the excess electron while retaining the anion geometry, the bridging C–C bond retains covalent character with a relatively similar bond order to that of the anion bridging bond. Thus, the excess electron appears not to be solely responsible for the binding of the two acetonitrile moieties in the dimer anion, but it rather causes changes in the electronic structure and geometry of the acetonitrile molecule that facilitates the formation of the bridging bond and stabilizes the anion dimer structure. As for the geometry and BCP properties, the AIM atomic charges and unpaired spin populations in the acetonitrile dimer anion do not differ much in the

gas-phase and in the presence of solvent (*cf.* Table 17). In agreement with experimental EPR measurements,[333] the majority part of the unpaired spin density (*ca.*80%) is concentrated on the nitrogen atoms.

In contrast to the valence-bound acetonitrile dimer anion, the solvated monomer acetonitrile anion is characterized by a significantly smaller ellipticity of the carbon-nitrogen bond, relative to that for the acetonitrile molecule, which suggests that it retains its triple bond character to a greater extent despite a bent C–C–N structure. The unpaired spin population of the cyanide carbon atom is much larger than for the dimer anion, and in fact, it is almost equal to that of the nitrogen atom (*cf.* Table 17). Inspection of the Laplacian of the electron density contour map for the valence-bound acetonitrile monomer anion (*cf.* Figure 41) suggests the presence of a non-bonded charge concentration on the cyanide carbon atom similar to the "lone-pair" non-bonded maxima in $\nabla^2\rho(r)$ for carbon-centered radicals and carbenes (*cf.* insets in Figure 41). Indeed, the analysis of the Laplacian of the electron density distribution around the cyanide carbon atom reveals the presence of a local minimum (indicated as a purple star and labeled as VSCC for valence-shell charge concentration in Figure 41). The properties of this critical point of the Laplacian of the electron density are very similar to the VSCC critical points in carbon-centered radicals and carbenes (*cf.* Table 18). In fact, the "lone-pair" character of these charge concentrations gradually increases from the acetonitrile monomer anion to the carbon-centered radical and to the carbene. Thus, the cyanide carbon atom in the valence-bound acetonitrile monomer anion appears to possess partial radical character, while in the dimer anion, this carbon atom is involved in covalent bonding with the cyanide carbon atom of the other acetonitrile moiety.

Table 17. Integrated AIM properties for the atoms in valence-bound acetonitrile anions and the acetonitrile molecule [a]

	atom[b]	N(Ω)	q(Ω)	σ(Ω)
$(CH_3CN)_2^{\bullet-}$	N	8.300	-1.300	0.421
	C_1	5.182	+0.818	0.014
	CH_3	9.048	-0.048	0.068
$(CH_3CN)_2$ [d]	N	8.021	-1.021	
	C_1	5.188	+0.812	
	CH_3	8.794	+0.206	
$(CH_3CN)_2^{\bullet-}$ [c]	N	8.338	-1.338	0.421
	C_1	5.183	+0.817	0.016
	CH_3	8.986	+0.014	0.065
$CH_3CN^{\bullet-}$ [c]	N	8.493	-1.493	0.404
	C_1	5.443	+0.557	0.394
	CH_3	9.066	-0.066	0.203
CH_3CN	N	8.258	-1.258	
	C_1	4.998	+1.002	
	CH_3	8.745	+0.255	
CH_3CN [c]	N	8.316	-1.316	
	C_1	4.982	+1.018	
	CH_3	8.704	+0.296	

[a] Electron populations (N(Ω)), atomic charges (q(Ω)), and spin populations (σ(Ω)).
[b] The methyl group properties are the sum of the hydrogen and carbon atomic properties.
[c] Solvation effects included using the CPCM continuum solvation model of refs. [350,351]
[d] "Vertical neutral" dimer in the equilibrium geometry of the anion

Table 18. Properties of the non-bonded minima of the Laplacian of the electron density (charge concentrations) on the carbon atom for the valence-bound acetonitrile monomer anion, and carbon-centered radical and carbene prototype[a]

	r, Å	ρ	$\nabla^2\rho$
$CH_3CN^{\bullet-}$	0.488	0.222	-0.638
CH_3CO	0.477	0.249	-0.924
CH_3COH	0.456	0.330	-1.584

[a] Distance from the respective nuclei r (in Å), electron density (ρ), the Laplacian of the electron density ($\nabla^2\rho$) in atomic units. Calculated based on PBEO/aug-pc-1 electron densities and using the CPCM continuum solvation model of Refs. [350,351]

Based on the spin densities obtained from EPR experiments, Williams and Sprague[333] proposed that the electronic structure of the valence-bound monomer anion can be described by a combination of three resonance structures, shown below, and arising from localization of the excess electron on the nitrogen and carbon atoms:

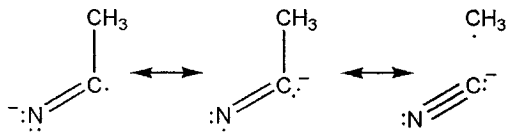

Although these resonance structures are consistent with the unpaired spin density distribution (*cf.* Figure 40), the unpaired spin atomic populations (*cf.* Table 17) and the formation of a VSCC critical point at the cyanide carbon atom (*cf.* Figure 41), they can not explain the significant increase of the negative charge (-0.066 e) at the methyl group, compared to that of the neutral acetonitrile molecule (+0.296 e). Thus, it appears necessary to also include a resonance structure with a negatively charged methyl carbon atom to fully account for the electronic structure of the valence-bound monomer anion:

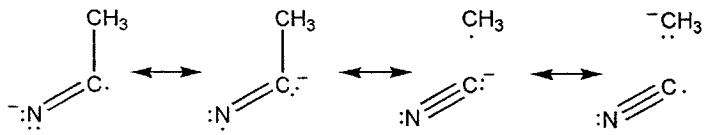

Likewise, the electronic structure of the valence-bound dimer anion can be represented as a combination of six resonance structures (the dashed line represents a one-electron bond between cyanide carbon atoms):

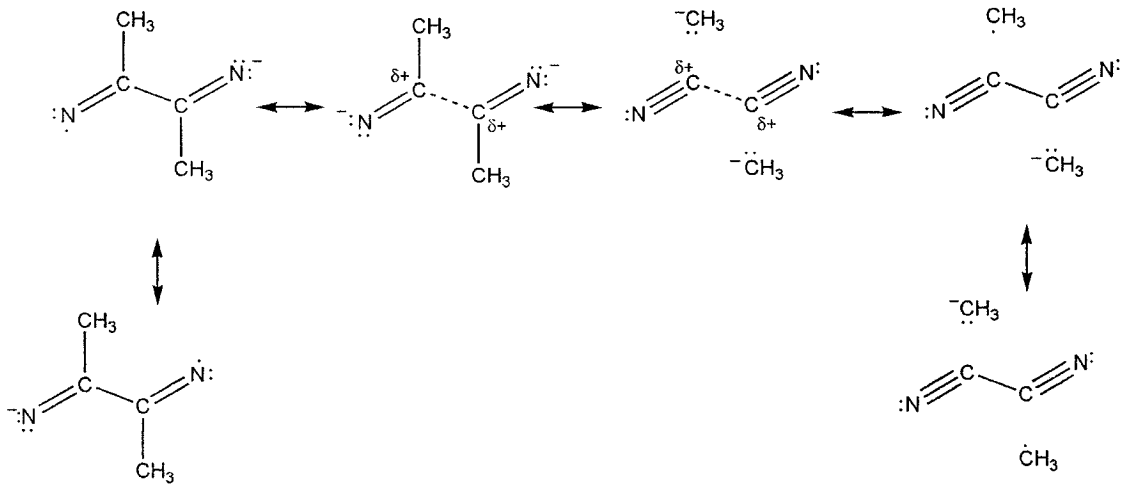

Greater delocalization of the excess charge and unpaired spin leads to a higher stability for the valence-bound dimer anion, compared to the monomer anion. Although these resonance structures are a very approximate way to qualitatively represent the complex electronic structure of the valence-bound acetonitrile anions, they seem to be in reasonable agreement with the quantitative results of AIM analysis and provide important insight into the structure of these peculiar species.

To summarize, the addition of an excess electron to the valence orbitals of acetonitrile molecules can lead to formation of a dimer radical anion which appears to be thermodynamically metastable in the gas phase and stable in liquid acetonitrile, or sufficiently large acetonitrile clusters. The electronic structure of this dimer radical anion is fairly complex and characterized by high delocalization of the excess electron and a weak covalent bridging bond between the cyanide carbon atoms of the two acetonitrile moieties. The acetonitrile monomer radical anion does not exist in the gas phase, but it exists in polar environments. However, the lower delocalization of the excess electron and the presence of a "radical center" or "lone pair" on the cyanide carbon atom, as inferred from AIM analysis, makes this anion extremely reactive.

VII.5. Concluding remarks

In this work, we have investigated the structure and stability of the acetonitrile anions $(CH_3CN)_n^-$ n = 1, 2 in the gas phase and in the presence of solvent, with particular attention to acetonitrile dimer anions. In the gas phase, the excess electron can be loosely trapped in the field of molecular dipoles, giving rise to two possible isomers of the dipole-bound acetonitrile dimer anion $(CH_3CN)_2^-$. For the first isomer, the excess electron is bound by the aggregate dipole moment of the collinear acetonitrile dimer. In this typical dipole-bound cluster anion, the excess electron is located outside the cluster, and the geometry of the dimer anion is essentially the same as that of the neutral dimer. For the other isomer, the excess electron is trapped inside the solvent cluster, "sandwiched" between the acetonitrile dipoles arranged in a head-to-head fashion. The very existence of this "solvated electron" structure is due to the presence of the excess electron. While it is not the most thermodynamically stable structure at low temperatures, the very flat potential energy surface of the "solvated electron" isomer leads to high entropy, and therefore higher stability at room temperature.

Topologically, the excess electron in the dipole-bound acetonitrile dimers manifests itself as a very diffuse region of charge concentration (where the Laplacian of the electron density is negative) outside of the acetonitrile molecules and referred to as "dipole-bound charge concentration". Furthermore, the excess electron in the "solvated electron" isomer gives rise to a non-nuclear maximum of electron density, or non-nuclear attractor (NNA) and a corresponding pseudo-atom of electron density. Thus, the "solvated" excess electron exists as a distinct topological entity which connects two acetonitrile molecules with each other via "e^--bond picture".

Two acetonitrile molecules can also accept the excess electron into their valence orbitals to form a valence-bound acetonitrile dimer radical-anion $(CH_3CN)_2^{\bullet -}$. In this

case, the addition of the electron initiates a substantial reorganization of the electronic structure of the acetonitrile moieties, which facilitates formation of a covalent bond between the cyanide carbon atoms and efficient delocalization and stabilization the excess electron. Although metastable in the gas phase, this acetonitrile anion radical dimer is stable in the condensed phase and, as recent experiments suggest, even in relatively small gas-phase acetonitrile clusters. A single acetonitrile molecule can also bind an excess electron in a valence orbital in a polar environment, giving rise to a very reactive radical anion. Indeed, the addition of the excess electron leads to formation of a reactive center at the cyanide carbon atom, which manifests itself topologically as a local minimum of the Laplacian of the electron density. Thus, depending on the environment, the interaction of acetonitrile molecules with an excess electron can give rise to a very rich and interesting topology of the electron density.

There is still much to be learned about the electronic structure, stability, photochemistry and reactivity of acetonitrile anions in various environments, the gas phase, clusters and liquid phase. Specifically, one of the most interesting problems is the interrelation and interconversion (via non-adiabatic transitions) between the dipole-bound and valence bound anions in finite-size acetonitrile clusters. The dipole- and valence-bound dimer anions possess very different geometries, thus this interconversion is likely to involve more than two acetonitrile molecules. The relaxation of photoexcited iodide-acetonitrile clusters is known to be a very efficient way of producing acetonitrile cluster anions,[61] and large acetonitrile clusters $(CH_3CN)_n$, $n>10$ may bind an excess electron as a valence-bound anion. Thus, experimental femtosecond spectroscopy studies of the relaxation dynamics of photoexcited iodide-acetonitrile clusters $I^-(CH_3CN)_n$, $n > 10$ may reveal extremely interesting dynamical features related to interconversion of the dipole-bound to valence-bound electronic states of the acetonitrile cluster anions. On the theoretical side, calculations of the couplings between these states

over extended regions of the potential energy surface is an equally important, but demanding problem.[80,326] In general, studies of acetonitrile anions may significantly advance to our understanding of the interaction of electrons with closed-shell molecules.

VII.6. Supporting information

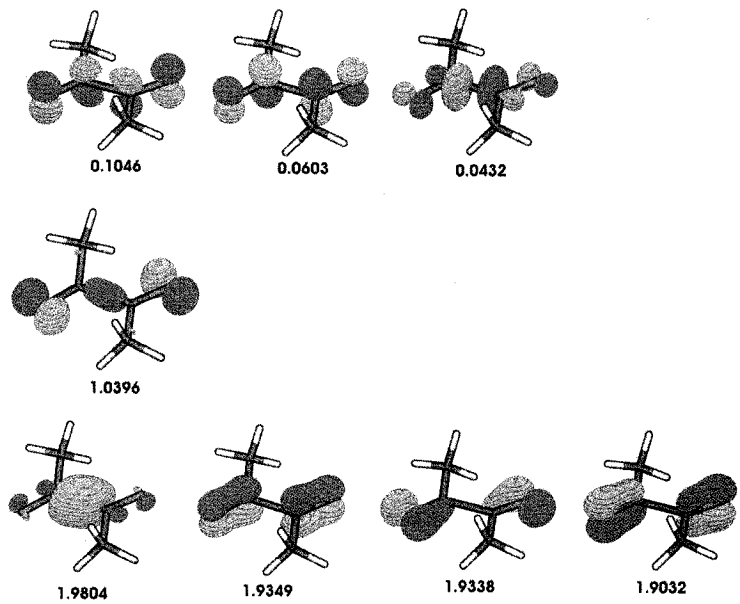

Figure 42. Active space CASSCF/SVP+ , natural orbitals and occupations numbers for the acetonitrile valence-bound dimer anion

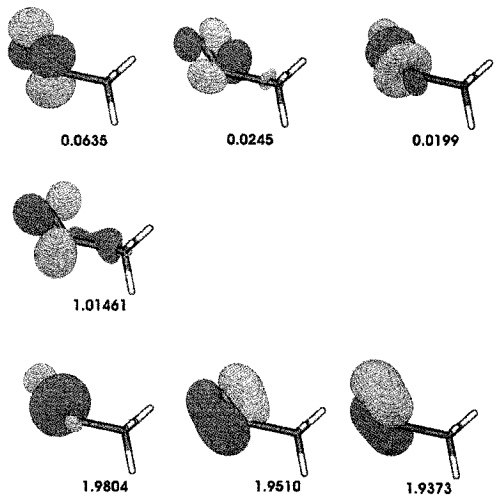

Figure 43. Active space CASSCF/SVP+, natural orbitals and occupation numbers for the solvated acetonitrile valence-bound monomer anion

VII.6.a.Cartesian coordinates and energies

Dipole-bound acetonitrile dimer anion, collinear head-to-tail isomer; UMP2/SVP+

```
Charge = -1; multiplicity = 2
E(UMP2)=-264.7528231 Hartree, <S2>=0.75001
C,0.,0.,-2.6109329256
N,0.,0.,-1.4246814131
C,0.,0.,-4.081840651
H,0.0000001321,-1.0269817681,-4.4495891001
H,-0.8893923665,0.5134907696,-4.4495891001
H,0.8893922343,0.5134909985,-4.4495891001
C,0.,0.,3.1611398418
N,0.,0.,4.3485783412
C,0.,0.,1.6891146256
H,-0.0000001315,1.0221119115,1.3122011531
H,-0.8851748151,-0.5110560697,1.3122011531
H,0.8851749466,-0.5110558419,1.3122011531
```

Dipole-bound acetonitrile dimer anion, head-to-head "solvated electron" isomer; UMP2/SVP+

```
E(UMP2)=-264.7480417 Hartree, <S2>=0.750044
C,0.,0.,3.7238991484
C,0.,0.,5.196392899
N,0.,0.,6.3840140866
C,0.,0.,-3.7238991484
C,0.,0.,-5.196392899
```

N,0.,0.,-6.3840140866
H,-0.0000000214,1.0262844639,3.3542049532
H,0.888788428,-0.5131422134,3.3542049532
H,-0.8887884065,-0.5131422505,3.3542049532
H,0.0000000214,-1.0262844639,-3.3542049532
H,0.8887884065,0.5131422505,-3.3542049532
H,-0.888788428,0.5131422134,-3.3542049532

Valence-bound acetonitrile dimer anion, PBEO/ aug-pc-1 in solution (acetonitrile, CPCM model)

Charge = -1; multiplicity = 2
E(SCF)=-265.2082012 Hartree, $<S^2>$=0.762128
C,-0.0671412453,0.8284315465,0.0300744341
N,-1.1679930113,1.3745007605,0.0961140601
C,0.0644703511,-0.8286927475,0.0286905843
N,1.1550130474,-1.3757701407,0.189471127
C,1.2927669586,1.4695981597,-0.050182973
C,-1.282292314,-1.4685737881,-0.1802801753
H,1.2289409172,2.5459252418,0.1435646301
H,-1.2358706093,-2.5466029335,0.0089024662
H,1.9679673424,0.9807692058,0.6640798219
H,1.7241044673,1.3063429386,-1.0479644222
H,-2.0196979727,-0.9858282213,0.4740975878
H,-1.6214069001,-1.2962995932,-1.211587614

Valence-bound acetonitrile monomer anion, PBEO/aug-pc-1 calculations in solution (acetonitrile, CPCM model)

Charge = -1; multiplicity = 2
E(SCF)=-132.541658 Hartree, $<S^2>$=0.751424
C,0.2953350283,-0.3953632176,-0.0001758765
N,1.363040921,0.1795089817,0.
C,-1.1331270615,0.0859725158,0.
H,-1.1870852688,1.1963055057,-0.0060498765
H,-1.6659269889,-0.3032515837,-0.8790698765
H,-1.6615219907,-0.2932725829,0.8861161235

Chapter VIII

Conclusions

The main objective of this Thesis was to improve our understanding of the properties and time-evolution of the charge-transfer-to-solvent excited states of small halide-solvent clusters, with particular attention to the clusters formed by the iodide anion with acetonitrile molecules. An array of methods of modern computational and theoretical chemistry has been employed to investigate the structure, photochemistry and dynamics of these systems. However, due to the complex nature of the cluster CTTS excited states, a truly quantitative treatment of the photoexcitation and excited state relaxation dynamics requires not only basic insight into the nature of the CTTS excited states, but also a solid understanding of the ground and ionized states of halide-solvent clusters.

The objective of Chapter II was to perform a preliminary quantum-chemical study of the photoexcitation of the binary iodide-acetonitrile complex leading to charge-transfer-to-solvent precursor states with relatively simple electronic structure theory calculations. The basic picture which emerged from these calculations is that, upon photoexcitation, an electron is transferred from one of the iodide valence p orbitals to the acetonitrile molecule, where it is stabilized by interactions with the acetonitrile dipole. A similar picture applies to the photoexcitation of iodide-water clusters. Although this preliminary investigation provided important insight into the most basic properties of the CTTS states of iodide-acetonitrile clusters, it clearly suggested that, in order to obtain a truly quantitative description of CTTS photoexcitation, one needs to apply more advanced techniques that correctly treat the excited electron as well as spin-orbit coupling effects.

Reliable modeling of the excited states of halide-acetonitrile clusters requires an accurate treatment of the ground-state geometries and binding energies. Hitherto, several hypotheses regarding the nature of the interaction between substituted methanes YCH_3 and halide ions have been proposed in the literature, which ranged from purely

electrostatic ion-dipole attraction models to regular, or even improper blue-shifting hydrogen bonding. The situation was especially unclear in the case of halide-acetonitrile complexes and clusters, since several recent theoretical and experimental works provided fairly contradictory results on the prevalent role of either ion-dipole interactions or hydrogen bonding. To address this problem, in Chapter III we performed a systematic computational study of the structures, binding energies and potential energy surfaces for a series of binary halide-acetonitrile clusters $X^-(CH_3CN)$. Extensive testing of the various model chemistries, an in-depth investigation of the complex potential energy surfaces and the nature of bonding revealed a very subtle interplay between the ion-dipole interactions and hydrogen bonding in halide-acetonitrile clusters, as well as in similar systems, where a halide ion interacts with a methyl group of a solvent molecule. The binary iodide-acetonitrile complex appears to be the only halide-acetonitrile cluster with no hydrogen-bonded isomer and a single linear structure, determined exclusively by ion-dipole interactions, as the only minimum on the potential energy surface (PES). The other binary halide-acetonitrile complexes and even larger iodide-acetonitrile clusters appear to have hydrogen-bonded isomers as local or global minima on the PES. Also, the results of this in-depth computational investigation lead to a re-evaluation of the results of a few recent theoretical and computational studies of similar systems.

However, extensive knowledge of ground state iodide-solvent clusters is not the only prerequisite to a deep understanding of the CTTS excited states of these clusters, since open-shell ionized iodide-solvent clusters with a neutral iodine atom, presents a number of challenges due to the (quasi)degeneracy of the ground electronic state and strong spin-orbit interactions. Some of these issues are addressed in Chapter IV. First, a detailed study of the nature of the interaction in polar or ionic clusters involving the iodine atom has been performed on the paradigm diatomic complex made up of the

sodium cation and the iodine atom $Na^+\cdots I^\cdot$. Second, accurate potential curves obtained in this work were necessary for simulations of NaI photodissociation and femtosecond spectroscopy performed in our laboratory. It was found that the potential curves for the first two electronic Λ-S states have very different character. Whereas the potential for the $^2\Pi$ state has a well depth of ~10 kcal/mol, the $^2\Sigma$ state is essentially unbound. This difference has been rationalized in terms of the anisotropic interaction of the quadrupole moment of the iodine atom with the sodium cation, which is stabilizing in the case of the $^2\Pi$ state and destabilizing in the case of the $^2\Sigma$ state. It was found that inclusion of spin-orbit coupling does not affect the X (Ω = 3/2) ground state, which retains its $^2\Pi$ character, but it results in two Ω = 1/2 spin-orbit states, with mixed $^2\Sigma$ and $^2\Pi$ character and binding energies roughly half of that of the ground spin-orbit state. Complete basis set extrapolations were used to obtain binding energies, equilibrium geometries and spectroscopic parameters of the $Na^+\cdots I^\cdot$ complex, and to parameterize model potentials for further use in molecular dynamics simulations.

The main objective of Chapter V was to use the important insight obtained from studies presented in the preceding chapters to perform a detailed investigation of the photoexcitation and CTTS excited-state relaxation dynamics of the binary iodide-acetonitrile complex. The nature of photoexcitation and the various ingredients of the CTTS excitation energy have been discussed in detail. The anisotropy of the interaction of the neutral iodine atom and polar acetonitrile molecule in the excited and ionized states of the iodide-acetonitrile complex is similar to the sodium cation – iodine atom complex discussed in Chapter IV. However, in this case the strong ion-quadrupole interactions are changed to significantly weaker dipole-quadrupole interactions. The spin-orbit mixing between the electronic states due to the different orientation of the half-filled *p*-orbital of the iodine atom with respect to the acetonitrile molecule was also found to be similar to that of the $Na^+\cdots I^\cdot$ complex. Further, it was shown that a correct

treatment of spin-orbit coupling effects and the systematic error arising in the problems the calculations of the ionization potential of the iodide anion leads to a truly quantitative description of photoexcitation and excited-state potential energy surfaces of the binary iodide-acetonitrile complex. Inspection of the accurate potential energy curves for the excited and ionized states of the iodide-acetonitrile complex and the dependence of the vertical detachment energy on the position of the neutral iodine atom revealed interesting features, somewhat reminiscent of the experimental results obtained for the relaxation of photoexcited iodide-water clusters. It appears that, at short distances from the charged solvent molecule, the iodine atom greatly destabilizes the dipole-bound excited electron due to exchange repulsion, whereas at longer distances, it can in fact slightly stabilize it, most probably due to dispersion interactions.

The information on the potential energy curves helped develop an efficient approach for first-principles excited-state molecular dynamics simulations of the CTTS relaxation dynamics. Using this approach, realistic *ab initio* molecular dynamics simulations of the CTTS excited-state relaxation dynamics for a small iodide-solvent cluster have been performed for the first time, and the time-evolution of the excited electron vertical detachment energy (VDE), discussed in connection with available experimental data for the relaxation dynamics of more complex iodide-water clusters. It appears that the evolution of the excess electron VDE during the relaxation of the photoexcited binary iodide-acetonitrile complex has very similar features to the those for vertical detachment energy dynamics observed experimentally in the relaxation of iodide-water clusters $I^-(H_2O)_n$.

The relaxation mechanism of the CTTS excited state of binary iodide-acetonitrile clusters is probably one of the simplest cases of CTTS relaxation dynamics. The considerably more complex excited-state dynamics of iodide-water clusters has been a matter of debate in the scientific literature for quite some time. The objectives of

Chapter VI was to perform a preliminary investigation of charge-transfer-to-solvent excited-state dynamics of model $I^-(H_2O)_3$ clusters in order to gain some insight into the general features of the relaxation process of photoexcited $I^-(H_2O)_n$ clusters. It has been found that the relaxation of the excited $I^-(H_2O)_3$ cluster is characterized by rapid motion of water molecules and slow recoil motion of the iodine atom. Thus, in the case of photoexcited iodide-water clusters, both the solvent reorganization and the iodine atom motion appear to be important for interpreting the results of femtosecond photoelectron spectroscopy experiments.

The relaxation of photoexcited iodide-acetonitrile complexes is known to produce acetonitrile cluster anions. However, their structure, stability and electronic structure are not very well known. Thus, the objective of Chapter VII was to perform an investigation of the various ways acetonitrile molecules can interact with an excess electron, with particular attention to their geometry, stability and the electronic structure, including the topology of the electron density distribution. It was shown that there are two possible isomers for the dipole-bound acetonitrile anion. In the first isomer, the excess electron resides outside the cluster, trapped in the field of the aggregate cluster dipole moment (classical dipole-bound electron). In the second isomer, the excess electron is "sandwiched" between the solvent molecules inside the cluster ("solvated electron"). Interestingly, the very flat potential energy surface of the "solvated electron" isomer leads to high entropy, and therefore higher stability at room temperature, although it is energetically less stable than the classical dipole-bound isomer at low temperatures.

Topologically, the excess electron in the dipole-bound acetonitrile dimers manifests itself as a very diffuse region of charge concentration (where the Laplacian of the electron density is negative) outside of the acetonitrile molecules and referred to as "dipole-bound charge concentration". Furthermore, the excess electron in the "solvated

electron" acetonitrile dimer anion was found to give rise to a non-nuclear maximum of electron density and a corresponding pseudo-atom of electron density. Basically, the "solvated" excess electron exists as a distinct topological entity which connects two acetonitrile molecules with each other.

Recent experimental studies suggested that relatively small acetonitrile clusters can not only support an excess electron in a dipole-bound or "solvated electron" fashion, but they can also accept the excess electron into their valence orbitals. Hence, both dipole-bound and valence bound acetonitrile dimer anions have been investigated (Chapter VII). In the case of the valence-bound acetonitrile dimer anion, the excess electron causes a substantial reorganization of the electronic structure of the acetonitrile molecules leading to formation of a covalent bond between the cyanide carbon atoms and efficient delocalization and stabilization of the excess electron. Although metastable in the gas phase, this acetonitrile anion radical dimer is stable in the condensed phase and, as recent experiments suggest, even in relatively small gas-phase acetonitrile clusters. A single acetonitrile molecule can also bind an excess electron in a valence orbital in a polar environment, giving rise to a transient radical anion.

To summarize, this thesis presented a theoretical investigation of various aspects of the charge-transfer-to-solvent excited states of the halide-polar solvent clusters, including the properties of the ground, excited and ionized states of these clusters, the excited state relaxation dynamics and its products. We hope that the insight gained in this work will help better understand the properties of gas-phase clusters and, ultimately, the condensed phase.

References

(1) Dye, J. L. *Scientific American* **1967**, *216*, 77.
(2) Kraus, C. A. *J. Am. Chem. Soc.* **1908**, *30*, 1323.
(3) Hart, E. J.; Anbar, M. *The Hydrated Electron*; Wiley-Interscience: New York, 1970.
(4) Boudaiffa, B.; Cloutier, P.; Hunting, D.; Huels, M. A.; Sanche, L. *Science* **2000**, *287*, 1658.
(5) Ferris, J. P.; Antonucci, F. R. *J. Am. Chem. Soc.* **1972**, *94*, 8091.
(6) Pearson, G. S.; Magee, R. S. *Pure Appl. Chem.* **2002**, *74*, 187.
(7) Jortner, J. *Mol. Phys.* **1962**, *5*, 257.
(8) Copeland, D. A.; Kestner, N. R.; Jortner, J. *J. Chem. Phys.* **1970**, *53*, 1189.
(9) Kevan, L.; Fueki, K.; Feng, D.-F.; Christoffersen, R. E. *J. Phys. Chem.* **1971**, *75*, 2297.
(10) Feng, D.-F.; Kevan, L. *Chem. Rev.* **1980**, *80*, 1.
(11) Rossky, P. J.; Schnitker, J. *J. Phys. Chem.* **1988**, *92*, 4277.
(12) Wong, K. F.; Rossky, P. J. *J. Chem. Phys.* **2002**, *116*, 8418.
(13) Nicolas, C.; Boutin, A.; Levy, B.; Borgis, D. *J. Chem. Phys.* **2003**, *118*, 9689.
(14) Borgis, D.; Staib, A. *Chem. Phys. Lett.* **1994**, *230*, 405.
(15) Wallqvist, A.; Thirumalai, D.; Berne, B. J. *J. Chem. Phys.* **1986**, *85*, 1583.
(16) Berne, B. J.; Thirumalai, D. *Annu. Rev. Phys. Chem.* **1986**, *37*, 401.
(17) Hummer, G.; Pratt, L. R.; Garcia, A. E.; Berne, B. J.; Rick, S. W. *J. Phys. Chem. B* **1997**, *101*, 3017.
(18) Barnett, R. N.; Landman, U.; Makov, G.; Nitzan, A. *J. Chem. Phys.* **1990**, *93*, 6226.
(19) Barnett, R. N.; Landman, U.; Nitzan, A. *J. Chem. Phys.* **1988**, *89*, 2242.
(20) Fermi, E.; Teller, E. *Phys. Rev.* **1947**, *72*, 399.
(21) Crawford, O. H. *Mol. Phys.* **1973**, *26*, 139.
(22) Garrett, W. R. *Chem. Phys. Lett.* **1970**, *5*, 393.
(23) Garrett, W. R. *J. Chem. Phys.* **1978**, *69*, 2621.
(24) Stockdale, J. A.; Davis, F. J.; Compton, R. N.; Klots, C. E. *J. Chem. Phys.* **1974**, *60*, 4279.
(25) Haberland, H.; Schindler, H. G.; Worsnop, D. R. *B. Bunsen Ges. Phys. Chem.* **1984**, *88*, 270.
(26) Jordan, K. D.; Wang, F. *Annu. Rev. Phys. Chem.* **2003**, *54*, 367.
(27) Kim, J.; Becker, I.; Cheshnovsky, O.; Johnson, M. A. *Chem. Phys. Lett.* **1998**, *297*, 90.
(28) Jordan, K. D. *Science* **2004**, *306*, 618.
(29) Bragg, A. E.; Verlet, J. R. R.; Kammrath, A.; Cheshnovsky, O.; Neumark, D. M. *J. Am. Chem. Soc.* **2005**, *127*, 15283.
(30) Bragg, A. E.; Verlet, J. R. R.; Kammrath, A.; Cheshnovsky, O.; Neumark, D. M. *Science* **2004**, *306*, 669.
(31) Paik, D. H.; Lee, I.-R.; Yang, D.-S.; Baskin, J. S.; Zewail, A. H. *Science* **2004**, *306*, 672.
(32) Hammer, N. I.; Shin, J.-W.; Headrick, J. M.; Diken, E. G.; Roscioli, J. R.; Weddle, G. H.; Johnson, M. A. *Science* **2004**, *306*, 675.

(33) Verlet, J. R. R.; Bragg, A. E.; Kammrath, A.; Cheshnovsky, O.; Neumark, D. M. *Science* **2005**, *307*, 93.
(34) Verlet, J. R. R.; Kammrath, A.; Griffin, G. B.; Neumark, D. M. *J. Chem. Phys.* **2005**, *123*, 231102.
(35) Turi, L.; Sheu, W.-S.; Rossky, P. J. *Science* **2005**, *309*, 914.
(36) Verlet, J. R. R.; Bragg, A. E.; Kammrath, A.; Cheshnovsky, O.; Neumark, D. M. *Science* **2005**, *310*, 1769b.
(37) Turi, L.; Sheu, W.-S.; Rossky, P. J. *Science* **2005**, *310*, 1769c.
(38) *Science* **2004**, *309*, 2017.
(39) Jordan, K. D.; Luken, W. *J. Chem. Phys.* **1976**, *64*, 2760.
(40) Jordan, K. D.; Wendoloski, J. J. *Chem. Phys.* **1977**, *21*, 145.
(41) Skurski, P.; Gutowski, M.; Simons, J. *Int. J. Quant. Chem.* **2000**, *80*, 1024.
(42) Gutowski, M.; Skurski, P.; Boldyrev, A. I.; Simons, J.; Jordan, K. D. *Phys. Rev. A* **1996**, *54*, 1906.
(43) Skurski, P.; Gutowski, M. *J. Chem. Phys.* **1998**, *108*, 6303.
(44) Gutowski, M.; Skurski, P. *J. Phys. Chem. B* **1997**, *101*, 9143.
(45) Gutowski, M.; Skurski, P. *J. Chem. Phys.* **1997**, *107*, 2968.
(46) Gutowski, M.; Skurski, P.; Jordan, K. D.; Simons, J. *Int. J. Quant. Chem.* **1997**, *64*, 183.
(47) Gutowski, M.; Jordan, K. D.; Skurski, P. *J. Phys. Chem. A* **1998**, *102*, 2624.
(48) Gutowski, M.; Hall, C. S.; Adamowicz, L.; Hendricks, J. H.; de Clercq, H. L.; Lyapustina, S. A.; Nilles, J. M.; Xu, S. J.; Bowen, K. H., Jr. *Phys. Rev. Lett.* **2002**, *88*, 143001/1.
(49) Blandamer, M. J.; Fox, M. F. *Chem. Rev.* **1970**, *70*, 59.
(50) Jortner, J.; Ottolenghi, M.; Stein, G. *J. Phys. Chem.* **1964**, *68*, 247.
(51) Platzman, R.; Frank, J. *Z. Phys.* **1954**, *138*, 411.
(52) Ferraudi, G. J. *Elements of inorganic photochemistry*; Wiley: New York, 1988.
(53) Sheu, W.-S.; Rossky, P. J. *J. Phys. Chem.* **1996**, *100*, 1295.
(54) Staib, A.; Borgis, D. *J. Chem. Phys.* **1996**, *104*, 9027.
(55) Borgis, D.; Staib, A. *J. Chem. Phys.* **1996**, *104*, 4776.
(56) Martini, I. B.; Barthel, E. R.; Schwartz, B. J. *Science* **2001**, *293*, 462.
(57) Kloepfer, J. A.; Vilchiz, V. H.; Lenchenkov, V. A.; Chen, X.; Bradforth, S. E. *J. Chem. Phys.* **2002**, *117*, 766.
(58) Kloepfer, J. A.; Vilchiz, V. H.; Lenchenkov, V. A.; Germaine, A. C.; Bradforth, S. E. *J. Chem. Phys.* **2000**, *113*, 6288.
(59) Combariza, J. E.; Kestner, N. R.; Jortner, J. *J. Chem. Phys.* **1994**, *100*, 2865.
(60) Dessent, C. E., H.; Bailey, C. G.; Johnson, M. A. *J. Chem. Phys.* **1995**, *102*, 6335.
(61) Dessent, C. E., H.; Bailey, C. G.; Johnson, M. A. *J. Chem. Phys.* **1995**, *103*, 2006.
(62) Markovich, G.; Pollack, S.; Giniger, R.; Cheshnovsky, O. *J. Chem. Phys.* **1994**, *101*, 9344.
(63) Markovich, G.; Perera, L.; Berkowitz, M. L.; Cheshnovsky, O. *J. Chem. Phys.* **1996**, *105*, 2675.
(64) Dessent, C. E., H.; Kim, J.; Johnson, M. A. *Acc. Chem. Res.* **1998**, *31*, 527.
(65) Hiraoka, K.; Mizuse, S.; Yamabe, S. *J. Phys. Chem.* **1988**, *92*, 3943.
(66) Dessent, C. E. H.; Kim, J.; Johnson, M. A. *J. Phys. Chem.* **1996**, *100*, 12.

(67) Buck, U.; Gu, X. J.; Krohne, R.; Laurensten, C. *Chem. Phys. Lett.* **1990**, *174*, 247.
(68) Serxner, D.; Dessent, C. E., H.; Johnson, M. A. *J. Chem. Phys.* **1996**, *105*, 7231.
(69) Lehr, L.; Zanni, M. T.; Frischkorn, C.; Weinkauf, R.; Neumark, D. M. *Science* **1999**, *284*, 635.
(70) Kammrath, A.; Verlet, J. R. R.; Bragg, A. E.; Griffin, G. B.; Neumark, D. M. *J. Phys. Chem. A* **2005**, *109*, 11475.
(71) Davis, A. V.; Zanni, M. T.; Weinkauf, R.; Neumark, D. M. *Chem. Phys. Lett.* **2002**, *353*, 455.
(72) Chen, H.-Y.; Sheu, W.-S. *Chem. Phys. Lett.* **2001**, *335*, 475.
(73) Chen, H.-Y.; Sheu, W.-S. *Chem. Phys. Lett.* **2002**, *353*, 459.
(74) Adamowicz, L. *J. Chem. Phys.* **1989**, *91*, 7787.
(75) Compton, R. N.; Carman, H. S., Jr.; Desfrancois, C.; Abdoul-Carmine, H.; Schermann, J. P.; Hendricks, J. H.; Lyapustina, S. A.; Bowen, K. H. *J. Chem. Phys.* **1996**, *105*, 3472.
(76) Gutsev, G. L.; Bartlett, R. J. *J. Chem. Phys.* **1996**, *105*, 8785.
(77) Desfrancois, C.; Schermann, J. P. *Chem. Soc. Rev.* **2002**, *31*, 269.
(78) Dessent, C. E. H.; Johnson, M. A. *J. Am. Chem. Soc.* **1997**, *119*, 5067.
(79) Laerdahl, J. K.; Uggerud, E. *Int. J. Mass Spec.* **2002**, *214*, 277.
(80) Sommerfeld, T. *Phys. Chem. Chem. Phys.* **2002**, *4*, 2511.
(81) Stein, G.; Treinin, A. *Trans. Fraday Soc.* **1959**, *55*, 1086.
(82) Assel, M.; Laenen, R.; Laubereau, A. *Chem. Phys. Lett.* **1998**, *289*, 267.
(83) Kloepfer, J. A.; Vilchiz, V. H.; Lenchenkov, V. A.; Bradforth, S. E. *Chem. Phys. Lett.* **1998**, *298*, 120.
(84) Sheu, W. S.; Rossky, P. G. *J. Phys. Chem.* **1996**, *100*, 1295
(85) Bernstein, E. R. *Chemical Reactions in Clusters*; Oxford University Press: New York, 1996.
(86) Becker, I.; Cheshnovsky, O. *J. Chem. Phys.* **1999**, *110*, 6288.
(87) Zanni, M. T.; Frischkorn, C.; Davis, A. V.; Neumark, D. M. *J. Phys. Chem. A* **2000**, *104*, 2527
(88) Majumdar, D.; Kim, J.; Kim, K. S. *J. Chem. Phys.* **2000**, *112*, 101.
(89) Chen, H.-Y.; Sheu, W.-S. *J. Am. Chem. Soc.* **2000**, *122*, 7534.
(90) Lee, M. L.; Kim, K. S. *J. Chem. Phys.* **2001**, *114*, 4461.
(91) Hehre, W. J.; Radom, L.; Schleyer, P. v. R.; Pople, J. A. *Ab Initio Molecular Orbital Theory*; John Wiley and Sons: New York et al., 1985.
(92) Foresman, J. B.; Head-Gordon, M.; Pople, J. A.; Frisch, M. J. *J. Phys. Chem.* **1992**, *96*, 135.
(93) Casida, M. E.; Jamorski, C.; Casida, K. C.; Salahub, D. R. *J. Chem. Phys.* **1998**, *108*, 4439.
(94) Becke, A. D. *J. Chem. Phys.* **1993**, *98*, 5648.
(95) Stanton, J. F.; Bartlett, R. J. *J. Chem. Phys.* **1993**, *89*, 7029.
(96) McLean, A. D.; Chandler, G. S. *J. Chem. Phys.* **1980**, *72*, 5639.
(97) Bergner, A.; Dolg, M.; Kuechle, W.; Stoll, H.; Preuss, H. *Mol. Phys.* **1993**, *80*, 1431.
(98) Glukhovtsev, M. N.; Pross, A.; McGrath, M. P.; Radom, L. *J. Chem. Phys.* **1995**, *103*, 1878.
(99) Bader, R. F. W. *Atoms in Molecules: A Quantum Theory*; Oxford Univ. Press: Oxford, 1990.
(100) Frisch, M. J., et al., *Gaussian 98*, Revision A.11; Gaussian, Inc.: Pittsburgh, PA, 2002.

(101) Schmidt, M. W.; Baldridge, K. K.; Boatz, J. A.; Elbert, S. T.; Gordon, M. S.; Jensen, J. H.; Koseki, S.; Matsunaga, N.; Nguyen, K. A. *J. Comput. Chem.* **1993**, *14*, 1347.

(102) Werner, H.-J.; Knowles, P. J.; Lindh, R.; Schuetz, M., et al., MOLPRO version 2002.6, a package of ab initio programs, see http://www.molpro.net.

(103) Nguyen, T.-N.; Peslherbe, G. H. *J. Phys. Chem. A* **2003**, *107*, 1540.

(104) Kim, K. S.; Park, I.; Lee, S.; Cho, K.; Lee, J. Y.; Kim, J.; Joannopoulos, J. D. *Phys. Rev. Lett.* **1996**, *76*, 956.

(105) Pauling, L. *The Nature of the Chemical Bond*; Cornell University Press: Ithaca, N.Y, 1940.

(106) Scheiner, S. *Hydrogen Bonding: A Theoretical Perspective*; Oxford Univ Press: New York, 1997.

(107) Jeffery, G. A. *An Introduction to Hydrogen Bonding*; Oxford University Press: Oxford, 1997.

(108) Desiraju, G. R.; Steiner, T. *The Weak Hydrogen Bond In Structural Chemistry and Biology*; Oxford University Press: Oxford, 1999.

(109) Steiner, T. *Angew. Chem. Int. Ed.* **2002**, *41*, 48.

(110) Desiraju, G. R. *Acc. Chem. Res.* **2002**, *35*, 565.

(111) Alkorta, I.; Rozas, I.; Elguero, J. *Chem. Soc. Rev.* **1998**, *27*, 163.

(112) Donohue, J. In *Structural Chemistry and Molecular Biology*; Rich, A., Davidson, N., Eds.; W. H. Freeman: San Francisco, 1968; pp 459.

(113) Desiraju, G. R. *Acc. Chem. Res.* **1991**, *24*, 290.

(114) Desiraju, G. R. *Acc. Chem. Res.* **1996**, *29*, 441.

(115) Raymo, F. M.; Bartberger, M. D.; Houk, K. N.; Stoddart, J. F. *J. Am. Chem. Soc.* **2001**, *123*, 9264.

(116) Scheiner, S.; Kar, T. *Journal of Physical Chemistry B* **2005**, *109*, 3681.

(117) Castellano, R. K. *Current Organic Chemistry* **2004**, *8*, 845.

(118) Hobza, P.; Havlas, Z. *Chem. Rev.* **2000**, *100*, 4253.

(119) Gu, Y.; Kar, T.; Scheiner, S. *J. Am. Chem. Soc.* **1999**, *121*, 9411.

(120) Barnes, A. J. *J. Mol. Struct.* **2004**, *704*, 3.

(121) Li, X.; Liu, L.; Schlegel, H. B. *J. Am. Chem. Soc.* **2002**, *124*, 9639.

(122) Hermansson, K. *J. Phys. Chem. A* **2002**, *106*, 4695.

(123) Alabugin, I. V.; Manoharan, M.; Peabody, S.; Weinhold, F. *J. Am. Chem. Soc.* **2003**, *125*, 5973.

(124) Masunov, A.; Dannenberg, J. J.; Contreras, R. H. *J. Phys. Chem. A* **2001**, *105*, 4737.

(125) Herrebout, W. A.; Delanoye, S. N.; van der Veken, B. J. *J. Phys. Chem. A* **2004**, *108*, 6059.

(126) Gregoire, G.; Brenner, V.; Millie, P. *J. Phys. Chem. A* **2000**, *104*, 5204.

(127) Shi, Z.; Boyd, R. J. *J. Am. Chem. Soc.* **1990**, *112*, 6789.

(128) Kryachko, E. S.; Zeegers-Huyskens, T. *J. Phys. Chem. A* **2002**, *106*, 6832.

(129) Mollner, A. K.; Brooksby, P. A.; Loring, J. S.; Bako, I.; Palinkas, G.; Fawcett, W. R. *J. Phys. Chem. A* **2004**, *108*, 3344.

(130) Hobza, P.; Havlas, Z. *Theor. Chem. Acc.* **2002**, *108*, 325.

(131) Gonzales, J. M.; Cox, R. S., III; Brown, S. T.; Allen, W. D.; Schaefer, H. F., III. *J. Phys. Chem. A* **2001**, *105*, 11327.

(132) Ayala, R.; Martinez, J. M.; Pappalardo, R. R.; Marcos, E. S. *J. Phys. Chem. A* **2000**, *104*, 2799.

(133) Rode, M. F.; Roszak, S.; Szymczak, J. J.; Sadlej, J.; Leszczynski, J. *J. Chem. Phys.* **2004**, *121*, 6277.

(134) Li, C.; Ross, P.; Szulejko, J. E.; McMahon, T. B. *J. Am. Chem. Soc.* **1996**, *118*, 9360.
(135) Dunning Jr., T. H. *J. Chem. Phys.* **1989**, *90*, 1007.
(136) Martin, J. M. L.; Sundermann, A. *J. Chem. Phys.* **2001**, *114*, 3408.
(137) Sadlej, A. J. *Theor. Chim. Acta* **1992**, *81*, 339.
(138) Boys, S. F.; Bernardi, F. *Mol. Phys.* **1970**, *19*, 553.
(139) van Duijneveldt, F. B.; van Duijneveldt-van de Rijdt, J. G. C. M.; van Lenthe, J. H. *Chem. Rev.* **1994**, *94*, 1873.
(140) AIMPAC. Available from Professor R. F. W. Bader, McMaster University, Hamilton, ON L8S 4M1, Canada, and from AIMPAC web-site (http://www.chemistry.mcmaster.ca/aimpac/).
(141) Reed, A. E.; Weinstock, R. B.; Weinhold, F. *J. Chem. Phys.* **1985**, *83*, 735.
(142) Glendening, E. D.; Reed, A. E.; Carpenter, F.; Weinhold, F. NBO Version 3.1.
(143) Besler, B. H.; Merz, K. M.; Kollman, P. A. *J. Comput. Chem.* **1990**, *11*, 431.
(144) Singh, U. C.; Kollman, P. A. *J. Comput. Chem.* **1984**, *5*, 129.
(145) Van Voorhis, T.; Scuseria, G. E. *J. Chem. Phys.* **1998**, *109*, 400.
(146) Meot-Ner (Mautner), M. M.; Lias, S. G. Binding Energies Between Ions and Molecules, and The Thermochemistry of Cluster Ions. In *NIST Chemistry WebBook, NIST Standard Reference Database Number 69*; Linstrom, P. J., Mallard, W. G., Eds.; National Institute of Standards and Technology: Gaithersburg MD (http://webbook.nist.gov), 2003.
(147) Mueller, W.; Flesch, J.; Meyer, W. *J. Chem. Phys.* **1984**, *80*, 3297.
(148) Leclercq, J. M.; Allavena, M.; Bouteiller, Y. *J. Chem. Phys.* **1983**, *78*, 4606.
(149) Bouteiller, Y.; Behrouz, H. *J. Chem. Phys.* **1992**, *96*, 6033.
(150) Hobza, P.; Havlas, Z. *Theor. Chem. Acc.* **1998**, *99*, 372.
(151) Simon, S.; Duran, M.; Dannenberg, J. J. *J. Chem. Phys.* **1996**, *105*, 11024.
(152) Simon, S.; Duran, M.; Dannenberg, J. J. *J. Phys. Chem. A* **1999**, *103*, 1640.
(153) Salvador, P.; Duran, M. *J. Chem. Phys.* **1999**, *111*, 4460.
(154) Simon, S.; Bertran, J.; Sodupe, M. *J. Phys. Chem. A* **2001**, *105*, 4359.
(155) Yamdagni, R.; Kebarle, P. *J. Am. Chem. Soc.* **1972**, *94*, 2940.
(156) Stone, A. J. *The Theory of Intermolecular Forces*; Clarendon Press: Oxford, 1996.
(157) Popelier, P. L. A. *Atoms in Molecules: An Introduction*; Prentice Hall: Harlow et al., 2000.
(158) Choi, S. C.; Boyd, R. J. *Canad. J. Chem.* **1986**, *64*, 2042.
(159) Boyd, R. J.; Choi, S. C. *Chem. Phys. Lett.* **1986**, *129*, 62.
(160) Carroll, M. T.; Bader, R. F. W. *Mol. Phys.* **1988**, *65*, 695.
(161) Carroll, M. T.; Chang, C.; Bader, R. F. W. *Mol. Phys.* **1988**, *63*, 387.
(162) Jonas, V.; Frenking, G.; Reetz, M. T. *J. Am. Chem. Soc.* **1994**, *116*, 8741.
(163) Koch, U.; Popelier, P. L. A. *J. Phys. Chem.* **1995**, *99*, 9747.
(164) Bone, R. G. A.; Bader, R. F. W. *J. Phys. Chem.* **1996**, *100*, 10892.
(165) Popelier, P. L. A. *J. Phys. Chem. A* **1998**, *102*, 1873.
(166) Gonzalez, L.; Mo, O.; Yanez, M.; Elguero, J. *J. Chem. Phys.* **1998**, *109*, 2685.
(167) Rozas, I.; Alkorta, I.; Elguero, J. *J. Am. Chem. Soc.* **2000**, *122*, 11154.
(168) Cremer, D.; Kraka, E. *Angew. Chem. Int. Ed.* **1984**, *23*, 627.

(169) Koch, W.; Frenking, G.; Gauss, J.; Cremer, D.; Collins, J. R. *J. Am. Chem. Soc.* **1987**, *109*, 5917.
(170) Espinosa, E.; Molins, E.; Lecomte, C. *Chem. Phys. Lett.* **1998**, *285*, 170.
(171) Espinosa, E.; Lecomte, C.; Molins, E. *Chem. Phys. Lett.* **1999**, *300*, 745.
(172) Espinosa, E.; Molins, E. *J. Chem. Phys.* **2000**, *113*, 5686.
(173) Espinosa, E.; Alkorta, I.; Rozas, I.; Elguero, J.; Molins, E. *Chem. Phys. Lett.* **2001**, *336*, 457.
(174) Espinosa, E.; Alkorta, I.; Elguero, J.; Molins, E. *J. Chem. Phys.* **2002**, *117*, 5529.
(175) Arnold, W. D.; Oldfield, E. *J. Am. Chem. Soc.* **2000**, *122*, 12835.
(176) Ranganathan, A.; Kulkarni, G. U.; Rao, C. N. R. *J. Phys. Chem. A* **2003**, *107*, 6073
(177) Coppens, P.; Abramov, Y.; Carducci, M.; Korjov, B.; Novozhilova, I.; Alhambra, C.; Pressprich, M. R. *J. Am. Chem. Soc.* **1999**, *121*, 2585.
(178) Madsen, G. K. H.; Iversen, B. B.; Larsen, F. K.; Kapon, M.; Reisner, G. M.; Herbstein, F. H. *J. Am. Chem. Soc.* **1998**, *120*, 10040.
(179) Arnold, W. D.; Sanders, L. K.; McMahon, M. T.; Volkov, R. V.; Wu, G.; Coppens, P.; Wilson, S. R.; Godbout, N.; Oldfield, E. *J. Am. Chem. Soc.* **2000**, *122*, 4708.
(180) Koch, D. M.; Peslherbe, G. H. *Chem. Phys. Lett.* **2002**, *359*, 381.
(181) Wang, Y.; Balbuena, P. B. *J. Phys. Chem. A* **2001**, *105*, 9972.
(182) Scheiner, S.; Kar, T. *J. Phys. Chem. A* **2002**, *106*, 1784.
(183) Reed, A. E.; Curtiss, L. A.; Weinhold, F. *Chem. Rev.* **1988**, *88*, 899.
(184) Weinhold, F. Natural bond orbital methods. In *Encyclopedia of computational chemistry*; Schleyer, P. v. R., Ed.; John Wiley and Sons: Chichester, 1998; Vol. 3rd; pp 1792.
(185) Steiner, P. A.; Gordy, W. *J. Mol. Spectrosc.* **1966**, *21*, 291.
(186) Lide, D. R. *The CRC Handbook of Chemistry and Physics*, 75th edition ed.; CRC Press: Boca Raton, Florida, 1994.
(187) Benzel, M. A.; Dykstra, C. E. *J. Chem. Phys.* **1983**, *78*, 4052.
(188) Kar, T.; Scheiner, S. *J. Chem. Phys.* **2003**, *119*, 1473.
(189) Bertolasi, V.; Gilli, P.; Ferretti, V.; Gilli, G. *Chem. Eur. J.* **1996**, *2*, 925.
(190) Timerghazin, Q. K.; Nguyen, T.-N.; Peslherbe, G. H. *J. Chem. Phys.* **2002**, *116*, 6867.
(191) Barone, V.; Cossi, M.; Tomasi, J. *J. Comput. Chem.* **1998**, *19*, 404.
(192) Shimanouchi, T. Molecular Vibrational Frequencies. In *NIST Chemistry WebBook, NIST Standard Reference Database Number 69*; Linstrom, P. J., Mallard, W. G., Eds.; National Institute of Standards and Technology: Gaithersburg MD (http://webbook.nist.gov), 2003.
(193) Hohenberg, P.; Kohn, W. *Phys. Rev.* **1964**, B864.
(194) Vosko, S. H.; Wilk, L.; Nusair, M. *Can. J. Phys.* **1980**, *58*, 1200.
(195) Becke, A. D. *Phys. Rev. A* **1988**, *38*, 3098.
(196) Lee, C.; Yang, W.; Parr, R. G. *Phys. Rev. B* **1988**, *37*, 785.
(197) Burke, K.; Perdew, J. P.; Wang, Y. *Electronic Density Functional Theory: Recent Progress and New Directions, [Proceedings of the International Workshop on Electronic Density Functional Theory: Recent Progress and New Directions], Nathan, Australia, July 14-19, 1996* **1998**, 81.
(198) Perdew, J. P.; Burke, K.; Ernzerhof, M. *Phys. Rev. Lett.* **1996**, *77*, 3865.
(199) Adamo, C.; Barone, V. *J. Comput. Chem.* **1998**, *19*, 418.
(200) Gill, P. M. W. *Mol. Phys.* **1996**, *89*, 433.
(201) Adamo, C.; Barone, V. *Chem. Phys. Lett.* **1997**, *274*, 242.
(202) Chalasinski, G.; Szczesniak, M. M. *Chem. Rev.* **2000**, *100*, 4227.

(203) Arnold, D. W.; Bradforth, S. E.; Kim, E. H.; Neumark, D. M. *J. Chem. Phys.* **1995**, *102*, 3510.
(204) Arnold, D. W.; Bradforth, S. E.; Kim, E. H.; Neumark, D. M. *J. Chem. Phys.* **1995**, *102*, 3493.
(205) Zhao, Y. X.; Yourshaw, I.; Reiser, G.; Arnold, C. C.; Neumark, D. M. *J. Chem. Phys.* **1994**, *101*, 6538.
(206) Yourshaw, I.; Zhao, Y. X.; Neumark, D. M. *J. Chem. Phys.* **1996**, *105*, 351.
(207) Yourshaw, I.; Lenzer, T.; Reiser, G.; Neumark, D. M. *J. Chem. Phys.* **1998**, *109*, 5247.
(208) Lenzer, T.; Furlanetto, M. R.; Asmis, K. R.; Neumark, D. M. *J. Chem. Phys.* **1998**, *109*, 10754.
(209) Lenzer, T.; Furlanetto, M. R.; Pivonka, N. L.; Neumark, D. M. *J. Chem. Phys.* **1999**, *110*, 6714.
(210) Lenzer, T.; Yourshaw, I.; Furlanetto, M. R.; Reiser, G.; Neumark, D. M. *J. Chem. Phys.* **1999**, *110*, 9578.
(211) Lenzer, T.; Yourshaw, I.; Furlanetto, M. R.; Pivonka, N. L.; Neumark, D. M. *J. Chem. Phys.* **2001**, *115*, 3578.
(212) Buchachenko, A. A.; Krems, R. V.; Szczesniak, M. M.; Xiao, Y. D.; Viehland, L. A.; Chalasinski, G. *J. Chem. Phys.* **2001**, *114*, 9919.
(213) Sanov, A.; Faeder, J.; Parson, R.; Lineberger, W. C. *Chem. Phys. Lett.* **1999**, *313*, 812.
(214) Kowal, M.; Gora, R. W.; Roszak, S.; Leszczynski, J. *J. Chem. Phys.* **2001**, *115*, 9260.
(215) Roszak, S.; Kowal, M.; Gora, R. W.; Leszczynski, J. *J. Chem. Phys.* **2001**, *115*, 3469.
(216) Roeselova, M.; Mucha, M.; Schmidt, B.; Jungwirth, P. *J. Phys. Chem. A* **2002**, *106*, 12229.
(217) Robertson, W. H.; Johnson, M. A. *Annu. Rev. Phys. Chem.* **2003**, *54*, 173.
(218) Rose, T. S.; Rosker, M. J.; Zewail, A. H. *J. Chem. Phys.* **1988**, *88*, 6672.
(219) Rosker, M. J.; Rose, T. S.; Zewail, A. H. *Chem. Phys. Lett.* **1988**, *146*, 175.
(220) Rosker, M. J.; Dantus, M.; Zewail, A. H. *Science (Washington, DC, United States)* **1988**, *241*, 1200.
(221) Rose, T. S.; Rosker, M. J.; Zewail, A. H. *J. Chem. Phys.* **1989**, *91*, 7415.
(222) Mokhtari, A.; Cong, P.; Herek, J. L.; Zewail, A. H. *Nature (London, United Kingdom)* **1990**, *348*, 225.
(223) Cong, P.; Mokhtari, A.; Zewail, A. H. *Chem. Phys. Lett.* **1990**, *172*, 109.
(224) Engel, V.; Metiu, H. *Chem. Phys. Lett.* **1989**, *155*, 77.
(225) Jouvet, C.; Martrenchard, S.; Solgadi, D.; Dedonder-Lardeux, C.; Mons, M.; Gregoire, G.; Dimicoli, I.; Piuzzi, F.; Visticot, J. P.; Mestdagh, J. M.; D'Oliveira, P.; Meynadier, P.; Perdrix, M. *J. Phys. Chem. A* **1997**, *101*, 2555.
(226) Gregoire, G.; Mons, M.; Dimicoli, I.; Piuzzi, F.; Charron, E.; Dedonder-Lardeux, C.; Jouvet, C.; Martrenchard, S.; Solgadi, D.; Suzor-Weiner, A. *European Physical Journal D: Atomic, Molecular and Optical Physics* **1998**, *1*, 187.
(227) Gregoire, G.; Mons, M.; Dedonder-Lardeux, C.; Jouvet, C. *European Physical Journal D: Atomic, Molecular and Optical Physics* **1998**, *1*, 5.
(228) Gregoire, G.; Mons, M.; Dimicoli, I.; Dedonder-Lardeux, C.; Jouvet, C.; Martrenchard, S.; Solgadi, D. *J. Chem. Phys.* **2000**, *112*, 8794.
(229) Dedonder-Lardeux, C.; Gregoire, G.; Jouvet, C.; Martrenchard, S.; Solgadi, D. *Chem. Rev.* **2000**, *100*, 4023.
(230) Peslherbe, G. H.; Ladanyi, B. M.; Hynes, J. T. *J. Phys. Chem. A* **1998**, *102*, 4100.

(231) Stibbe, D. T.; Charron, E.; Brenner, V.; Millie, P.; Suzor-Weiner, A. *J. Chem. Phys.* **2002**, *116*, 10753.
(232) Charron, E.; Suzor-Weiner, A. *J. Chem. Phys.* **1998**, *108*, 3922.
(233) Stibbe, D. T.; Charron, E.; Suzor-Weiner, A. *J. Chem. Phys.* **2001**, *115*, 10425.
(234) Werner, H. J.; Knowles, P. J. *J. Chem. Phys.* **1988**, *89*, 5803.
(235) Knowles, P. J.; Werner, H. J. *Chem. Phys. Lett.* **1988**, *145*, 514.
(236) Knowles, P. J.; Hampel, C.; Werner, H. J. *J. Chem. Phys.* **1993**, *99*, 5219.
(237) Watts, J. D.; Gauss, J.; Bartlett, R. J. *J. Chem. Phys.* **1993**, *98*, 8718.
(238) Werner, H. J.; Knowles, P. J. *J. Chem. Phys.* **1985**, *82*, 5053.
(239) Knowles, P. J.; Werner, H. J. *Chem. Phys. Lett.* **1985**, *115*, 259.
(240) Langhoff, S. R.; Davison, E. R. *Int. J. Quant. Chem.* **1974**, *8*, 61.
(241) Blomberg, M. R. A.; Siegbahn, P. E. M. *J. Chem. Phys.* **1983**, *78*, 5682.
(242) Simons, J. *J. Phys. Chem.* **1989**, *93*, 626.
(243) Woon, D. E.; Dunning, T. H., Jr. *J. Chem. Phys.* **1995**, *103*, 4572.
(244) Peterson, K. A. *J. Chem. Phys.* **2003**, *119*, 11099.
(245) Peterson, K. A.; Figgen, D.; Goll, E.; Stoll, H.; Dolg, M. *J. Chem. Phys.* **2003**, *119*, 11113.
(246) Peterson, K. A.; Woon, D. E.; Dunning, T. H., Jr. *J. Chem. Phys.* **1994**, *100*, 7410.
(247) MOLPRO. is a package of ab initio programs written by H.-J. Werner and P. J. Knowles, version 2002.6, with contributions from R. D. Amos, A. Bernhardsson, A. Berning, P. Celani, D. L. Cooper, M. J. O. Deegan, A. J. Dobbyn, F. Eckert, C. Hampel, G. Hetzer, T. Korona, R. Lindh, A. W. Lloyd, S. J. McNicholas, F. R. Manby, W. Meyer, M. E. Mura, A. Nicklass, P. Palmieri, R. Pitzer, G. Rauhut, M. Schьtz, H. Stoll, A. J. Stone, R. Tarroni, and T. Thorsteinsson.
(248) Le Roy, R. LEVEL 7.1: A Computer Program for Solving the Radial Schrodinger Equation for Bound and Quasibound Levels, University of Waterloo Chemical Physics Research Report CP-642R.
(249) Alekseyev, A. B.; Liebermann, H.-P.; Lingott, R.; Buenker, R. J.; Wright, J. S. *Mol. Phys.* **1997**, *91*, 777.
(250) Hollas, J. M. *High Resolution Spectroscopy*, 2nd ed.; J. Wiley: Chichester ; New York, 1998.
(251) Dunning, T. H.; Hay, P. J. *J. Chem. Phys.* **1978**, *69*, 134.
(252) Faeder, J.; Delaney, N.; Maslen, P. E.; Parson, R. *Chem. Phys.* **1998**, *239*, 525.
(253) Klos, J. A.; Chalasinski, G.; Szczsniak, M. M.; Werner, H.-J. *J. Chem. Phys.* **2001**, *115*, 3085.
(254) Bellert, D.; Breckenridge, W. H. *Chem. Rev.* **2002**, *102*, 1595.
(255) Meuwly, M.; Hutson, J. M. *J. Chem. Phys.* **2003**, *119*, 8873.
(256) Cybulski, S. M.; Burcl, R.; Szczesniak, M. M.; Chalasinski, G. *J. Chem. Phys.* **1996**, *104*, 7997.
(257) Sansonetti, J. E.; Martin, W. C. *Handbook of Basic Atomic Spectroscopic Data (http://physics.nist.gov/PhysRefData/Handbook/index.html)*; National Institute of Standards and Technology: Gaithersburg, MD 20899, 2005.
(258) Hay, P. J.; Dunning, T. H., Jr. *J. Chem. Phys.* **1977**, *66*, 1306.
(259) Haberland, H. *Z. Phys. A* **1982**, *307*, 35.
(260) Alekseyev, A. B.; Liebermann, H.-P.; Buenker, R. J.; Balakrishnan, N.; Sadeghpour, H. R.; Cornett, S. T.; Cavagnero, M. J. *J. Chem. Phys.* **2000**, *113*, 1514.
(261) Alekseyev, A. B.; Liebermann, H.-P.; Buenker, R. J. *Recent Advances in Computational Chemistry* **2004**, *5*, 65.

(262) Shepler, B. C.; Peterson, K. A. *J. Phys. Chem. A* **2003**, *107*, 1783.
(263) Becker, C. H.; Casavecchia, P.; Lee, Y. T.; Olson, R. E.; Lester, W. A., Jr. *J. Chem. Phys.* **1979**, *70*, 5477.
(264) Aquilanti, V.; Luzzatti, E.; Pirani, F.; Volpi, G. G. *J. Chem. Phys.* **1980**, *73*, 1181.
(265) Aquilanti, V.; Candori, R.; Pirani, F. *J. Chem. Phys.* **1988**, *89*, 6157.
(266) Buchachenko, A. A.; Jakowski, J.; Chalasinski, G.; Szczesniak, M. M.; Cybulski, S. M. *J. Chem. Phys.* **2000**, *112*, 5852.
(267) Dunning, T. H., Jr. *J. Phys. Chem. A* **2000**, *104*, 9062.
(268) Woon, D. E.; Dunning, T. H., Jr. *J. Chem. Phys.* **1994**, *101*, 8877.
(269) Peterson, K. A.; Woon, D. E.; Dunning, T. H.; Jr. *J. Chem. Phys.* **1994**, *100*, 7410.
(270) Feller, D. *J. Chem. Phys.* **1992**, *96*, 6104.
(271) Feller, D. *J. Chem. Phys.* **1993**, *98*, 7059.
(272) Feller, D.; Peterson, K. A. *J. Chem. Phys.* **1998**, *108*, 154.
(273) Feller, D.; Glendening, E. D.; Woon, D. E.; Feyereisen, M. W. *J. Chem. Phys.* **1995**, *103*, 3526.
(274) Feller, D. *Chem. Phys. Lett.* **2000**, *322*, 543.
(275) Kenny, J. P.; Allen, W. D.; Schaefer III, H. F. *J. Chem. Phys.* **2003**, *118*, 7353.
(276) Fanourgakis, G. S.; Apra, E.; Xantheas, S. S. *J. Chem. Phys.* **2004**, *121*, 2655.
(277) Xantheas, S. S.; Apra, E. *J. Chem. Phys.* **2004**, *120*, 823.
(278) Halpern, A. M.; Glendening, E. D. *J. Chem. Phys.* **2003**, *119*, 11186.
(279) Feller, D.; Dixon, D. A.; Nicholas, J. B. *J. Phys. Chem. A* **2000**, *104*, 11414.
(280) Giese, T. J.; York, D. M. *J. Chem. Phys.* **2004**, *120*, 7939.
(281) Cybulski, S. M.; Toczylowski, R. R. *J. Chem. Phys.* **1999**, *111*, 10520.
(282) Crozet, P.; Ross, A. J.; Vervloet, M. *Annu. Rep. Prog. Chem., Sect. C: Phys. Chem.* **2002**, *98*, 33.
(283) Pratt, D. W. *Annu. Rev. Phys. Chem.* **1998**, *49*, 481.
(284) Engel, V.; Metiu, H.; Almeida, R.; Marcus, R. A.; Zewail, A. H. *Chem. Phys. Lett.* **1988**, *152*, 1.
(285) Xie, J.; Zare, R. N. *J. Chem. Phys.* **1990**, *93*, 3033.
(286) Buchachenko, A. A.; Szczesniak, M. M.; Chalasinski, G. *J. Chem. Phys.* **2001**, *114*, 9929.
(287) Buchachenko, A. A.; Szczesniak, M. M.; Klos, J.; Chalasinski, G. *J. Chem. Phys.* **2002**, *117*, 2629.
(288) Born, M.; Mayer, J. E. *Z. Phys.* **1932**, *75*, 1.
(289) London, F. *Z. Physik. Chem. B* **1930**, *11*, 222.
(290) Press, W. H.; Teukolsky, S. A.; Vetterling, W. T.; Flannery, B. P. *Numerical Recipes, the Art of Scientific Computing, Second Edition*; Cambridge University Press: Cambridge, England, 1992.
(291) Jortner, J.; Levine, R.; Ottolenghi, M.; Stein, G. *J. Phys. Chem.* **1961**, *65*, 1232.
(292) Crowell, R. A.; Lian, R.; Shkrob, I. A.; Bartels, D. M.; Chen, X.; Bradforth, S. E. *J. Chem. Phys.* **2004**, *120*, 11712.
(293) Martini, G. B.; Barthel, E. R.; Schwartz, B. J. *Science* **2001**, *293*, 462.
(294) Martini, I. B.; Barthel, E. R.; Schwartz, B. J. *J. Am. Chem. Soc.* **2002**, *124*, 7622.

(295) Robertson, W. H.; Johnson, M. A. *Annu. Rev. Phys. Chem.* **2003**, *54*, in press.
(296) Vila, F. D.; Jordan, K. D. *J. Phys. Chem. A* **2002**, *106*, 1391.
(297) Bradforth, S. E.; Jungwirth, P. *J. Phys. Chem. A* **2002**, *106*, 1286.
(298) Timerghazin, Q. K.; Peslherbe, G. H. *Chem. Phys. Lett.* **2002**, *354*, 31.
(299) Rode, M. F.; Roszak, S.; Szymczak, J. J.; Sadlej, J.; Leszczynski, J. *J. Chem. Phys.* **2004**, *121*, 6277.
(300) Lee, H. M.; Kim, K. S. *Mol. Phys.* **2004**, *102*, 2485.
(301) Lee, H. M.; Suh, S. B.; Kim, K. S. *J. Chem. Phys.* **2003**, *119*, 7685.
(302) Timerghazin, Q. K.; Peslherbe, G. H. *J. Am. Chem. Soc.* **2003**, *125*, 9904.
(303) Kolaski, M.; Lee, H. M.; Pak, C.; Dupuis, M.; Kim, K. S. *J. Phys. Chem. A* **2005**, *109*, 9419.
(304) Stoll, H.; Metz, B.; Dolg, B. *J. Comput. Chem.* **2002**, *23*, 767.
(305) Werner, H.-J. *Mol. Phys.* **1996**, *89*, 645.
(306) Alfonso, D. R.; Jordan, K. D. *J. Chem. Phys.* **2002**, *116*, 3612.
(307) Mitin, A. V.; Hirsch, G.; Buenker, R. J. *Chem. Phys. Lett.* **1996**, *259*, 151.
(308) Clark, T.; Chandrasekhar, J.; Spitznagel, G. W.; Schleyer, P. v. R. *J. Comput. Chem.* **1983**, *4*, 294.
(309) Stevens, W. J.; Krauss, M.; Basch, H.; Jasien, P. G. *Can J Chem* **1992**, *70*, 612.
(310) Check, C. E.; Faust, T. O.; Bailey, J. M.; Wright, B. J.; Gilbert, T. M.; Sunderlin, L. S. *J. Phys. Chem. A* **2001**, *105*, 8111.
(311) Peslherbe, G. H.; Wang, H. B.; Hase, W. L. *Adv Chem Phys* **1999**, *105*, 171.
(312) Hase, W. L.; Duchovic, R. J.; Hu, X.; Komornicki, A.; Lim, K.; D.Lu; Peslherbe, G. H.; Swamy, K. N.; Van de Linde, S. R.; Wang, H.; Wolf, R. J. *QCPE* **1996**, *16*, 671.
(313) Stewart, J. J. P.; Davis, L. P.; Burggraf, L. W. *J. Comput. Chem.* **1987**, *8*, 1117.
(314) Bolton, K.; Hase, W. L.; Peslherbe, G. H. Direct Dynamics Simulations of Reactive Systems. In *Multidimensional Molecular Dynamics Methods*; Thompson, D. L., Ed.; World Scientific Publishing Co., 1998.
(315) Timerghazin, Q. K.; Koch, D. M.; Peslherbe, G. H. *J. Chem. Phys.* **2006**, *124*, xxxxx.
(316) Desfrancois, C.; Abdoulcarime, H.; Khelifa, N.; Schermann, J. P. *Phys. Rev. Lett.* **1994**, *73*, 2436.
(317) Timerghazin, Q. K.; Nguyen, T.-N.; Peslherbe, G. H. *J. Am. Chem. Soc.* **2006**, *to be submitted.*
(318) Hall, C. S.; Adamowicz, L. *Mol. Phys.* **2002**, *100*, 3469.
(319) Klots, C. E. *Nature* **1987**, *327*, 222.
(320) Hay, P. J.; Wadt, W. R. *J. Chem. Phys.* **1985**, *82*, 270.
(321) Desfrancois, C.; Abdoul-Carime, H.; Schermann, J.-P. *International Journal of Modern Physics B* **1996**, *10*, 1339.
(322) Compton, R. N.; Hammer, N. I. *Advances in Gas Phase Ion Chemistry* **2001**, *4*, 257.
(323) Desfrancois, C.; Bouteiller, Y.; Schermann, J. P.; Radisic, D.; Stokes, S. T.; Bowen, K. H.; Hammer, N. I.; Compton, R. N. *Phys. Rev. Lett.* **2004**, *92*.
(324) Gutowski, M.; Skurski, P.; Li, X.; Wang, L. S. *Phys. Rev. Lett.* **2000**, *85*, 3145.
(325) Lecomte, F.; Carles, S.; Desfrancois, C.; Johnson, M. A. *J. Chem. Phys.* **2000**, *113*, 10973.

(326) Sommerfeld, T. *J. Phys. Chem. A* **2004**, *108*, 9150.
(327) Scheer, A. M.; Aflatooni, K.; Gallup, G. A.; Burrow, P. D. *Phys. Rev. Lett.* **2004**, *92*, 068102/1.
(328) Hashemi, R.; Illenberger, E. *J. Phys. Chem.* **1991**, *95*, 6402.
(329) Bailey, C. G.; Dessent, C. E. H.; Johnson, M. A.; Bowen, K. H. *J. Chem. Phys.* **1996**, *104*, 6976.
(330) Desfrancois, C.; Abdoul-Carime, H.; Khelifa, N.; Schermann, J. P.; Brenner, V.; Millie, P. *J. Chem. Phys.* **1995**, *102*, 4952.
(331) Mitsui, M.; Ando, N.; Kokubo, S.; Nakajima, A.; Kaya, K. *Phys. Rev. Lett.* **2003**, *91*.
(332) Burrow, P. D.; Howard, A. E.; Johnston, A. R.; Jordan, K. D. *J. Phys. Chem.* **1992**, *96*, 7570.
(333) Williams, F.; Sprague, E. D. *Acc. Chem. Res.* **1982**, *15*, 408.
(334) Shkrob, I. A.; Takeda, K.; Williams, F. *J. Phys. Chem. A* **2002**, *106*, 9132.
(335) Shkrob, I. A.; Sauer, M. C., Jr. *J. Phys. Chem. A* **2002**, *106*, 9120.
(336) Xia, C.; Peon, J.; Kohler, B. *J. Chem. Phys.* **2002**, *117*, 8855.
(337) Bonin, M. A.; Tsuji, K.; Williams, F. *Nature* **1968**, *218*, 946.
(338) Balaj, O. P.; Balteanu, I.; Fox-Beyer, B. S.; Beyer, M. K.; Bondybey, V. E. *Angew Chem Int Edit* **2003**, *42*, 5516.
(339) Scuseria, G. E.; Schaefer III, H. F. *J. Chem. Phys.* **1989**, *90*, 3700.
(340) Dunning Jr., T. H.; Hay, P. J. In *Methods of Electronic Structure Theory*; Schaefer III, H. F., Ed.; Plenum Press: New York, 1977; Vol. 3.
(341) Eade, R. H. A.; Robb, M. A. *Chem. Phys. Lett.* **1981**, *83*, 362.
(342) Celani, P.; Werner, H. J. *J. Chem. Phys.* **2000**, *112*, 5546.
(343) Koch, W.; Holthausen, M. C. *A Chemist's Guide to Density Functional Theory, 2nd Edition*, 2001.
(344) Cremer, D.; Kraka, E.; Szalay, P. G. *Chem. Phys. Lett.* **1998**, *292*, 97.
(345) Jensen, F. *J. Chem. Phys.* **2001**, *115*, 9113.
(346) Jensen, F. *J. Chem. Phys.* **2002**, *116*, 7372.
(347) Jensen, F. *J. Chem. Phys.* **2002**, *117*, 9234.
(348) Jensen, F. *J. Chem. Phys.* **2003**, *118*, 2459.
(349) Frisch, M. J., et al., *Gaussian 03*, Revision B.05; Gaussian, Inc.: Pittsburgh, PA, 2003.
(350) Cossi, M.; Rega, N.; Scalmani, G.; Barone, V. *J. Comput. Chem.* **2003**, *24*, 669.
(351) Cossi, M.; Barone, V.; Robb, M. A. *J. Chem. Phys.* **1999**, *111*, 5295.
(352) Popelier, P. L. A.; Stone, A. J.; Wales, D. J. *Faraday Discussions* **1994**, *97*, 243.
(353) Siebers, J. G.; Buck, U.; Beu, T. A. *Chemical Physics* **1998**, *239*, 549.
(354) Siebers, J. G. "Simulation of structure and vibrational spectra of small molecular clusters," Max-Planck-Institut Stromungsforschung,Goettingen,Germany. FIELD URL:, 1997.
(355) Reimers, J. R.; Hall, L. E. *J. Am. Chem. Soc.* **1999**, *121*, 3730.
(356) Cabaleiro-Lago, E. M.; Hermida-Ramon, J. M.; Pena-Gallego, A.; Martinez-Nunez, E.; Fernandez-Ramos, A. *Theochem* **2000**, *498*, 21.
(357) Ford, T. A.; Glasser, L. *International Journal of Quantum Chemistry* **2001**, *84*, 226.
(358) Hall, C. S.; Adamowicz, L. *J. Phys. Chem. A* **2002**, *106*, 6099.
(359) Skurski, P.; Simons, J. *J. Chem. Phys.* **2002**, *116*, 6118.
(360) Tsurusawa, T.; Iwata, S. *Chem. Phys. Lett.* **1999**, *315*, 433.

(361) Hao, X.-Y.; Li, Z.-R.; Wu, D.; Wang, Y.; Li, Z.-S.; Sun, C.-C. *J. Chem. Phys.* **2003**, *118*, 83.
(362) Kim, K. S.; Park, I.; Lee, S.; Cho, K.; Lee, J.; Kim, J.; Joannopoulos, J. D. *Phys. Rev. Lett.* **1996**, *76*, 956.
(363) Hammer, N. I.; Roscioli, J. R.; Johnson, M. A. *J. Phys. Chem. A* **2005**, *109*, 7896.
(364) Bader, R. F. W.; Bayles, D.; Heard, G. L. *J. Chem. Phys.* **2000**, *112*, 10095.
(365) Bader, R. F. W.; Platts, J. A. *J. Chem. Phys.* **1997**, *107*, 8545.
(366) Mei, C. J.; Edgecombe, K. E.; Smith, V. H.; Heilingbrunner, A. *Int. J. Quant. Chem.* **1993**, *48*, 287.
(367) Edgecombe, K. E.; Esquivel, R. O.; Smith, V. H.; Mullerplathe, F. *J. Chem. Phys.* **1992**, *97*, 2593.
(368) Madsen, G. K. H.; Blaha, P.; Schwarz, K. *J. Chem. Phys.* **2002**, *117*, 8030.
(369) Timerghazin, Q. K.; Rizvi, I.; Peslherbe, G. H. *manuscript in preparation.*

(361) Hao, X.-Y.; Li, Z.-R.; Wu, D.; Wang, Y.; Li, Z.-S.; Sun, C.-C. *J. Chem. Phys.* **2003**, *118*, 83.
(362) Kim, K. S.; Park, I.; Lee, S.; Cho, K.; Lee, J.; Kim, J.; Joannopoulos, J. D. *Phys. Rev. Lett.* **1996**, *76*, 956.
(363) Hammer, N. I.; Roscioli, J. R.; Johnson, M. A. *J. Phys. Chem. A* **2005**, *109*, 7896.
(364) Bader, R. F. W.; Bayles, D.; Heard, G. L. *J. Chem. Phys.* **2000**, *112*, 10095.
(365) Bader, R. F. W.; Platts, J. A. *J. Chem. Phys.* **1997**, *107*, 8545.
(366) Mei, C. J.; Edgecombe, K. E.; Smith, V. H.; Heilingbrunner, A. *Int. J. Quant. Chem.* **1993**, *48*, 287.
(367) Edgecombe, K. E.; Esquivel, R. O.; Smith, V. H.; Mullerplathe, F. *J. Chem. Phys.* **1992**, *97*, 2593.
(368) Madsen, G. K. H.; Blaha, P.; Schwarz, K. *J. Chem. Phys.* **2002**, *117*, 8030.
(369) Timerghazin, Q. K.; Rizvi, I.; Peslherbe, G. H. *manuscript in preparation.*